THE IMPACT OF PLEIOTROPHIN ON BREAST CANCER PROGRESSION

APPROVED BY SUPERVISORY COMMITTEE
(14 spaces down)

NOTE: The top line is for the Supervising Professor's name. There should be as many lines as there are members of the committee. All signatures must be original and in ink. Adjust "Approved by Supervisory Committee" line upward if the committee list is very large.

Rolf A. Brekken, Ph.D.

Melanie H. Cobb, Ph.D.

Philipp E. Scherer, Ph.D.

Paul C. Sternweis, Ph.D.

DEDICATION/ACKNOWLEDGEMENTS

I would like to thank the my advisor, Rolf A. Brekken, members of my Graduate Committee, my graduate program chair, members of the Brekken Lab, and my wife Susie.

THE IMPACT OF PLEIOTROPHIN EXPRESSION IN BREAST CANCER PROGRESSION

by

NOAH BRUCE SORRELLE

DISSERTATION / THESIS

Presented to the Faculty of the Graduate School of Biomedical Sciences

The University of Texas Southwestern Medical Center at Dallas

In Partial Fulfillment of the Requirements

For the Degree of

DOCTOR OF PHILOSOPHY

The University of Texas Southwestern Medical Center at Dallas

Dallas, Texas

May, 2019

THE IMPACT OF PLEIOTROPHIN EXPRESSION IN BREAST CANCER PROGRESSION

Publication No._____

Noah Bruce Sorrelle, Ph.D.

The University of Texas Southwestern Medical Center at Dallas, 2019

Supervising Professor: **Rolf A. Brekken, Ph.D.**

Breast cancer is the most frequent type of cancer, despite being largely restricted to women. Over the past few decades, cancer biologists have made great strides in understanding the factors that drive breast cancer tumorigenesis and progression. However, the significance of many factors, such as Pleiotrophin, remain uncharacterized.

Pleiotrophin (Ptn), a neurite outgrowth factor and a heparin-binding cytokine, is reportedly expressed in many types of cancer, including breast cancer. Despite being identified as a secreted factor produced by breast cancer cells in 1991, its

functional significance in breast cancer is uncertain. Previous studies into this question were limited by available tools for specifically perturbing or knocking out *Ptn* genetically. Further, they were also limited in scope, focusing only on select characteristics of the tumor progression and the microenvironment. Curiously, research into Ptn's impact in breast cancer came to a halt in 2007, leaving the very question of Ptn's functional significance unanswered.

Using pharmacologic and genetic methods, I tested the impact of Ptn perturbation in multiple preclinical models of breast cancer. Ptn perturbation only impacted primary tumor growth in a single model. In contrast, Ptn perturbation resulted in reduced pulmonary metastatic burden in every model tested thus far. This effect does not appear to be due to Ptn's direct impact on cancer cell phenotype, growth, or migration. Anti-Ptn therapy did not affect epithelial-to-mesenchymal transition of cancer cells, nor did Ptn directly promote cancer cell proliferation or migration in vitro.

These results suggest that Ptn's effects are through changes in the tumor microenvironment. By immunohistochemistry and flow cytometry, I observed that there was less neutrophil infiltration and macrophage/metastatic lesion coupling in vivo. This result was interesting as both neutrophils and macrophages are implicated in promoting pulmonary metastasis in preclinical models of breast cancer. Using a cytokine/chemokine array, I observed that Ptn perturbation resulted in the reduction

of macrophage and neutrophil chemokines, including MCP-1 and CXCL5, respectively.

In contrast to previous reports, Ptn perturbation did not result in changes in angiogenesis, epithelial-to-mesenchymal transition, or markers of cell proliferation or apoptosis. Some of these reported activities may have resulted from off-target effects of the tools used at the time.

Overall, the experimental strategies and specificity of the tools used in my thesis work have provided more accurate insights into the activity of Ptn. Additionally, the results suggest that Ptn is a potent driver of pulmonary metastasis in breast cancer and that targeting Ptn may an effective therapeutic strategy to treat metastatic breast cancer.

TABLE OF CONTENTS

PRIOR PUBLICATIONS

1. **Sorrelle N** et al. 2019. Pleiotrophin promotes breast cancer metastasis through recruitment if pro-metastatic myeloid cells. Manuscript under preparation.
2. **Sorrelle N**, Ganguly D, Dominguez ATA, Zhang Y, Huang H, Dahal LN, Burton N, Zeimys A, Brekken RA. Improved multiplex immunohistochemistry for immune microenvironment evaluation of mouse formalin-fixed paraffin-embedded tissues. *Journal of Immunology*. 2019 Jan 1;202(1):292-299.
3. Weckbach LT, [and 20 others, including **Sorrrelle N**]. 2018. Midkine Drives Cardiac Inflammation by mediating NETosis and Neutrophil Trafficking in Myocarditis. *J Exp Med.* 2019 Jan 15. pii:jem.20181102
4. Du W, Huang H, **Sorrelle N**, Brekken RA. Sitravatinib potentiates immune checkpoint blockade in refractory cancer models. *JCI Insight*. 2018 Nov 2;3(21). PMID: 30385724
5. Zhang Y, Kirane A, Huang H, **Sorrelle NB**, Burrows FJ, Dellinger MT, Brekken RA. Cyclooxygenase-2 inhibition potentiates the efficacy of vascular endothelial growth factor blockade and promotes an immune stimulatory microenvironment in preclinical models of pancreatic cancer. Mol Cancer Res. 2018 Oct 17. pii: molcanres.0427.2018. PMID: 30333153
6. Ludwig KF, Du W, **Sorrelle N**, et al. 2018. Small molecule Axl inhibition targets tumor immune suppression and enhances chemotherapy in pancreatic cancer. *Cancer Research.* 78(1):246-255.
7. **Sorrelle N**, Dominguez AT, Brekken RA. 2017. From top to bottom: midkine and pleiotrophin as emerging players in immune regulation. *J Leukoc Biol*. 102(2):277-286.
8. **Sorrelle N**, Brekken RA. 2016. Vascular Endothelial Growth Factor Receptor 2 (VEGFR2). Atlas Genet Cytogenet Oncol Haematol. 2016; 20(7):392-402.
9. Kirane A, Ludwig KF, **Sorrelle N**, et al. 2015. Warfarin Blocks Gas6-Mediated Axl Activation Required for Pancreatic Cancer Epithelial Plasticity and Metastasis. *Cancer Res*. 75(18):3699-705.
10. Huang R, [and 9 others, including **Sorrelle N**]. 2012. Enzyme functional evolution through improved catalysis of ancestrally non-preferred substrates. *Proceedings of the National Academy of Sciences*. 109(8): pg. 2966-2971

LIST OF FIGURES

LIST OF TABLES

LIST OF ABBREVIATIONS

Alk	Anaplastic Lymphoma Kinase
DKO	Double Knockout
DNA	Deoxyribose Nucleic Acid
cDNA	Complementary DNA
EMT	Epithelial-to-Mesenchymal Transition
FBS	Fetal Bovine Serum
FFPE	Formalin-Fixed, Paraffin-Embedded
HSC	Hematopoietic Stem Cell
IHC	Immunohistochemistry
Lrp1	Low Density Lipoprotein Receptor-Related Protein 1
Mac-1	Integrin αMβ2; CD11b/CD18
Mcp1	Monocyte Chemoattractant Protein 1
Mdk	Midkine
NK cell	Natural Killer Cell
PBS	Phosphate-Buffered Saline
PCR	Polymerase Chain Reaction
Ptn	Pleiotrophin
RNA	Ribonucleic Acid
Sdc	Syndecan
Ptprz1	Protein Tyrosine Phosphatase, Receptor Type Z1
Tlr	Toll-like Receptor
WT	Wild-Type

CHAPTER ONE
Introduction

The Pleiotrophin/Midkine Family of Cytokines

Midkine (Mdk) and pleiotrophin (Ptn) comprise a two-member family of heparin-binding cytokines. Mdk and Ptn are roughly 50% homologous in amino acid sequence in mammals [2]. Mouse Mdk shares 87% homology in amino acid sequence with human Mdk while human PTN shares 97% amino acid sequence identity to mouse Ptn and shares 72% amino acid homology with *Xenopus laevis* [3]. Mdk was first identified as a highly expressed factor produced during the early stage of retinoic acid-driven differentiation of embryonal carcinoma cells [4]. In 1991, it was independently discovered as a growth factor in bovine brain that promoted the proliferation of bovine brain capillary cells in vitro [5]. Ptn was first discovered as a heparin-binding, soluble protein present in the developing rat brain that promoted neurite outgrowth in vitro [6].

Fitting their respective scientific origins, much of the focus on the Mdk/Ptn family has been on the function of Mdk/Ptn in angiogenesis, the central nervous system, and cancer. Although Ptn and Mdk are expressed in many different cancers,

little is known about their function in this regard. **Regulation and Expression of Ptn and Mdk**

Ptn and Mdk: General Expression Patterns

Mdk and Ptn are expressed widely during development, yet mice deficient in either Mdk or Ptn display no overt developmental defects [7]. However, Mdk and Ptn double knockout (DKO) mice exhibit a gene dosage effect. Mice null for Ptn or Mdk are born at expected mendelian ratios, while DKO mice are born at 33% of the expected ratio [7]. DKO mice also have a lower average weight and fail to gain significant weight on a high-calorie diet. In DKO males, 100% of individuals are fertile; conversely, 79% of females are sterile, which may be due to abnormal follicular maturation in ovaries and vaginal malformation. For more information on the function and expression of Mdk and Ptn in development, see Kadomatsu and Tsubota, 2013 [8].

The expression of Mdk and Ptn in healthy adult mice is highly restricted. In adults, significant Ptn expression is limited largely to the central nervous system with detectable low-level expression in the breast epithelium, placental tissue, testis, bladder, and stomach [9,10]. Conversely, Mdk is expressed in the kidney [11], gut [12], epidermis [13], and bronchial epithelium [14]**.** Interestingly, Ptn is upregulated significantly in multiple tissues of Mdk-deficient mice, but there are no detectable differences of Mdk expression in *Ptn*-null mice [15]. These results suggest that Ptn may compensate for the loss of Mdk, but the converse may not hold true.

In the bone marrow, endothelial cells of the hematopoietic stem cell niche produce Ptn [16]. Ptn expands long-term HSCs in vitro, and *Ptn*-null bone marrow has significantly less long-term HSCs, suggesting that Ptn is a critical HSC maintenance factor [16,17]. Consistent with this idea, the administration of recombinant Ptn helps alleviate myelosuppression and greatly improves survival of lethally-irradiated mice. In this context, Ptn administration increased the frequency of granulocyte-erythroid-macrophage-megakaryocyte-CFUs (GEMM-CFUs), the multipotent progenitors of myeloid cells. Mechanistically, Ptn-driven expansion of bone marrow c-Kit+;Sca-1+;Lin- (KSL) cells is mediated through Ptprz1, leading to Ras activation in KSL cells. The deletion of Ptprz1 or Ras-inhibition perturbed Ptn activity in vitro and in vivo [18]. Aberrant activation of Ras in hematopoietic cells can drive myeloproliferative disorders and leukemia, but the function of Ptn in this context is undetermined [19,20].

Gene Expression and the Ptn/Mdk Family: Upstream and Downstream Factors

Mdk and Ptn expression are elevated in response to inflammatory cytokines; Mdk induction may be driven by nuclear factor kappa-B (NFκB) as the Mdk promoter contains a putative NFκB-responsive element [21]. Ptn expression can be positively regulated by IFNβ and IFNγ [22,23]. For example, in THP-1 monocytic cells and mouse peritoneal macrophages, IFNγ promotes Ptn expression via an IFNγ responsive promoter element [23]. Additionally, high-molecular weight hyaluronan, an inhibitor of toll-like receptor 4 (Tlr4) activity, decreases the expression of Ptn in a murine model of Th1-type autoimmune disease, implicating Ptn as a Tlr4-responsive gene [24].

Tumor necrosis factor alpha (TNFα) can stimulate the expression of Mdk and Ptn in monocytes and tumor cells, validating Mdk/Ptn expression as effectors of inflammatory cytokine activity [25-27]. Lymphocytes are also reported to express Mdk or Ptn after stimulation. For instance, Mdk expression is elevated in T cells after activation with anti-CD3/CD28 antibodies and in peripheral blood lymphocytes in response to interleukin-2 (IL-2) or IFNγ [28]. However, neither CD3/CD28 activation, nor IL-2 or IFNγ treatment promotes Ptn expression in lymphocytes, demonstrating a differential regulation of Mdk and Ptn expression depending on the context. Overall, these data suggest that immune cells may be a significant source of Mdk/Ptn in inflammation and cancer.

Of the non-immune-affiliated cytokines, Mdk and Ptn are positively regulated by epidermal growth factor (EGF) [27,29] and fibroblast growth factor-10 (FGF-10) [29]. Ptn is also upregulated by fibroblast growth factor-2 (FGF2 or bFGF) [30] and platelet-derived growth factor [31,32], and is downregulated by vascular endothelial growth factor-A (VEGF-A) [33].

A variety of non-cytokine-related pathways can also affect the expression of Mdk and Ptn. For example, the activation of estrogen receptor beta (ERβ) and subsequent protein kinase C delta activation stimulates Mdk expression [34,35] while estrogen receptor alpha (ERα) can negatively regulate Mdk expression [36]. Further, retinoic acid stimulates Mdk expression but has no effect on Ptn expression even though the promoters for each gene contain putative retinoic acid-responsive

elements [37]. In contrast, progesterone and testosterone augment Ptn expression but not Mdk [38]. Additionally, Mdk and Ptn expression are reduced in response to glucocorticoid receptor activity [37,39].

Downstream of Mdk/Ptn, there is evidence that this family can influence the expression of immunomodulatory cytokines. IL-1β, IL-6, and TNFα are upregulated in peripheral blood mononuclear cells (PBMCs) in response to Ptn [40,41]. Furthermore, in a murine model of peritoneal fibrosis, *Ptn*-null mice had decreased IL-1β, TNFα, and TGFβ expression. Ptn also mediates the expression of VEGF-A in colorectal cell lines [42] and heparin-binding EGF (HB-EGF) in primary osteoblasts [43]. In an ischemic renal injury model, Mdk was shown to stimulate the expression of the chemokines, macrophage inflammatory protein-2 and monocyte chemoattractant protein-1 (MIP2/CXCL2 and MCP-1/CCL2, respectively) [44]. This supports an immunomodulatory function of Mdk/Ptn signaling through mediating the expression of cytokines and chemokines.

Mdk, but not Ptn, is expressed by human peripheral blood lymphocytes from healthy donors, and the expression of Mdk is transiently and robustly increased in T cells in response to CD28 activation, IL-2, IFNγ, or phytohemagglutinin (PHA) [28]. Mdk appears to bind and interact with NCL on the surface of T lymphocytes [45]. Furthermore, Mdk co-localizes with NCL on the cell surface and in nucleoli of PHA-stimulated T cells, suggesting that NCL may be responsible for the internalization and nuclear-localization of Mdk. Mdk binds to the C-terminal RGG domain of NCL,

and this interaction is proteoglycan-independent [45]. The binding of Mdk to NCL on T cells interferes with human immunodeficiency virus-1 (HIV-1) binding and subsequent infection, similar to the NCL-binding peptide, HB-19 [28,45]. Mdk interference with the HIV-1 infection of T cells requires the presence of extracellular Mdk prior to HIV-1 exposure, suggesting that Mdk/NCL binding is the primary mechanism in which Mdk antagonizes HIV-1 infection. Additionally, $CD4^{neg}$ Mdk-producing cells can protect $CD4^{+}$ non-Mdk producing cells from HIV-1 infection, demonstrating that the function of Mdk in blocking HIV-1 infection can be mediated in a paracrine fashion [28]. NCL-binding and HIV-blocking activities have also been validated for Ptn [46]. NCL-dependent cell surface binding of Ptn was inhibited in the presence of excess HB-19 or Mdk, suggesting that Ptn and Mdk recognize the same region on NCL [46].

In PBMCs, Ptn is mitogenic and induces the expression of IL-6, TNFα, and IL-1β [40]. The increase in these cytokines via Ptn, however, promotes HIV-1 replication in PBMCs infected in vitro or AIDS patient-derived PBMCs, an effect potentiated by IL-2 [41]. When lymphocytes (B and T cells) and monocytes were treated separately, the induction of proinflammatory cytokine production by Ptn was greatly reduced and no virus replication occurred [41]. This suggests that Ptn's capacity to modulate proinflammatory cytokine expression works via an undefined mechanism in a heterogenous population of immune cells that may be mediated, in part, by NCL.

Mdk promotes B-cell survival in vitro and in vivo [47]. This is mediated through Ptprz1, as B cells isolated from *Ptprz1*-null mice fail to respond to Mdk. *Ptprz1*-null B cells also fail to respond to macrophage migration inhibitory factor or hepatocyte growth factor, which may induce B cell survival through induction of Mdk expression [47]. Furthermore, *Ptprz1*-null mice have reduced mature B cells in the bone marrow, spleen, and lymph nodes, indicating an in vivo function of Mdk/Ptprz1 signaling in lymphoid tissue B cell survival. Given Ptn's ability to promote cell survival upon Ptprz1-ligation in other cell types [18], it may also support B cell survival, underlying the importance of observing Mdk/Ptn biology concomitantly.

Expression of Mdk/Ptn Family in Tissue Damage and Inflammatory Diseases

Mdk and Ptn expression are elevated after injury in many tissues, including brain [48,49], blood vessels [50], heart [51,52] and kidney [44]. Additionally, Ptn expression is increased in bone marrow endothelial cells in mice exposed to total-body irradiation [53]. In a study of the toxicity of depleted uranium on peritoneal macrophages, Mdk was identified as a responsive gene [54]. Furthermore, Ptn is increased in response to hydrogen peroxide [55] and the expression of Mdk and Ptn are increased after exposure to ethanol in vitro and in vivo [56,57]. These data support the Mdk/Ptn family as being effectors of oxidative stress.

The expression of Mdk/Ptn is also stimulated by hypoxia. Human umbilical vein endothelial cells (HUVECs), monocytes, and PMNs show increased Mdk

expression under hypoxic conditions [58]. In PMNs, this effect could be reproduced using cobalt chloride, indicating that Mdk is an hypoxia inducible factor 1 alpha (HIF1α)-responsive gene [58]. Indeed, HIF1α directly drives Mdk expression via a hypoxia-responsive element in the Mdk promoter [59]. Ptn expression is also elevated in response to hypoxia. For example, Ptn expression is increased in hepatic stellate cells and cardiomyocytes in response to hypoxia in vitro, and Ptn secretion is elevated by endothelial cells and macrophages in response to acute ischemic brain injury [49]. However, unlike Mdk, it is unknown whether Ptn itself is a HIF1α-responsive gene.

One function of Mdk/Ptn that is widely covered in the context of tissue damage is angiogenesis. In a model of hindlimb ischemia, *Mdk*-null mice exhibited impaired angiogenesis [58]. Ptn, which is often cited as a pro-angiogenic factor, is only weekly mitogenic for endothelial cells in vitro [60]. However, in a rat model of myocardial ischemia, Ptn promoted the development of functional blood vessels [61]. Furthermore, there are multiple reports of Ptn promoting tumor angiogenesis, although in some cases it may be angiostatic (for review, see Papadimitriou et al., [10]). It is clear that Mdk and Ptn are not required for developmental angiogenesis as there are no apparent vascular abnormalities in *Mdk*- or *Ptn*-null mice [10], suggesting that the pro-angiogenic activity of Mdk/Ptn is not central to their function in tissue homeostasis.

Mdk and Ptn are expressed in inflammatory conditions, including atherosclerosis [23], experimental autoimmune encephalitis [62,63], rheumatoid arthritis [25,64,65], and in models of ischemia-reperfusion injury [44,49]. Preclinical models of these pathological indications have yielded insight into the function of Mdk/Ptn in the immune system.

Mdk suppresses tolerogenic DC development through induction of IL-12 and SHP-2 by regulatory DCs (DCregs), but not conventional DCs. Further, Mdk reduces Stat3 activation in these cells in a SHP-2-dependent fashion. In a murine model of experimental autoimmune encephalitis (EAE), $CD4^+$ and $CD8^+$ T cells, as well as CD11b+ cells, express Mdk. In vitro, T cells activated with CD3 + CD28 mAbs express Mdk, and among T-cell subsets, Mdk is upregulated in Th1 cells. *Mdk*-null mice had superior clinical scores, explained by an increase in DCregs and regulatory T cells [66]. However, the receptor imparting these effects was unidentified.

Mice null for the Mdk/Ptn receptor, Sdc4, were also studied in a murine model of EAE. Inverse to the *Mdk*-null mice, *Sdc4*-null mice had worse disease [67]. The mechanism explaining the phenotype also arrived at myeloid/T-cell interactions. Binding of the DC receptor, DC-HIL, to Sdc4 on activated T cells reduces T-cell activation. When this interaction is perturbed, either by targeting DC-HIL on myeloid cells or Sdc4 on T cells, there is an increase in T cell activation and EAE is exacerbated [67]. Furthermore, the suppressive effect of Sdc4 on T cell activation was demonstrated by direct ligation [68]. Given the opposing effects of Mdk and DC-

HIL/Sdc4 perturbation in this model, it raises the question of the functional consequences of Mdk binding to Sdc4 on T cells. If Mdk competes with DC-HIL for binding Sdc4, and does not impair T-cell activation when bound, it may function to potentiate T-cell activation by disrupting DC-HIL/Sdc4 interaction, thus leading to worse disease. This would implicate a function of Mdk in immune checkpoint disruption, although more research is necessary to validate this.

Ptn is expressed highly in the lymph nodes of MRL-*lpr/lpr* mice, which is a model of Th1-type autoimmune disease [24]. In this model, there is lymphoaccumulation of double-negative T cells. The administration of high-molecular weight hyaluronan, which antagonizes Tlr4 activation and perturbs lipopolysaccharide-mediated lethality [69], greatly reduces the enlargement of submandibular lymph nodes, correlating with decreased Ptn expression. Treating double-negative T cells isolated from this model with Ptn attenuates apoptosis, suggesting that the presence of Ptn in lymph nodes may support the accumulation of double-negative T cells, outlining a possible role for Ptn in T cell survival. If surface NCL promotes double-negative T-cell survival as it does in other cell types, then Ptn/NCL may promote survival in this context based on the following observations: 1) The HB-19 peptide, which prevents Ptn/NCL binding, decreases the proliferation and migration of HUVECs in vitro in an NCL-dependent manner [70], 2) In the chick embyro chorioallantoic membrane (CAM) assay, Ptn is endogenously expressed and promotes angiogenesis mediated by NCL [71], 3) HB-19 reduces angiogenesis in

the CAM assay [72], 4) As stated above, the Mdk/Ptn family adheres to T cells, at least in part, through surface NCL, which is blocked by HB-19 [45,46]. Certainly more research is required to support this hypothesis.

Mdk/Ptn Family Receptors

Robust heparin-binding was one of the first characteristics identified in the Mdk/Ptn family [6,73]; thus, it comes as no surprise that the first receptors identified for Mdk/Ptn were heparin- and chondroitin-sulfate proteoglycans. Mdk and Ptn bind cell surface proteoglycans, including syndecans 1-4 (Sdc 1-4) and receptor protein tyrosine phosphatase beta (Ptprz1), with similar affinities. Sdc1 is primarily expressed on epithelial and malignant plasma cells, Sdc2 by fibroblasts and endothelial cells, Sdc3 is found almost exclusively in the central nervous system, while Sdc4 is expressed more widely [74]. However, like Mdk and Ptn, the expression of the syndecans is also modulated by tissue damage and inflammation [75-78]. In immune cells, the syndecans are mediators of migration, activation, and cell survival [76,78-92] (see Table 1) and are expressed broadly. The only well-characterized Mdk/Ptn/Sdc interaction is between Ptn and Sdc3. Ligation of Sdc3 by Ptn promotes neurite outgrowth and cell migration [93,94] (Figure 1). However, the biological contexts and consequences for specific Mdk/Ptn/Sdc interactions are largely unknown.

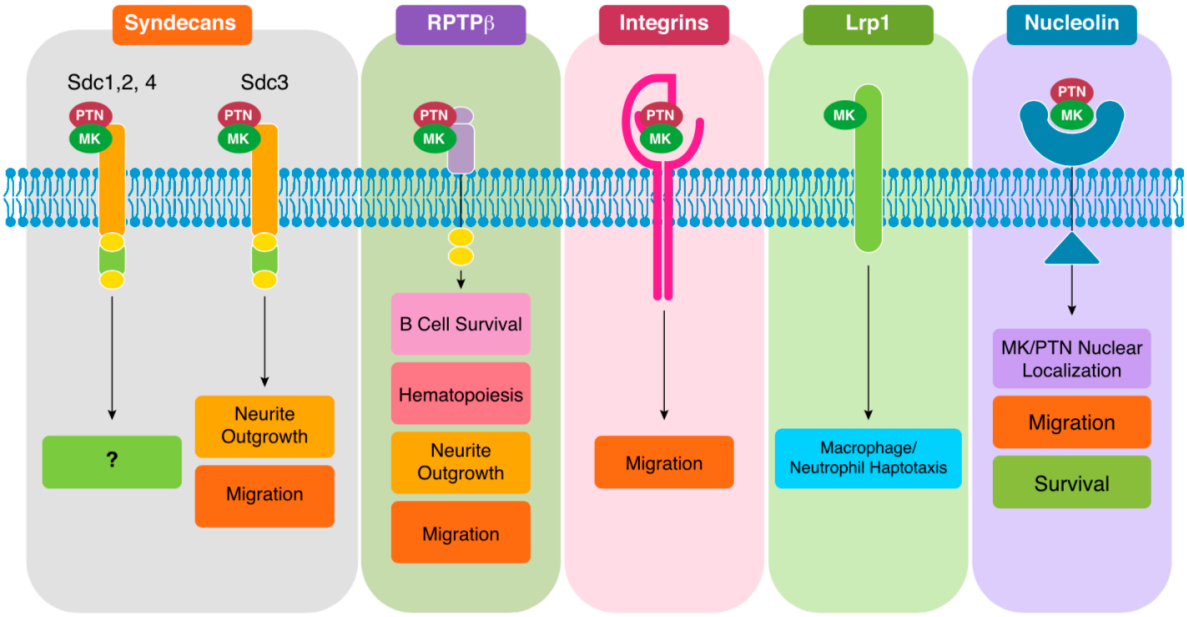

Figure 1.1. Known functions of Mdk/Ptn signaling through their receptors. Syndecans: Although Mdk/Ptn bind to Sdc 1, 2, and 4, the downstream effectors are unknown. Ptn binding to Sdc3 promotes neurite outgrowth and migration [93,94]. **RPTPβ (Ptprz1)**: Mdk/Ptn binding to RPTPβ promotes B cell survival, hematopoiesis, neutrite outgrowth, and migration [47,95]. **Integrins**: Mdk can directly interact with α4β1 and α6β1 integrins [96], while Ptn interacts with αvβ3 [97]; these interactions promote cell migration [96-98]. **Lrp1**: Mdk interacts with α4β1 and α6β1 while Ptn interacts with αvβ3. Lrp1 drives macrophage/neutrophil haptotaxis [99]. **Nucleolin**: Mdk/Ptn interaction with nucleolin promotes Mdk/Ptn nuclear localization, cell migration, and survival [71,98,100].

Mdk/Ptn/Ptprz1 interactions are characterized as driving neurite outgrowth and cell survival [18,95] (Figure 1); an effect mediated by activation of Anaplastic Lymphoma Kinase (ALK), which is a substrate of Ptprz1. Ligation of Ptprz1 by Ptn prevents Ptprz1 from dephosphorylating ALK, thus permitting ALK activity [101]. Ptprz1 was originally thought to be restricted to the central nervous system; however, it was recently identified on B cells and hematopoietic stem cells, where it functions to

promote cell survival [16,47], although ALK expression by B cells remains unreported. Whether Ptn or Mdk directly ligate ALK is disputed in the literature[102,103], but recent evidence demonstrates that FAM-150A/B are bona fide ligands for ALK[104-107]. Regardless, it is clear that, at least in the presence of Ptprz1, Mdk/Ptn and ALK biology are intertwined[17,101].

Non-proteoglycan receptors are also reported to interact with Mdk and Ptn. Mdk can directly interact with α4β1 and α6β1 integrins [96], while Ptn interacts with αvβ3 [97] (Figure 1). On immune cells, α6β1, α4β1 and αvβ3 mediate cell migration and adhesion, and α4β1 is also implicated in B and T cell development [108-113]. Direct Mdk/Ptn/integrin interactions promoting cell migration are implicated in multiple cell types, suggesting that these interactions perform a similar function on immune cells [96-98].

Mdk has also been identified as a high-affinity ligand for low-density lipoprotein receptor-related protein 1 (Lrp1) [114]. Lrp1 is thought to attenuate proinflammatory macrophage activation [115]. Mdk/Lrp1 signaling also promotes cell survival and may stimulate polymorphonuclear cell (PMN) haptotaxis [58,114,116]. Mdk and Ptn also bind to nucleolin (NCL), albeit with significantly lower affinity relative to other cell surface receptors [45,46,117]. NCL is ubiquitously expressed and may be involved in recognition of early apoptotic cells by macrophages [118]. The interaction between NCL and Mdk/Ptn promotes nuclear localization, endothelial cell migration, and cell survival [71,98,100] (Figure 1).

Table 1.1 Expression and reported functions of Mdk/Ptn receptors on immune cells

Receptor	Immune cell expression pattern	Comments
Syndecan-1	Expressed by immature DCs, pre-B cells, plasma cells, and thioglycollate-elicited peritoneal macrophages[79,80,85]	Promotes macrophage migration; expressed on macrophages in myocardial infarction[81,91]
		Sdc1-null mice are more susceptible to LPS-driven lethality[88]
Syndecan-2	Monocytes and macrophages, DCs, activated T cells[76,84,85,87,90]	Expression induced by LPS, IL-1a, or TNF-a on macrophages[76]
		Found on synovial fluid macrophages from rheumatoid arthritis patients[76]
		Delayed expression on activated T cells[87]
Syndecan-3	Peritoneal and splenic macrophages. May also be expressed by monocytes and DCs at low levels[85,89]	Sdc3-null mice have reduced leukocyte infiltration in a preclinical model of rheumatoid arthritis[91]
Syndecan-4	Expressed on DCs, monocytes, and macrophages[83-85]	Down-regulated on B cells undergoing isotype switching[82]
	Expressed by pre-B cells and most splenic macrophages[82]	Sdc4-null mice are more susceptible to LPS-mediated lethality[78]
	Rapidly induced on activated T cells[87,90]	Binding to DC-HIL at the immunologic synapse perturbs T cell activation[86]
	Expressed on a small subset (~10%) of splenic T cells[82]	Neutrophil migration[83]
		May regulate T cell proliferation[87]
Ptprz1	Found on HSCs and B cells[16,47]	Promotes HSC maintenance and B cell survival[16,47]
Lrp1	Macrophages, neutrophils[63,115]	Promotes PMN adhesion[63]
		Attenuates proinflammatory macrophage activation[115]
Nucleolin	Ubiquitously expressed[117]	May be involved in macrophage recognition of early apoptotic cells[118]
α4β1	T cells, B cells, DCs, monocytes, macrophages,	Implicated in migration; involved in B

	NK cells, neutrophils, eosinophils, basophils[111,113]	and T cell[108]
α6β1	Lymphocytes, monocytes and macrophages, granulocytes, neutrophils, eosinophils[112]	Adhesion and migration[112]
αvβ3	Monocytes, macrophages, DCs, neutrophils[110]	Implicated in migration and phagocytosis[109,110]
αMβ2 (Mac-1; CD11b/CD18)	Monocytes, granulocytes, macrophages, and NK cells[119,120]	Implicated in adhesion, migration, and cellular activation[121,122]

Listed are the purported receptors of the Mdk/Ptn family, the expression of those receptors on immune cells, and comments about the known functions of those receptors in immunity.

Understanding Mdk/Ptn signaling through their respective receptors is hampered by the fact that Mdk/Ptn interact with numerous cell surface proteins and their putative receptors also interact with a variety of other ligands. Thus, elucidating the functional contribution of Mdk/Ptn signaling requires knowledge of potential receptor expression. Table 1 provides a summary of Mdk/Ptn receptor expression and putative function on immune cells.

Mdk/Ptn Function in Myeloid Adhesion and Chemotaxis

Evidence from multiple models of inflammation implicates Mdk as a key factor in inflammatory cell infiltration. In preclinical models of kidney ischemia/reperfusion injury, rheumatoid arthritis [123], atherosclerosis [124,125], and EAE [126], Mdk-deficient mice exhibit significantly less tissue damage, which is associated with a reduction in leukocyte infiltration [127-129]. Specifically, in models of rheumatoid arthritis [123], kidney inflammation [44,128,129], and atherosclerosis [124], Mdk deficiency was associated with reduced neutrophil and macrophage recruitment at the site of injury. Takada et al. [64]

demonstrated that Mdk possesses chemotactic activity towards neutrophils in vitro [130]. Sato et al. [44] postulated that the reduced neutrophil and macrophage infiltration in *Mdk*-null mice in the ischemic renal injury model was due to a concomitant decrease in the chemokines MIP-2 and MCP-1. However, in a cisplatin-induced renal injury model, neutrophil recruitment was reduced in *Mdk*-null mice, but no change in a panel of chemokines was observed [128]. In the latter model, macrophage infiltration was not significantly decreased and no change in MCP-1 was observed, suggesting that the stimulus for inflammation or injury may impact the expression and subsequent contribution of Mdk to immune cell infiltration. Perhaps the fate of Mdk activity rests on the expression of Mdk receptors, which may be impacted differentially based on the nature of the stimulus.

Recently, Weckbach et al. [99] gained insight into how Mdk may mediate neutrophil infiltration in vivo, independent of its ability to induce the expression of other chemokines [99]. Weckbach et al. [99] observed that Mdk deficiency reduced leukocyte adhesion to cremaster muscle venules upon TNFα stimulation, while the number and velocity of rolling leukocytes was unaffected. In a hindlimb ischemia model, Mdk deficiency reduced PMN extravasation into inflamed tissue, which could be rescued by the introduction of exogenous Mdk. In an in vitro static adhesion assay, immobilized Mdk promoted PMN adhesion, while soluble Mdk had no effect. This corroborated the results from Takada et al. [64], which demonstrated that immobilized, not soluble, Mdk has chemotactic activity towards neutrophils [130].

Weckback et al. [99] observed that CD18 was not required for Mdk binding to PMN cells but is required for Mdk-mediated PMN adhesion. Lastly, Weckback et al. [99] demonstrated that Lrp1 is required for binding and activity of Mdk in PMN cells, suggesting that signaling downstream of this receptor promotes a high-affinity conformation of CD18. Indeed, using an antibody that recognizes the high-affinity conformation of CD18 (mAb24), it was demonstrated that PMNs bound to immobilized Mdk possessed increased high-affinity CD18. This increase was perturbed by using an inhibitor of Lrp1 [99].

Ptn may also have a direct on immune cell adhesion and recruitment. Similar to midkine, immobilized Ptn, not soluble, promotes migration of myeloid cells, suggesting that Ptn is a haptotactic factor[121]. Ptn haptotaxis may be mediated through Ptn/Mac-1 (CD11b/CD18) interaction on myeloid cells. This was demonstrated by the fact that Ptn-induced haptotaxis was markedly reduced in *Mac1*-null macrophages, relative to wild-type. Further, Shen et al. demonstrated that Ptn can directly interact with Mac-1.

The Expression and Impact of Ptn and Mdk Family in Cancer

The Mdk/Ptn family is highly expressed in multiple human cancers, including breast, pancreas, lung, and hematopoietic malignancies (for review, see [10]).

In 1992, Ptn was identified as a secreted growth factor produced by the human breast cancer cell line, MDA-MB-231[131].

Knowledge from preclinical models of cancer have yielded insight into the processes in which the Mdk/Ptn family participate. Mdk/Ptn are implicated in tumor angiogenesis, as proliferative drivers and factors in the resistance to apoptosis. For example, MCF7 cancer cells stably transfected to express high levels of Ptn grow robustly after in vivo injection in comparison to control transfected or untransfected MCF7 cells. This effect is mediated by Ptn-driven extracellular matrix remodeling, increased angiogenesis, and stimulation of stromal cells in the tumor microenvironment [132]. Further, MMTV-PyMT transgenic mice engineered to overexpress Ptn (MMTV-PyMT-Ptn) display more rapid development of scirrhous carcinoma type-breast cancer foci; scirrhous carcinoma is characterized by increased desmoplasia and it positively correlates clinically with increased lymph node metastasis [133] (although this was not assessed in MMTV-PyMT mice). MMTV-PyMT-Ptn tumors also exhibit increased extracellular matrix deposition and angiogenesis [132]. Similarly, in the SW-13 adrenal carcinoma line, the ectopic expression of Ptn greatly increased tumor growth and angiogenesis in vivo [134]. These data support a function of Ptn in tumor progression that centers on stromal cell activity, which may include tumor-associated myeloid cells as effectors of Ptn.

Mdk also drives tumor growth [135]. In the Lewis lung carcinoma model, *Mdk*-null mice had significantly reduced pulmonary metastasis [136]. Given Mdk's function in PMN recruitment (discussed below) and the ability of myeloid-derived suppressor

cells (MDSCs) to support metastasis, it would be interesting to see if PMN-MDSC numbers are reduced in Lewis lung tumors in *Mdk*-null mice.

The effect of the Mdk/Ptn family on angiogenesis is thought to be through the promotion of endothelial cell proliferation and tube formation [10]. However, there are conflicting reports about the angiogenic capacity of Mdk/Ptn on primary endothelial cells in vitro, particularly in the context of how Mdk/Ptn affect the activity of the principal angiogenic growth factor, VEGF-A [10,33,58,137]. Concomitant with the absence of vascular anomalies in *Ptn*-null embryos [7], this suggests that the mechanisms behind Ptn-mediated tumor angiogenesis may, in part, be due to its effects on other cell types in the tumor microenvironment. In fact, the effects of Ptn on tumor angiogenesis may be mediated by its effects on myeloid cells.

SPECIFIC AIMS OF DISSERTATION RESEARCH

To determine the relevance and function of Ptn in breast cancer, I developed the following specific aims:

1. Assess the expression and functional impact of Ptn on breast cancer cells
2. Determine the impact of Ptn-inhibition or genetic knockout in preclinical models of breast cancer

CHAPTER TWO

Pleiotrophin Promotes Metastasis in Prelinical Models of Breast Cancer

Introduction

One of the earliest papers on Ptn (1992) identified it as a factor produced and secreted by the MDA-MB-231 breast cancer cell line[131]. Naturally, this raised the question of its general expression and functional relevance in breast cancer. From 1992 to 2008, there were four papers that studied the functional relevance of Ptn in breast cancer. Two of the studies assessed the impact of truncated forms of Ptn on xenograft models of breast cancer. The truncated forms of Ptn reduced MDA-MB-231 tumor growth in vivo. The limitation of these studies is that it is uncertain what off-target effects overexpression of truncated Ptn may have, particularly because Ptn shares receptors with a plethora of other heparin-binding cytokines.

Both Choudhuri et al. (1997) and Chang et al. (2007) transfected MCF-7 cells to overexpress Ptn and observed that this increased MCF-7 xenograft growth in vivo. Chang et al. also compared tumor progression in wild-type MMTV-PyMT mice relative to MMTV-PyMT mice overexpressing Ptn. They did not observe a change in tumor growth or metastasis.

The expression and impact of Ptn in breast primary tumors remains controversial[138]. Some have reported high levels of Ptn in primary tumors while others have not[138,139]. What does appear consistent, however, is the elevation of Ptn levels in patient serum[139]. Further, there are multiple reports of upregulated Ptn

expression at metastatic sites in breast cancer patients, including lung[140], bone[140,141], and brain[141].

Curiously, there have been no additional published studies on the functional significance of Ptn in breast cancer since 2008. Given the limitation the prior studies, the question of Ptn's functional impact in breast cancer remains unanswered.

Using specific pharmacologic and genetic methods, I demonstrate that Ptn specifically promotes metastasis in preclinical models of breast cancer. To my knowledge, this is the first report of this activity in breast cancer, and the most convincing evidence for the function of Ptn in promoting metastasis in cancer. Based on my data, I hypothesize that this activity is through the unreported ability of Ptn to promote immune cell trafficking in vivo.

Using genetic and pharmacologic methods, we discovered that Ptn promotes pulmonary metastasis in multiple preclinical models of breast cancer. In vivo, Ptn inhibition results in reduces neutrophil recruitment at both the primary and metastatic sites. Further, this is correlated with a reduction in the neutrophil chemokine, CXCL5. As neutrophils have been recently implicated in promoting breast cancer metastasis[142], my data implicate Ptn as an upstream factor mediating this biology. Additionally, I also found that Ptn inhibition reduced macrophage recruitment to metastatic lesions in the lung.

Results

Ptn is upregulated in preclinical models of breast cancer

First, I tested if mouse breast cancer cell lines express Ptn in vitro. Using reverse transcriptase PCR, Ptn expression was undetectable (**Figure 2.1A**). Interestingly, I discovered that Ptn protein was readily detectable in mouse breast tumors and it is highly upregulated compared to healthy tissue (**Figure 2.1B-C**). Although expression cannot be detected in vitro, tumors formed from the breast cancer cell lines tested in Figure 2.1A are promoting Ptn expression in vivo.

Ptn inhibition reduces pulmonary metastasis, but not primary tumor growth, in preclinical models of breast cancer

Using the Ptn-blocking monoclonal antibody, 3B10, I next tested the impact of Ptn-inhibition on the 4T1, E0771, and MMTV-PyMT preclinical models of breast cancer. Ptn-inhibition did not impact growth of these breast cancer cell lines in vitro (**Figure 2.2A-C**). Although these cell lines do not express Ptn, it is readily detectable in fetal bovine serum used in the experimental condition (data not shown). In vivo, Ptn inhibition did not impact primary tumor growth in these models (**Figure 2.2D-F**). These results suggest that Ptn is not a direct growth promoting factor for breast cancer cells.

Conversely, I observed that anti-Ptn therapy significantly reduced pulmonary metastasis in the 4T1, E0771-LG, and MMTV-PyMT models of breast cancer (**Figure 2.3**). To rule out that the phenotype may be due to off-target effects of the antibody, I repeated the E0771-LG and MMTV-PyMT experiments in *Ptn*-null mice. *Ptn*-null mice are viable and exhibit no obvious developmental defects[7]. Similar to

A

Cell Line	Cancer	PTN (Cq)	Actin (Cq)
Met-1	Breast	ND	18.5
E0771	Breast	ND	17.0
4T1	Breast	ND	19.1
LLC	Lung	23	19.5

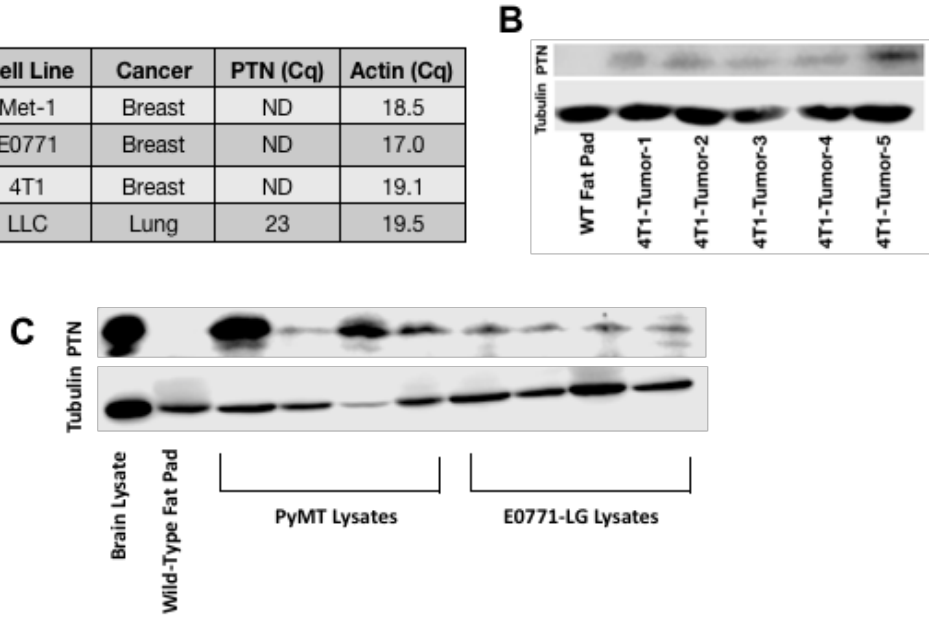

Figure 2.1: **Characterization of Ptn expression and the impact of Ptn-inhibition on primary tumor growth in preclinical models of breast cancer**. A) Mouse breast cancer cell lines were evaluated for *Ptn* expression by rt-PCR. LLC cells were used as a positive control. B) Western blot of Ptn and tubulin in wild-type fat pad or 4T1 tumors from BALB/C mice. C) Western blot of Ptn and tubulin in mouse brain (positive control), wild-type fat pad, or from PyMT or E0771-LG tumors.

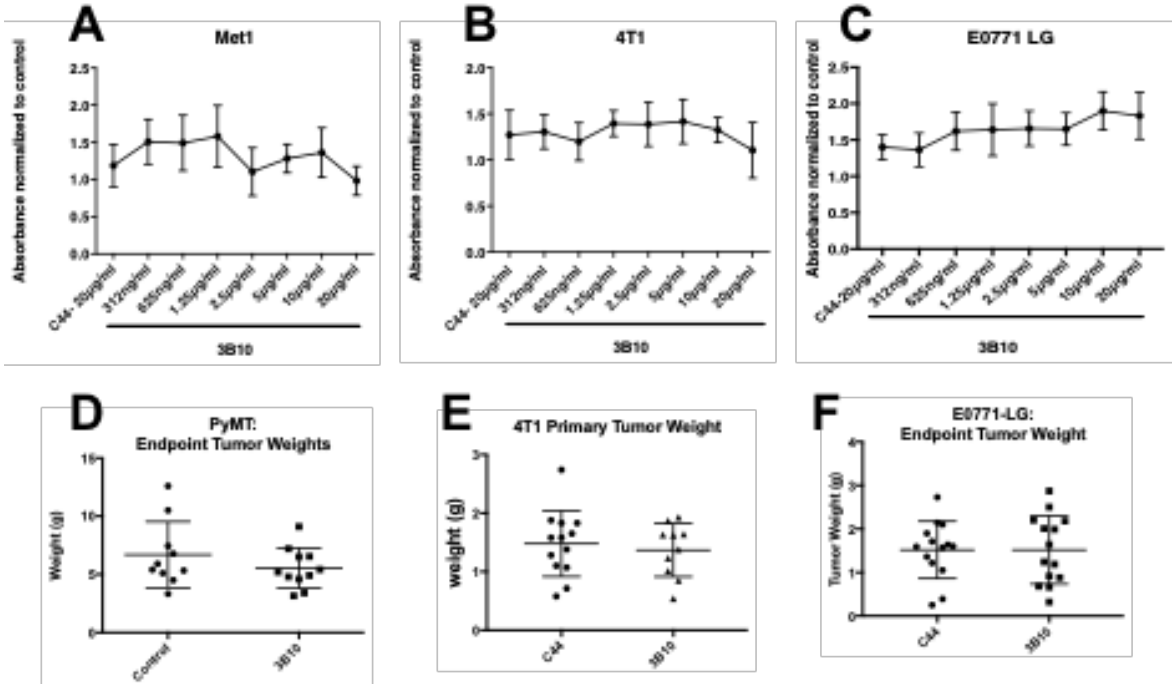

Figure 2.2: **Ptn-inhibition does not impact mouse breast cancer cell growth or primary tumor growth in preclinical models of breast cancer**. A) Mouse breast cancer cell lines were evaluated for *Ptn* expression by rt-PCR. LLC cells were used as a positive control. B) Western blot of Ptn and tubulin in wild-type fat pad or 4T1 tumors from BALB/C mice. D-F) Mice bearing MMTV-PyMT, 4T1, or E0771-LG tumors were treated twice weekly with control (C44) or anti-Ptn (3B10) antibodies. When the average control group tumor size reached 1500 cubic millimeters, mice were euthanized and tissues were collected, weighed, and stored for further analysis.

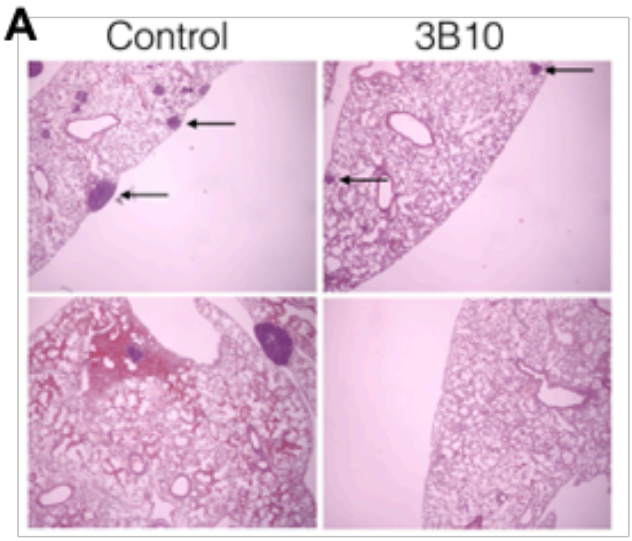
A
Control
3B10

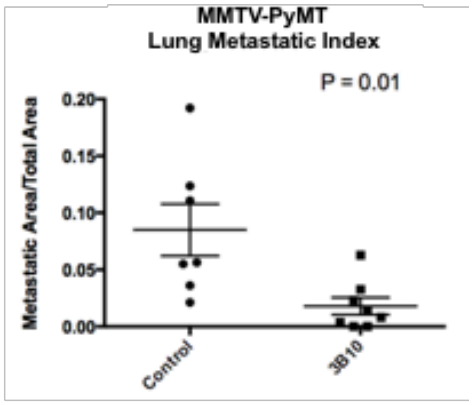
B
MMTV-PyMT
Lung Metastatic Index
P = 0.01
Metastatic Area/Total Area
0.20
0.15
0.10
0.05
0.00
Control
3B10

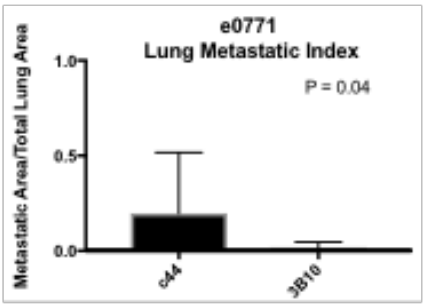
C
e0771
Lung Metastatic Index
P = 0.04
Metastatic Area/Total Lung Area
1.0
0.5
0.0
c44
3B10

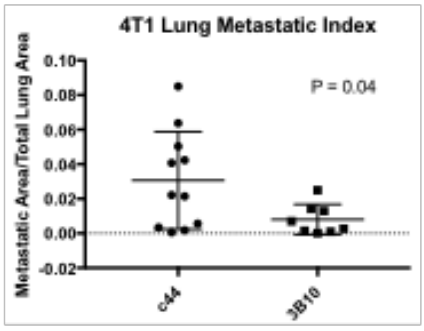
D
4T1 Lung Metastatic Index
P = 0.04
Metastatic Area/Total Lung Area
0.10
0.08
0.06
0.04
0.02
0.00
-0.02
c44
3B10

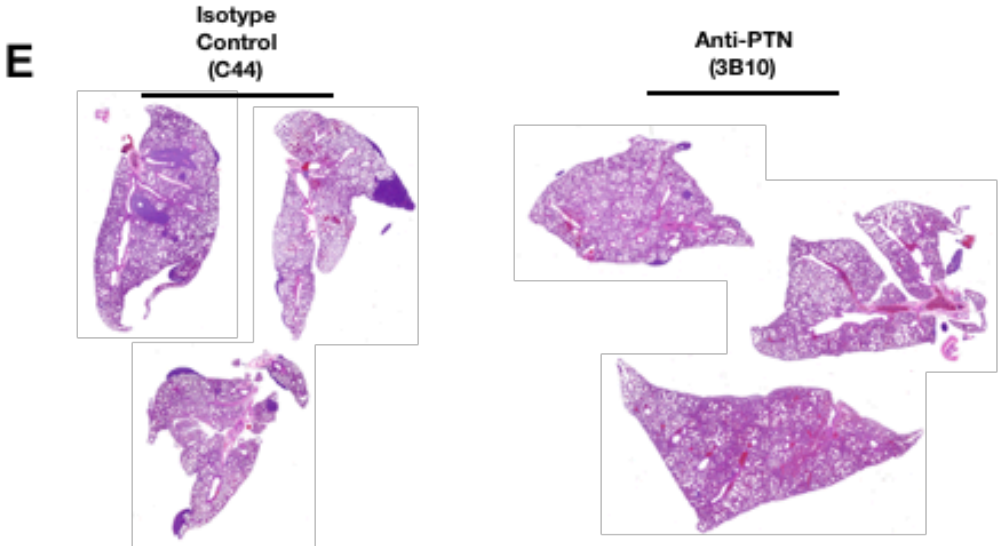
E
Isotype
Control
(C44)
Anti-PTN
(3B10)

Figure 2.3: **Ptn inhibition reduces pulmonary metastasis in preclinical models of breast cancer**. Mice bearing MMTV-PyMT, 4T1, or E0771-LG tumors were treated twice weekly with control (C44) or anti-Ptn (3B10) antibodies. When the average control group tumor size reached 1500 cubic millimeters, mice were euthanized and tissues were collected, weighed, and stored for further analysis. A) H&E of lungs from C44- or 3B10-treated mice. Arrows depict examples of metastatic lesions. B-D) Quantitation of the metastatic index was performed by dividing the metastatic area over the total lung area. Each point represents an individual mouse. E) Macroscopic H&Es of lungs from C44- or 3B10-treated mice. Statistics were performed in GraphPad Prism using the unpaired T Test. P values are annotated on each graph.

3B10, pulmonary metastasis was reduced in *Ptn*-null mice relative to control (**Figure 2.4**). Additionally, 3B10 only reduced metastatic burden significantly relative to control in wild-type, but not *Ptn*-null mice (**Figure 2.4B-D**). This validates that 3B10's activity is on-target and provides further support for the hypothesis that Ptn is a pro-metastatic factor in preclinical models of breast cancer.

Ptn does not impact angiogenesis, epithelial-to-mesenchymal transition, proliferative or apoptotic cell marker expression

In order to gain insight into how Ptn-inhibition or genetic deletion impacts tumor biology, I characterized control- and 3B10-treated tumors using histological and immunohistochemical methods. First off, H&E staining did not reveal any overt histologic impact of Ptn-inhibition (**Figure 2.5**). Next, I evaluated epithelial-to-mesenchymal transition (EMT). EMT is a phenotype in some cancers believed to promote metastasis[143]. Ptn may promote EMT in some cancers, such as prostate cancer[144]. I did not observer any changes in EMT markers in 3B10-treated mice compared to control (**Figure 2.6a**). This is corroborated by the H&E staining in which

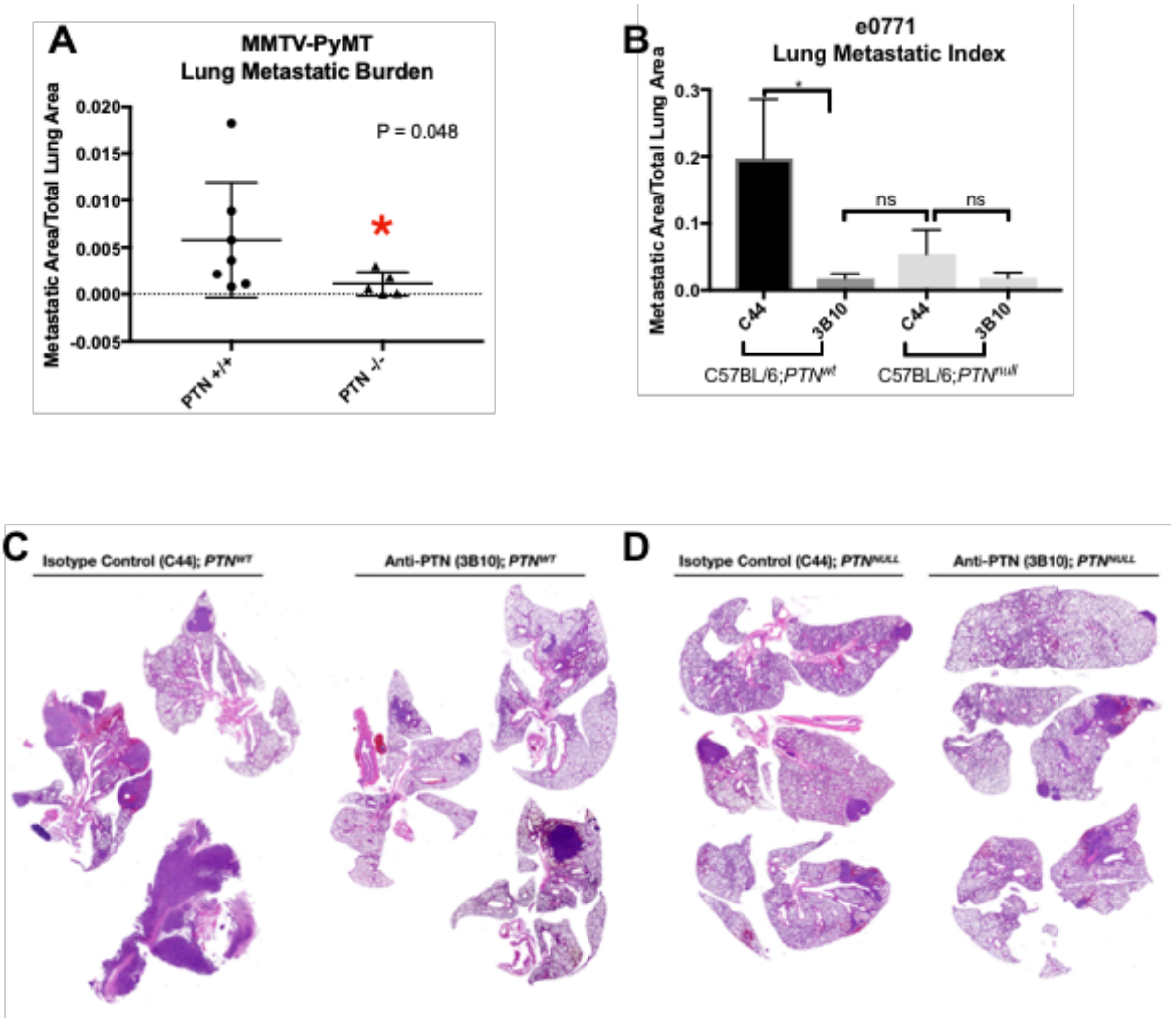

Figure 2.4: **Genetic deletion of Ptn recapitulates the anti-metastic effect of Ptn-inhibition in preclinical models of breast cancer**. A) MMTV-PyMT;$PTN^{+/+}$ and MMTV-PyMT;$PTN^{-/-}$ mice were sacked at 12 weeks of age and tissues were collected for further analysis. Metastatic index was performed by analyzing lung H&E sections from these mice. B-D) E0771-LG cells were injected into C57BL/6;PTNwt or C57BL/6;PTNwt mice. Once tumors reached 50 mm^3, mice were divided into treatment groups and treated twice weekly with control (C44) or anti-Ptn (3B10) antibodies. Mice were euthanized and tissue was collected for analysis once tumor burden in the control group reached an average of 1500 mm^3. B) Quantitation of the lung metastatic index in E0771-LG tumor-bearing mice. C-D) H&Es of representative lungs from the E0771-LG experiment. Statistics were performed using the unpaired T test. *, $p<0.05$.

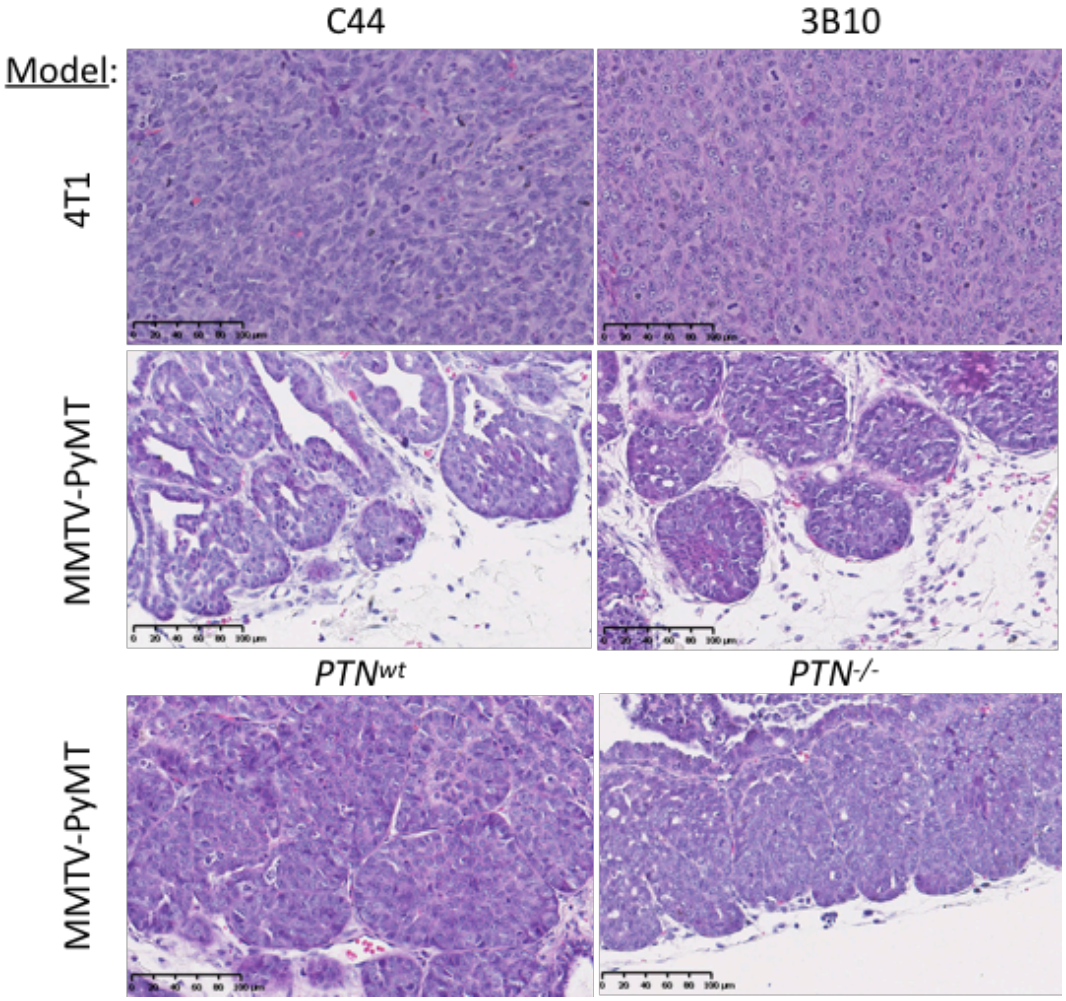

Figure 2.5: **PTN-inhibition or genetic knockout does not significantly impact primary tumor histology in preclinical models of breast cancer**. H&Es were performed on primary tumors collected from mice bearing 4T1 or MMTV-PyMT tumors.

morphological changes of the cancer cells, which are expected with EMT, were not observed (**Figure 2.5**).

Because Ptn is also implicated in angiogenesis[10,60,134], I stained the tissue for blood vessel markers(**Figure 2.6b-c**). 3B10 did not reduce tumor angiogenesis in any models tested. This is corroborated by the fact that 3B10 did not impact primary

tumor growth, given that tumor growth in these models is sensitive to inhibitors of angiogenesis.

To test the hypothesis that Ptn may be promoting the survival or proliferation of breast cancer cells at the metastatic site, I evaluated marker expression of apoptosis (cleaved caspace 3) and proliferation (Ki67) on pulmonary metastatic lesions. No changes in these markers were observed when Ptn was inhibited or genetically deleted (**Figure 2.7**).

Ptn inhibition reduces neutrophil recruitment and macrophage/metastatic lesion clustering

Thus far, my data suggested that the impact of Ptn in vivo could not be explained by its direct impact on breast cancer cells. Next, I looked for changes in the tumor stroma, starting with immune cell infiltration, given that immune cells can take part in the promotion or inhibition of metastatic growth.

First, I observed that there was a trend towards decreased myeloid lineage cells at the metastatic site in 3B10-treated mice (**Figure 2.8A-B**). Among myeloid lineage cells, I observed that there was a trend towards decreased macrophages.

Although the change in total macrophages wasn't statistically significant, I observed reduced macrophage clustering at metastatic lesions in the lung (**Figure 2.8C-D**). This was true across metastatic lesions of similar size.

Knowing that neutrophils are another possible myeloid cell that could be mediating metastatic changes in preclinical models of breast cancer[142], I assessed

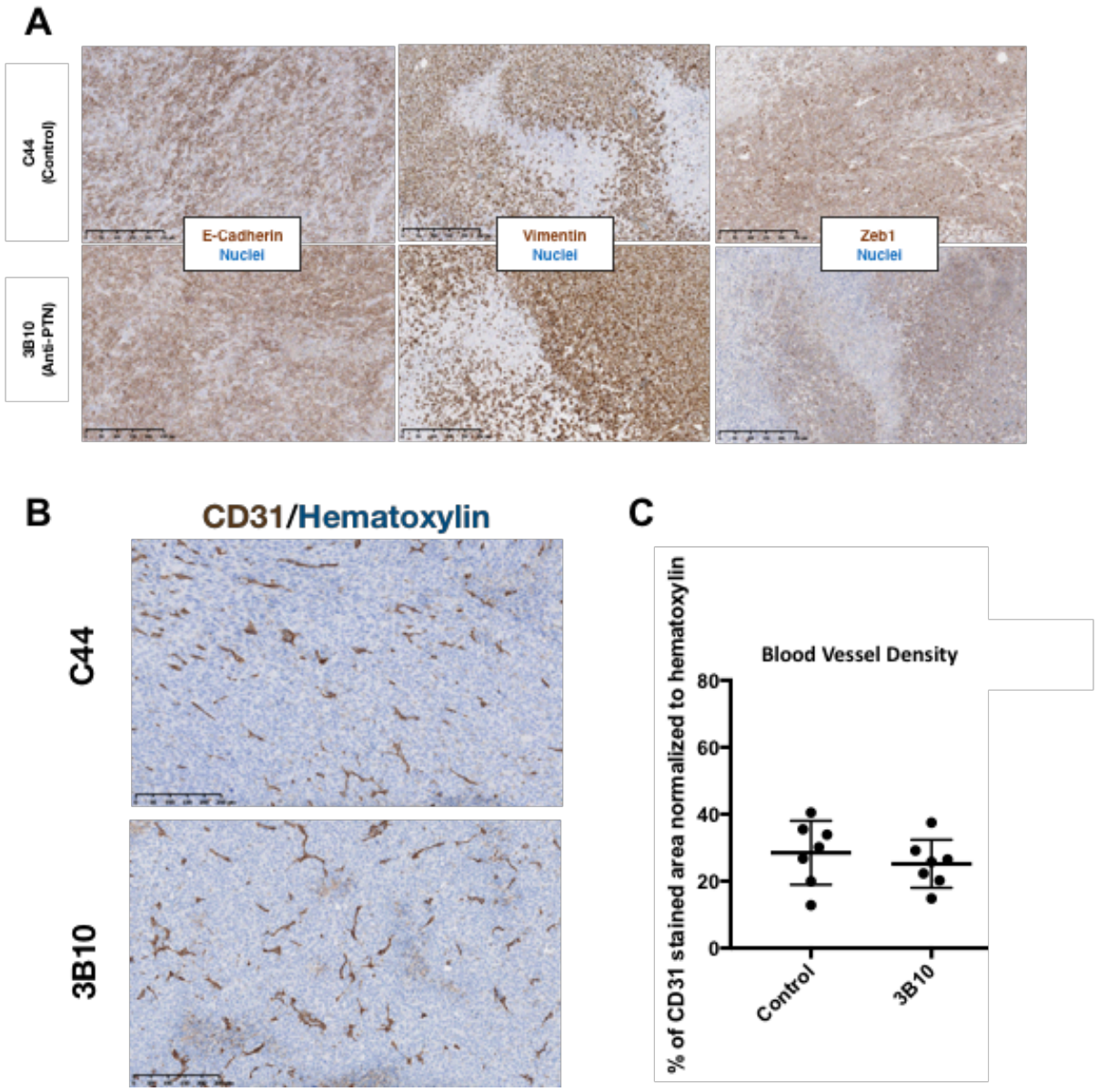

Figure 2.6: **Ptn inhibition does not impact angiogenesis or epithelial-to-mesenchymal transition in preclinical models of breast cancer**. A-B) Primary tumor tissue from 4T1 tumor-bearing mice was analyzed for expression of EMT markers (2.6A; E-cadherin, Vimentin, and Zeb1) or angiogenesis (2.6B; CD31) using immunohistochemistry. C) Quantitative comparison of blood vessel density between control- vs 3B10-treated 4T1 tumor-bearing mice.

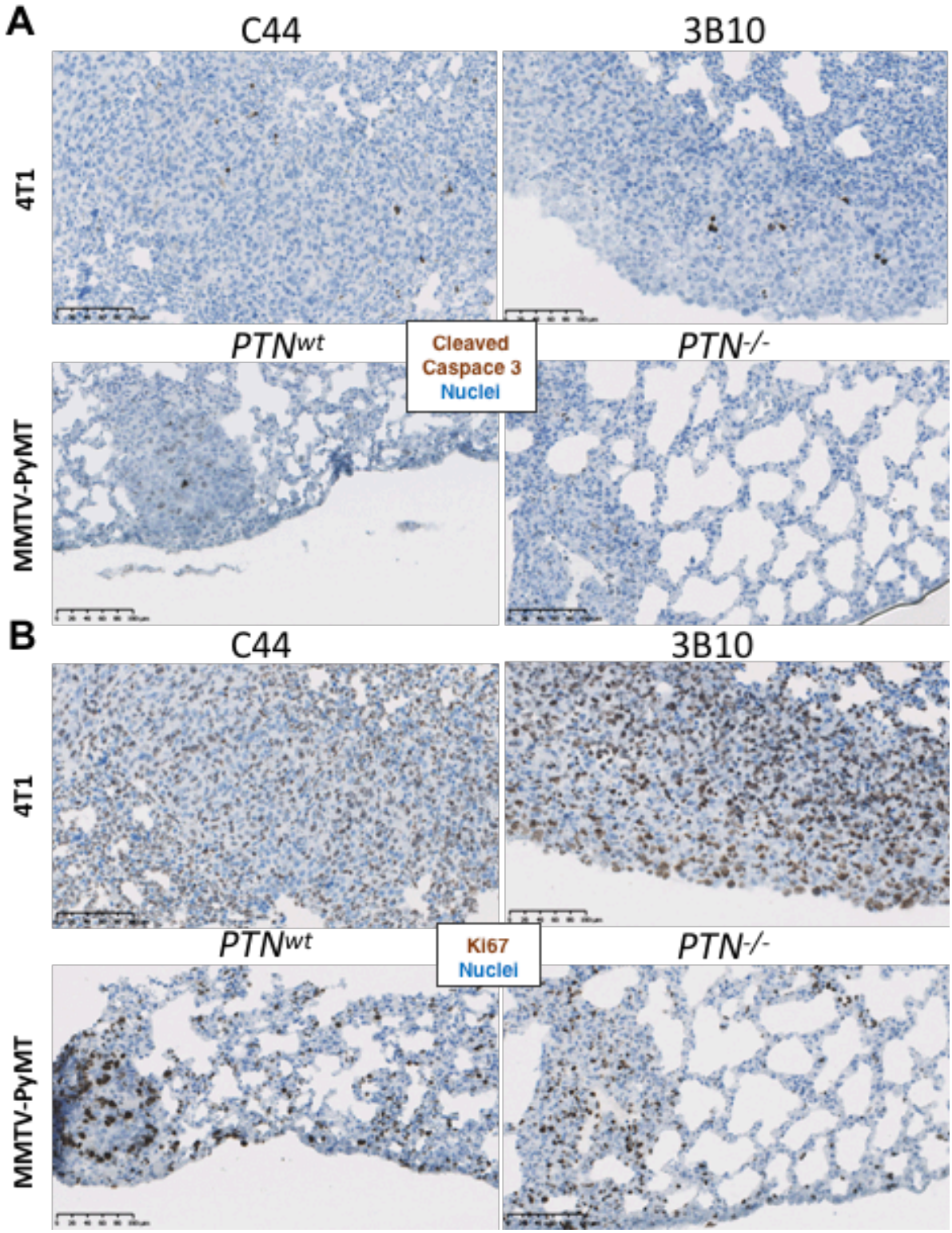
A
C44
3B10
4T1
PTNwt
Cleaved
Caspace 3
Nuclei
PTN-/-
MMTV-PyMT
B
C44
3B10
4T1
PTNwt
KI67
Nuclei
PTN-/-
MMTV-PyMT

Figure 2.7: **Ptn-inhibition or genetic deletion does not impact markers of apoptosis or proliferation of pulmonary metastatic lesions**. A-B) Metatstatic lesions in the lungs from control- or 3B10-treated mice bearing 4T1 tumors were assessed for markers of apoptosis (2.7A; cleaved caspace 3) or proliferation (2.7B; Ki67) via IHC.

the number of neutrophils at the primary and metastatic sites. By immunohistochemical analysis, I observed that Ptn-inhibition or genetic ablation resulted in a marked reduction of neutrophils in the primary tumor (**Figure 2.9A-B**). Using flow cytometry, I also observed that Ptn-inhibition reduced neutrophil number at the metastatic site.

In contrast to neutrophils or macrophages, there was no change in number or localization of relevantlymphoid lineage immune cells, including T cells, NK cells (**Figure 2.9D-E**).

Ptn modulates neutrophil chemokine expression and may also act as a direct haptotactic factor for neutrophils and macrophages

Knowing that Ptn impacted macrophage and neutrophil recruitment in vivo, I performed a cytokine and chemokine array to see if changes in these factors could explain the phenotype (**Figure 2.10A**). Notably, MCP1 and CXCL5 were top hits, which are macrophage and neutrophil chemotactic factors, respectively (**Figure 2.10B-D**). To see if Ptn could directly modulate cytokines and chemokines, I tested the effect of recombinant Ptn on macrophagesin vitro. Ptn was able to directly

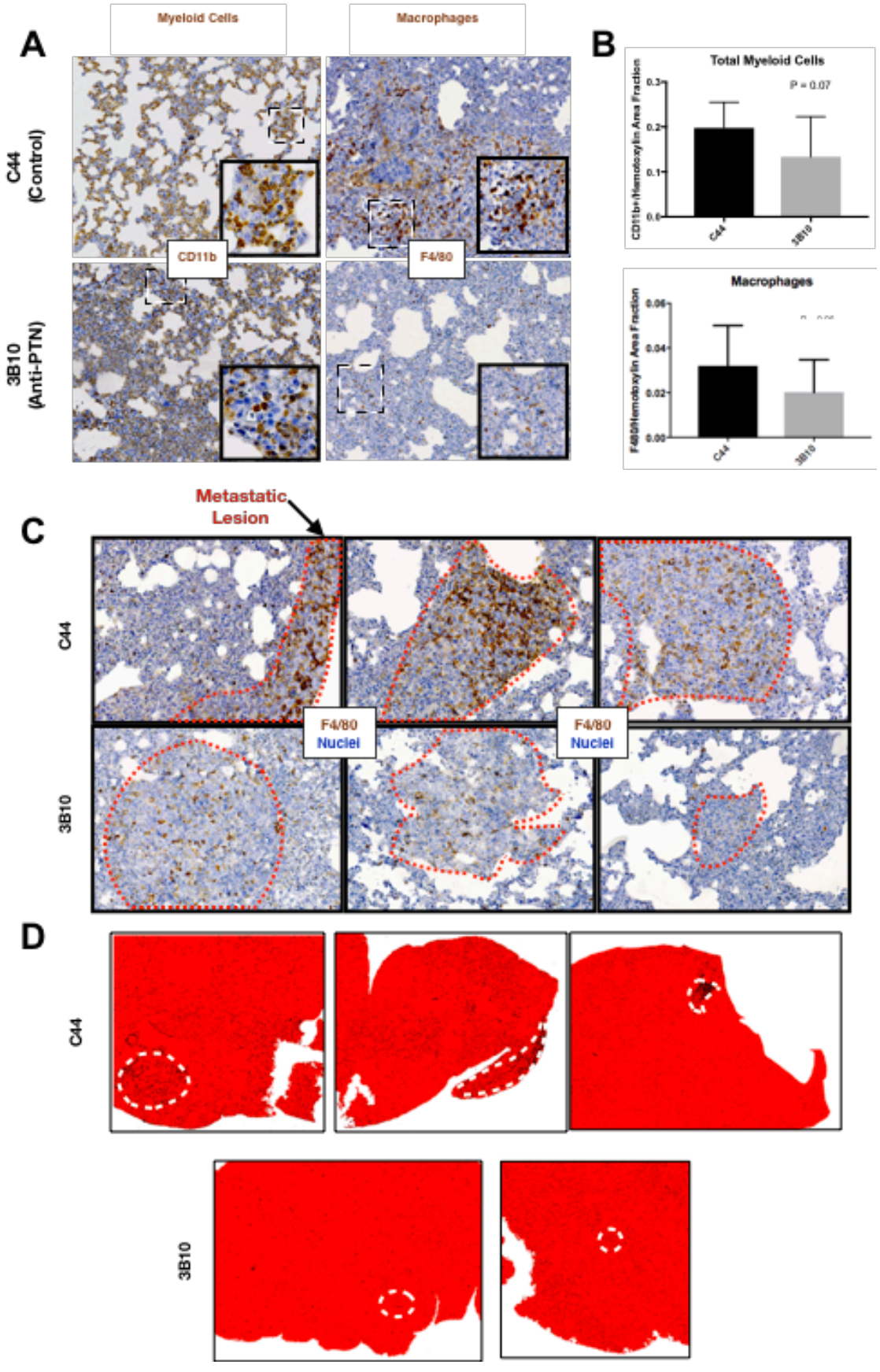
A
Myeloid Cells
Macrophages
C44 (Control)
3B10 (Anti-PTN)
CD11b
F4/80
B
Total Myeloid Cells
P = 0.07
CD11b+/Hemotoxylin Area Fraction
C44
3B10
Macrophages
F4/80/Hemotoxylin Area Fraction
C44
3B10
C
Metastatic Lesion
C44
3B10
F4/80
Nuclei
F4/80
Nuclei
D
C44
3B10

Figure 2.8: **Ptn-inhibition or genetic deletion does not impact markers of apoptosis or proliferation of pulmonary metastatic lesions**. Lungs from C44- or 3B10-treated 4T1 mice were DAB chromagen stained for CD11b and F4/80. B) Quantiation of this staining. **C)** Representative F4/80 staining at 10x magnification comparing macrophage density among similarly sized metastatic lesions. **D)** 4x images were processed to fill non-F480 regions in red and F480+ in black (right) to exhibit macrophage clustering.

promote expression of the some of the same cytokines and chemokines that were changed in response to Ptn-inhibition in vivo (**Figure 2.11A**).

Recent publications suggest that the Ptn/Mdk family may act directly to promote immune cell motility[121]. To test this, I performed transwell migration assays. I observed that Ptn could directly promote the migration of macrophages, but not cancer cells (**Figure 2.11B-C**). Overall, these data suggest to possible mechanisms, direct and indirect, in which Ptn may be promoting myeloid cell recruitment in preclinical models of breast cancer.

Discussion

In this study, I demonstrated that Ptn is a pro-metastatic factor in preclinical models of breast cancer. To the best of my knowledge, this is the first report claiming such activity. Further, I observed that Ptn did not impact primary tumor growth, in contrast to previous reports[132]. This may be due to the fact that previous studies relied on truncated Ptn or overexpression constructs, which may have unanticipated activities.

Additionally, I did not observe any impact of Ptn inhibition on tumor angiogenesis, epithelial-to-mesenchymal transition, or proliferative or apoptotic markers. Further, Ptn did not impact cancer cell growth or migration in vitro. These

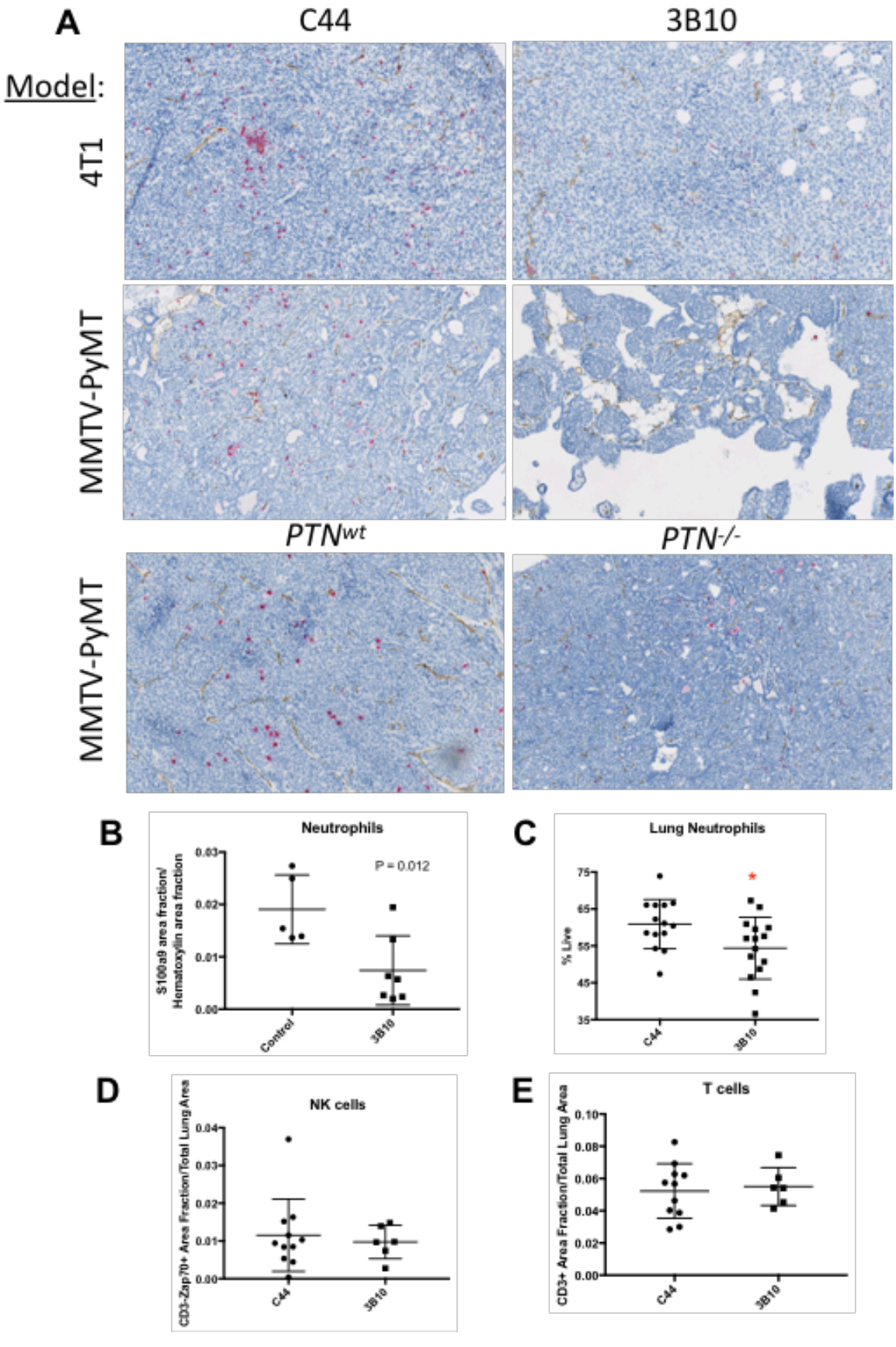
A
C44
3B10
Model:
4T1
MMTV-PyMT
PTNwt
PTN-/-
MMTV-PyMT
B
Neutrophils
S100a9 area fraction/ Hematoxylin area fraction
P = 0.012
Control
3B10
C
Lung Neutrophils
% Live
C44
3B10
D
NK cells
CD3-Zap70+ Area Fraction/Total Lung Area
C44
3B10
E
T cells
CD3+ Area Fraction/Total Lung Area
C44
3B10

Figure 2.9: **Ptn promotes expression of chemotactic factors and directly promotes myeloid cell haptotaxis**. A) Primary tumors were stained for neutrophils (S100A9) via IHC. B) Quantiation of the staining. C) Flow cytometry was performed using single cell suspensions from the lungs of 4T1 tumor-bearing mice. Neutrophils were identified as $CD11b^{+};Ly\text{-}6c^{-};Ly\text{-}6g^{+}$ cells. D-E) Double staining for CD3 and Zap70 was performed on the lungs from 4T1 tumor-bearing mice. T cells are identified as $CD3^{+};Zap70^{+}$ and NK cells are $CD3^{-};Zap70^{+}$. Statistics were performed using the unpaired T test. *, $p<0.05$.

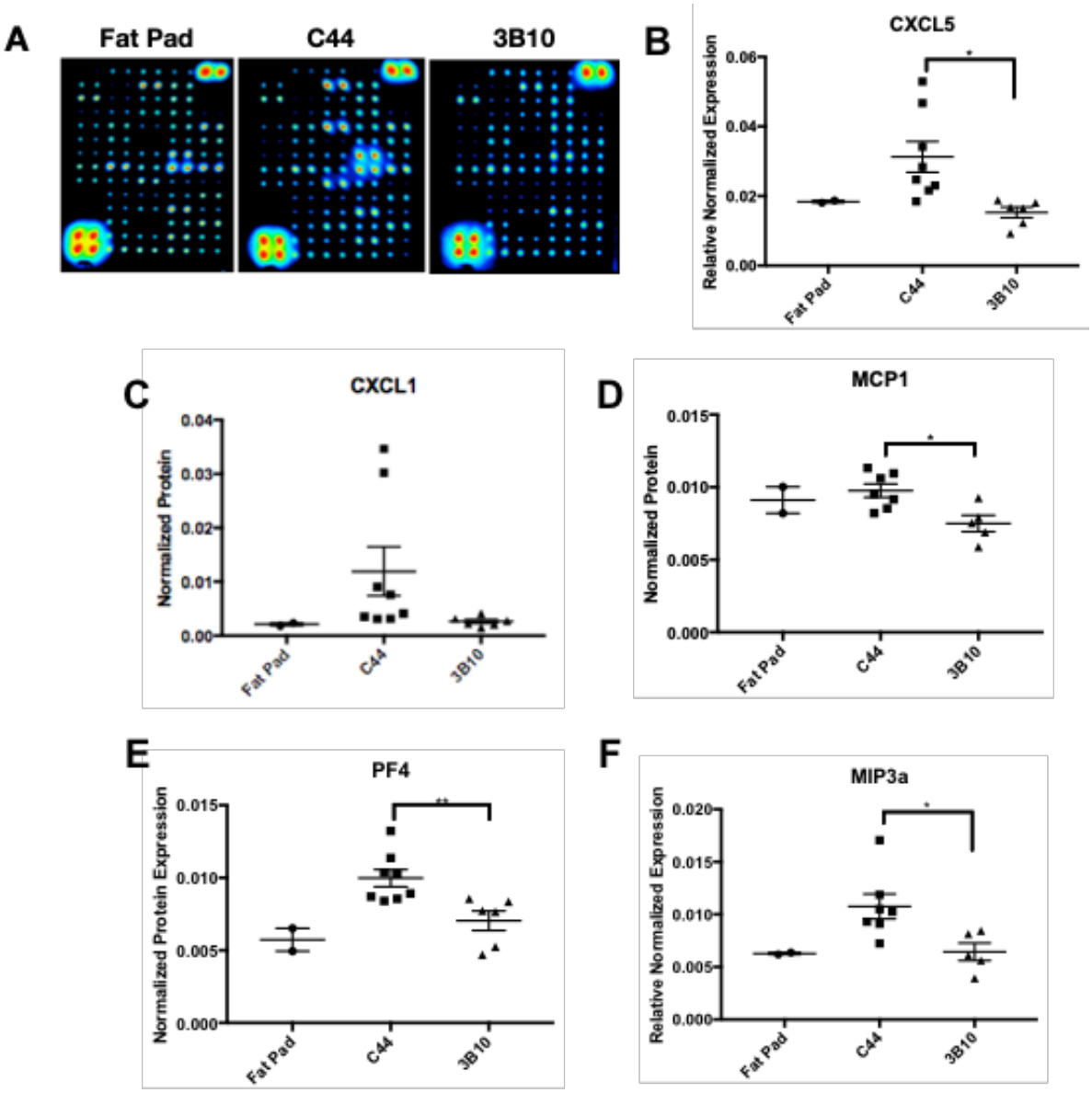

Figure 2.10: **Ptn-inhibition reduces expression of myeloid cell chemokines in the Met-1 model of breast cancer**. A cytokine/chemokine array (Abcam, ab133995) was used to assess changes between non-tumor bearing fat pad (Fat Pad), and C44- or 3B10-treated Met-1 tumors. **A)** An example of the raw data. **B-F)** Quantified changes for select cytokines/chemokines on the array. Statistics performed using the unpaired T test. *, $p<0.05$; **, $p<0.01$.

results corroborate the lack of impact of Ptn-inhibition or genetic deletion on primary tumor growth in vivo.

Instead, I observed that Ptn perturbation resulted in reduced recruitment and altered localization of myeloid cells, including macrophages and neutrophils, in both the primary tumor and metastatic site. This provides the first in vivo evidence of Ptn mediating myeloid cell recruitment.Not only did Ptn impact cytokine and chemokine expression, it could also directly support macrophage migration, corroborating the Shen et al.'s hypothesis[121]. This may be through direct interaction of Ptn and the myeloid cell integrin, Mac1 (CD11b/CD18)[121]. I plan to test this hypothesis by repeating the immune cell migration assays in the presence or absence of a Mac1-blocking antibody.

While midkine was previously proven to be involved in neutrophil trafficking (CITATION), this is the first report demonstrating that Ptn may share this function. This implies some functional redundancy between Ptn and Mdk, originally suggested by the severe gene dosage effect observed in Ptn and Mdk double knockout mice (CITATION).

Overall, my data demonstrate both the presence and importance of Ptn in preclinical models of breast cancer. Further, the data provide a strong rationale for further investigation into the mechanism behind Ptn's pro-metastatic effects.

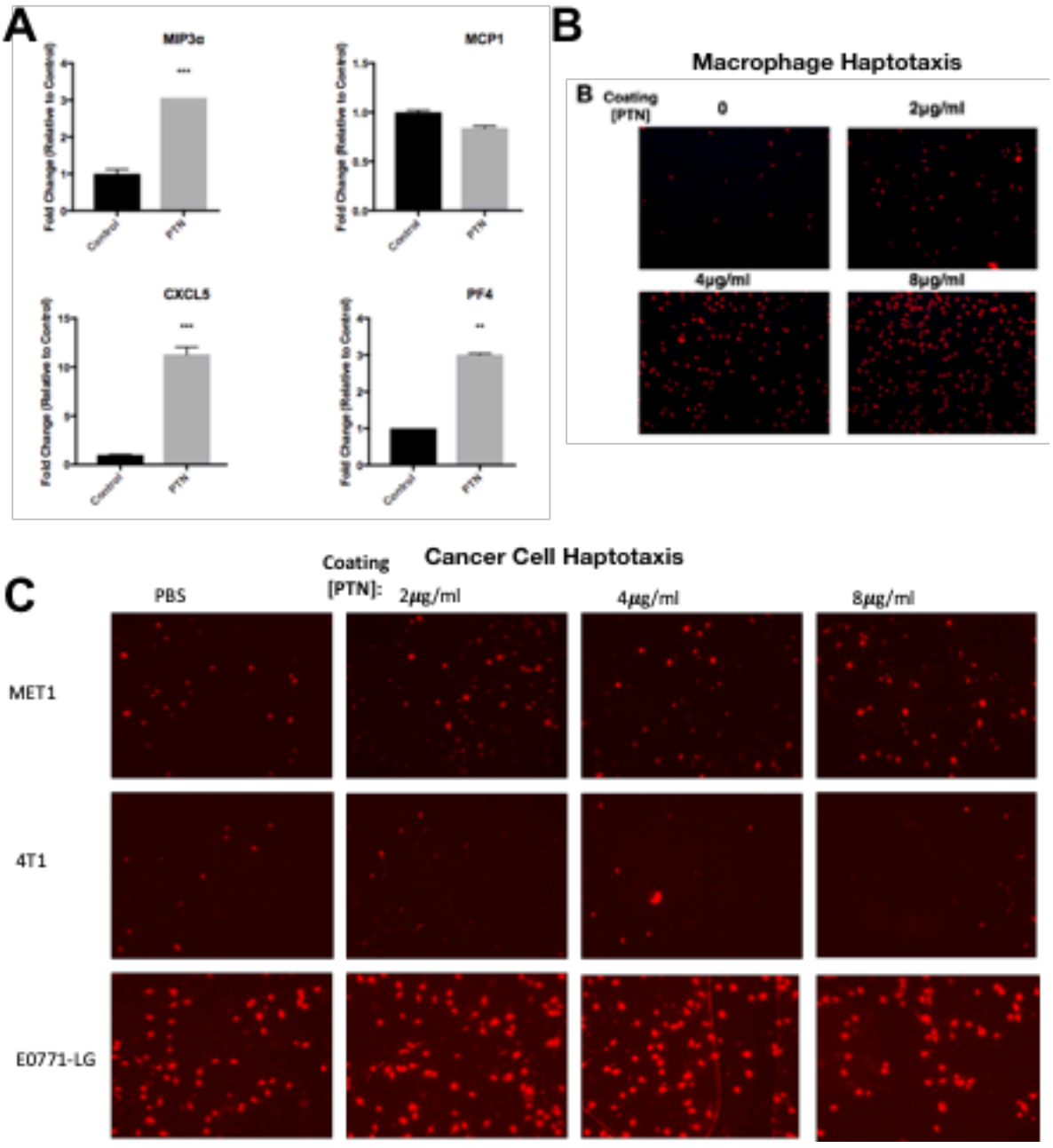

Figure 2.11: **Ptn promotes expression of chemotactic factors and directly promotes myeloid cell, but not cancer cell, haptotaxis in vitro**. **A)** RAW 264 macrophages were plated on petri dishes and treated for 2 hrs. For PTN treatment, the dishes were first coated with PTN (8 ug/mL) before plating the cells. For LPS treatment, cells were treated with 100 ng/mL LPS. cDNA was generated from extracted RNA and real-time PCR was performed. **B)** Transwell migration assay. Primary bone marrow derived macrophages were plated on trans wells coated with either 0, 2, 4, or 8 ug/mL PTN. After 2 hrs, cells were fixed, unmigrated cells were removed, and migrated cells were stained with DAPI for analysis. **C)** Transwell migration assay was performed as described in B. Migrated cells were stained with propidium iodide for analysis. Statistics performed using the unpaired T test. *, $p<0.05$; **, $p<0.01$; ***, $p<0.001$.

CHAPTER THREE
Improved multiplex immunohistochemistry for immune microenvironment evaluation of mouse formalin-fixed paraffin-embedded tissues

Immunohistochemistry (IHC) remains a critical tool for the analysis of immune cell dynamics in mouse models of disease. Flow cytometry (FC), used ubiquitously by immunology labs, provides absolute quantitation of different immune cell types. IHC complements FC, permitting validation of FC results and providing spatial data in context of intact tissue[145-148]. However, characterizing the immune landscape in formalin-fixed, paraffin-embedded (FFPE) mouse tissue remains a significant technical challenge for the field.

Zinc-salt fixation has been proposed as an alternative to formalin-fixation as a strategy to retain tissue morphology while resulting in less epitope masking [149,150]. Zinc-salt fixation may indeed have advantages; however, there are only limited IHC studies comparing the two fixation methods. Additionally, there are concerns that zinc-based fixatives may not penetrate tissues as effectively as formalin [151]. Further, to the best of our knowledge, the long-term stability of zinc-fixed tissue is unreported. Finally, formalin-fixation remains the most common fixation method for mouse tissues.

In this study, I developed an improved protocol for multiplex IHC of mouse FFPE tissues that met the following requirements: 1) reproducibility of staining across different tissues from different experiments; 2) consistent results with most antibodies used without laborious antibody-specific antigen retrieval optimization; 3)

ability to perform multiplex IHC.

Results

Methodological Assessment and Improvement

Development of a More Effective Standard Antigen Retrieval Protocol

One of the primary issues with formalin fixation is that the very chemical changes that induced by formalin to preserve tissue also result in modifying epitopes recognized by antibodies. Hypothetically, these modifications must be reversed for proper antibody recognition to occur.

In my experience, the efficacy of published antigen retrieval protocols vary wildly with different antibodies. To address this, I sought to develop a more consistent antigen-retrieval protocol. In accord with previous reports, I found that Tris-EDTA (pH 9.0) was optimal for most primary antibodies [152]. Further, I found that the addition of 10% glycerol significantly enhanced antigen retrieval in multiple cases (**Figure 3.1:A-L**). Additionally, I found that adding a short 10% neutral buffered fixation step after deparaffinization prevented tissue folding, which can be an issue with higher pH buffers during heat-induced epitope retrieval (HIER). This did not impact epitope detection (data not shown).

Assessment of Antibody Stripping Methods for Multiplex Staining

In our experience, the majority of effective antibodies for mouse FFPE tissue are rabbit IgG. This is a major barrier to multiplex staining, as signal detection and amplification techniques rely the utilization of anti-rabbit IgG secondary antibodies

that cannot distinguish between the different rabbit primary antibodies.

To address this, some labs produced methods for stripping off antibodies[150]. Combined with signal detection methods that are unaffected by stripping, this allows one to probe the tissue with one primary Ab, strip it off, then probe with another.

To strip, some groups utilize a short HIER-like step in citrate buffer (pH 6.2), while others have reported success with incubating the slides in a 100 mM glycine-tween buffer (pH 10.0) at room temperature [150]. I found that the glycine buffer-based stripping method failed to remove the primary antibody (**Figure 3.1:N, Q)**. In contrast, the short HIER-like step in citrate buffer worked effectively (**Figure 3.1-O, R**). I suspect heat-denaturing of high affinity antibodies is particularly important in this process.

Impact of Antibody Stripping Methods on Subsequent Staining

To evaluate the effect of the stripping step on antigen retrieval, we stained spleens after the primary antigen retrieval step ("Round 1," **Figure 3.2**). Second, we stained different spleen sections for the same markers after performing antigen retrieval and a single stripping step ("Round 2," **Figure 3.2**). Third, we repeated this on spleens that were subjected to antigen retrieval and two subsequent stripping steps ("Round 3," **Figure 3.2**). For the three antibodies tested on spleens (CD3, CD19, and Pax5), we did not observe significant differences in detection before or after the tissue was exposed to multiple stripping steps. However, this is not the case for every antibody/epitope (e.g. F4/80 [D2S9R]; **Figure 3.2:K-L**). Thus, labs

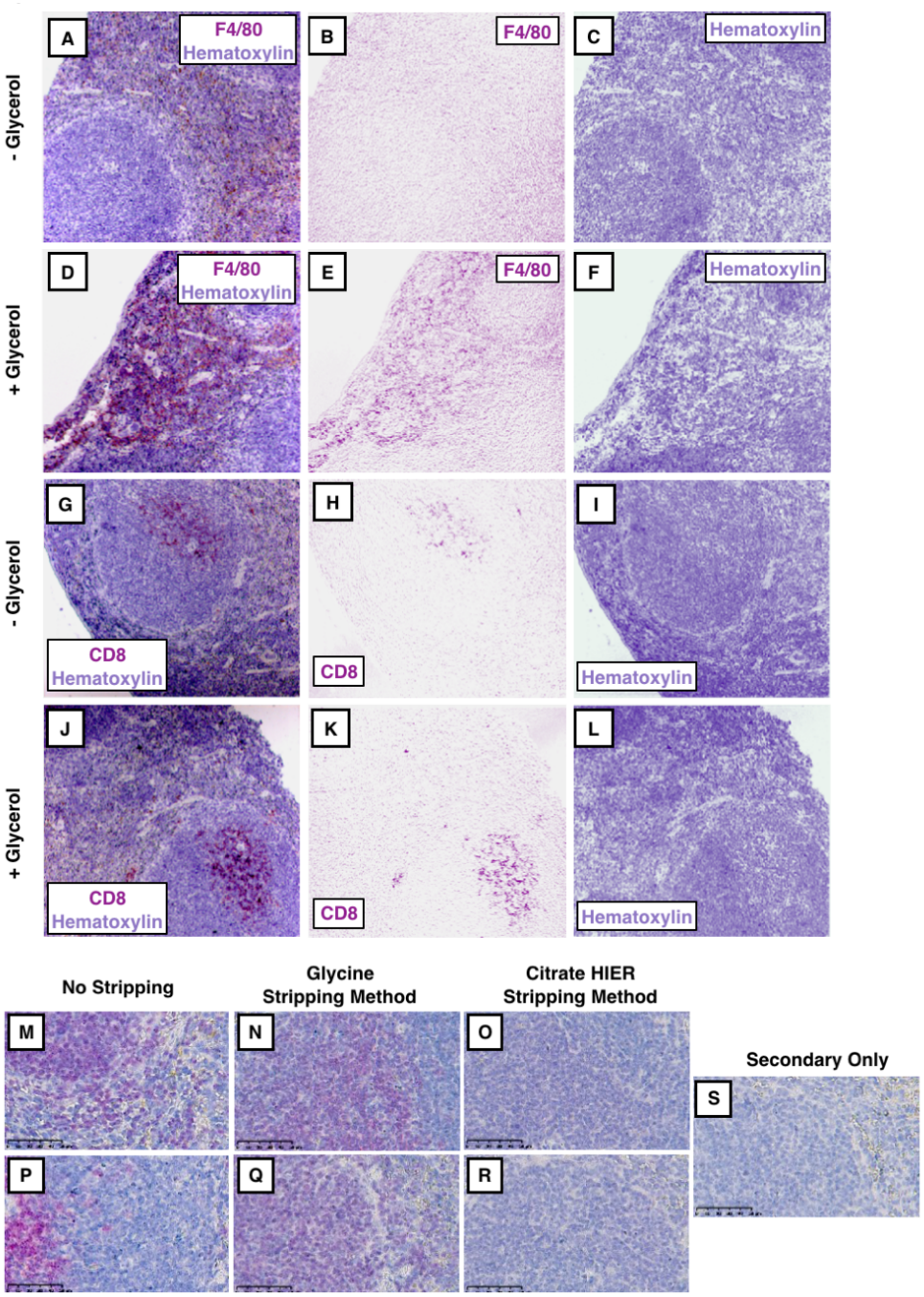

Figure 3.1: Comparison of antigen retrieval buffers and antibody stripping methods. (**A-L**) BALB/c spleens were stained with antibodies specific for F4/80 (SP115; A-F) or CD8 (G-L). Spleen sections were treated with antigen retrieval buffer with (D-F, J-L) or without (A-C, G-I) glycerol. For detection, Bajoran Purple was used as the chromogenic substrate, followed by a hematoxylin counterstain. Images (A, D, G, J) were deconvoluted into their respective hematoxylin (C, F, I, L) and Bajoran Purple (B, E, H, K) components using ImageJ software. Slides were scanned at 20X objective using the Hamamatsu NanoZoomer 2.0-HT. Images represent a 20X field-of-view. (**M-S**) Comparison of different antibody stripping methods. BALB/c spleens were probed for antibodies. First, tissues were treated with Pax5 (M-O), CD3 (PA1-29547; P-R), or secondary-only (S). Next, tissue was developed with chromogen before (M, P) or

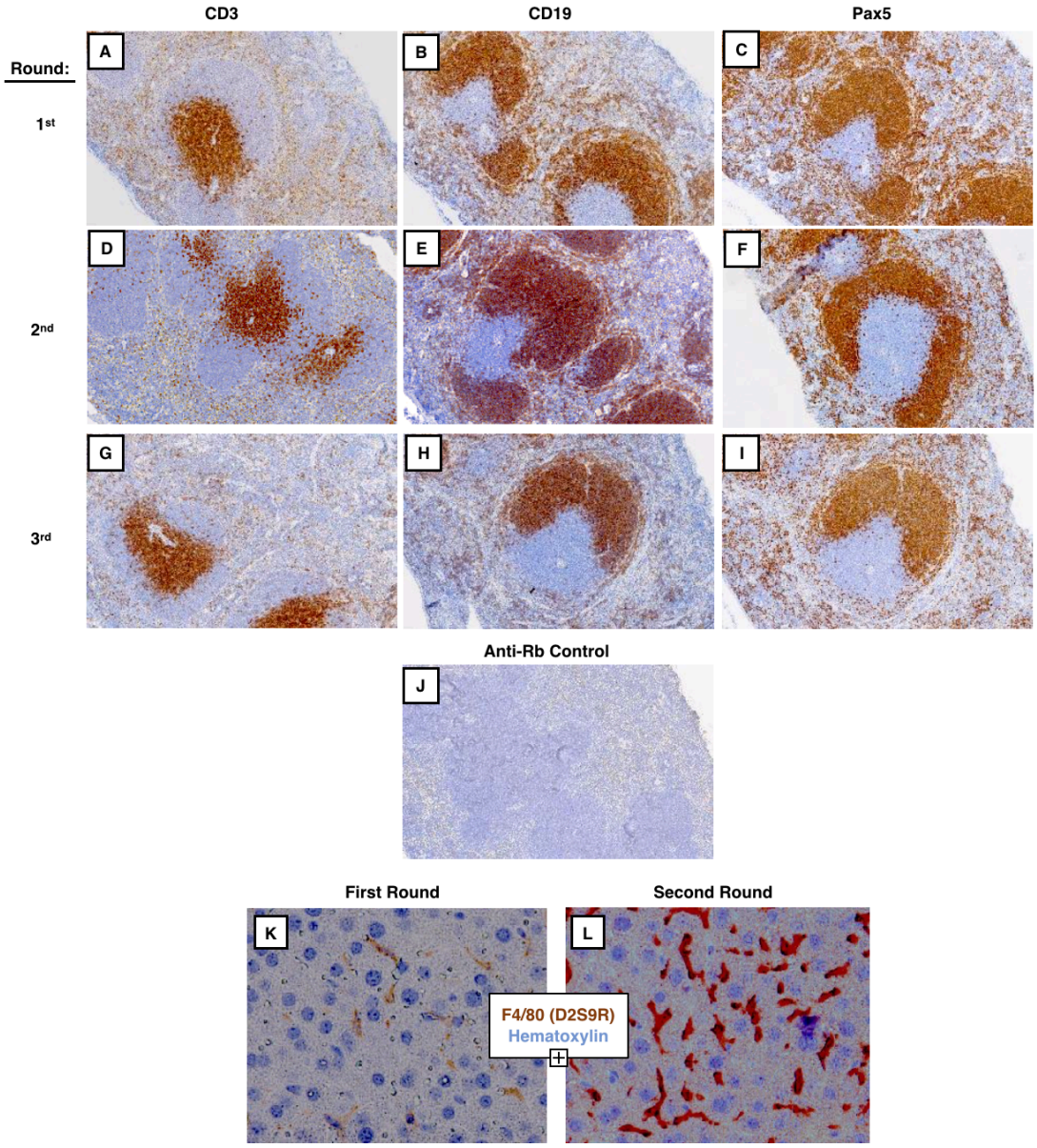

Figure 3.2: Sensitivity of antibodies to multiple rounds of antigen retrieval. (**A-J**) BALB/c spleens were stained for CD3 (PA1-29547; A, D, G), CD19 (B, E, H), or Pax5 (C, F, I) after antigen retrieval (1st round; A, B, C) or antibody stripping (2nd round; D, E, F) or a second round of antibody stripping (3rd round; G, H, I, J). (**K, L**) BALB/c livers were stained for F4/80 (D2S9R) after antigen retrieval minus (K) or plus (L) one round of antibody stripping. Betazoid DAB was used as the chromogenic substrate for detection. Slides were scanned at 20X using the Hamamatsu NanoZoomer 2.0-HT. (**A-J**) Spleen images represent a 10X field-of-view. (**K, L**) Liver images represent a 40X field-of-view.

should perform such testing to determine the order of staining for multiplex protocols involving antibody stripping steps.

Retaining Integrity of Nuclear Staining

After the primary antigen retrieval step and multiple iterations of stripping in multiplex staining, I found that the nuclear signal, via DAPI or hematoxylin, is lost if the staining is done over a longer timeframe (hours vs days; data not shown). I suspect that nuclear DNA is vulnerable to environmental DNase contamination after extensive destruction of formalin crosslinks. This issue was resolved by adding 2 mM EDTA to wash buffers and antibody diluents.

Development and Validation of an Immune Cell Antibody Panel for Mouse FFPE Tissue

Immune Cell Marker and Antibody Selection

Applying our revised protocol to test over 35 primary antibodies specific for mouse immune subsets, we developed a panel of lymphoid and myeloid cell markers **(Table 3.1**). These markers were chosen based on ImmGEN expression data (**Figure 3.3**, [1]), previous reports [153-158], and antibody availability. Using chromagen and fluorescence (via tyramide signal amplification) detection methods, we observed that each marker produced expected staining patterns corresponding with known localization and expression by the respective cell types of interest (**Figure 3.4,** [159]).

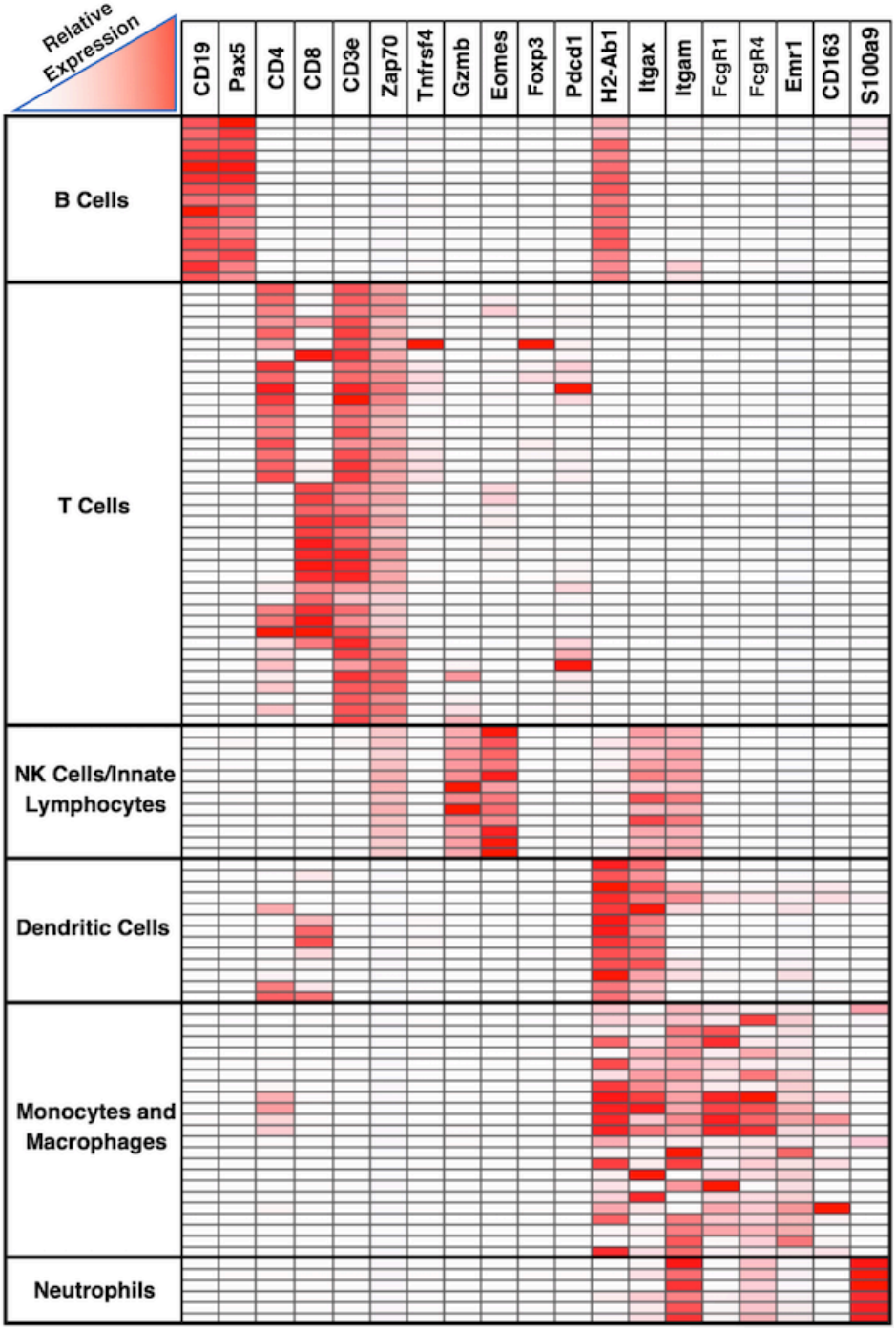

Figure 3.3: Heatmap depicting immune cell expression of markers utilized in our immunohistochemistry panel. Micro-array data from ImmGen showing relative expression levels of different markers by different cell types (http://www.immgen.org) [1]. Rows represent different immune cell populations, grouped by cell type. Columns represent genes.

Antibody Validation

To validate antibody specificity, we used two strategies. First, we stained tissue in which cell types/markers of interest are expected to be decreased compared to control. For the lymphoid panel, we stained spleens from wild-type, SCID, and NSG mice (**Figure 3.5:A-G1)**. Compared to wild-type, we observed a decrease in lymphoid cell markers in SCID and NSG spleens. For example, CD3 and CD19 (T cell and B cell markers, respectively) are completely absent in SCID and NSG tissue. As a positive control, CD11b, mostly a myeloid-lineage marker, was consistent across all groups (**Figure 3.5:B1-D1**).

For macrophage markers, we stained livers from control- or clodronate-liposome-treated mice, as clodronate liposomes deplete professional phagocytic cells, primarily macrophages [160,161]. Macrophage staining was markedly reduced in clodronate liposome-treated mice (**Figure 3.5:H1-Q1**).

For our second strategy to confirm antibody specificity, we utilized multiple antibodies for the same marker or cell type when possible. For example, we utilized two different antibodies for F4/80 (**Figure 3.5:H1-K1**). For B cells, we utilized two different B cell-specific markers, CD19 and Pax5 (**Figure 3.5:J-O**).

Multiplex Staining Strategies for Specific Immune Cell Identification

When developing the antibody panels, we found that for some cell types, such as DCs, neutrophils, and NK cells, antibodies for cell-specific markers were not available. To address this, we utilized multi-marker staining strategies.

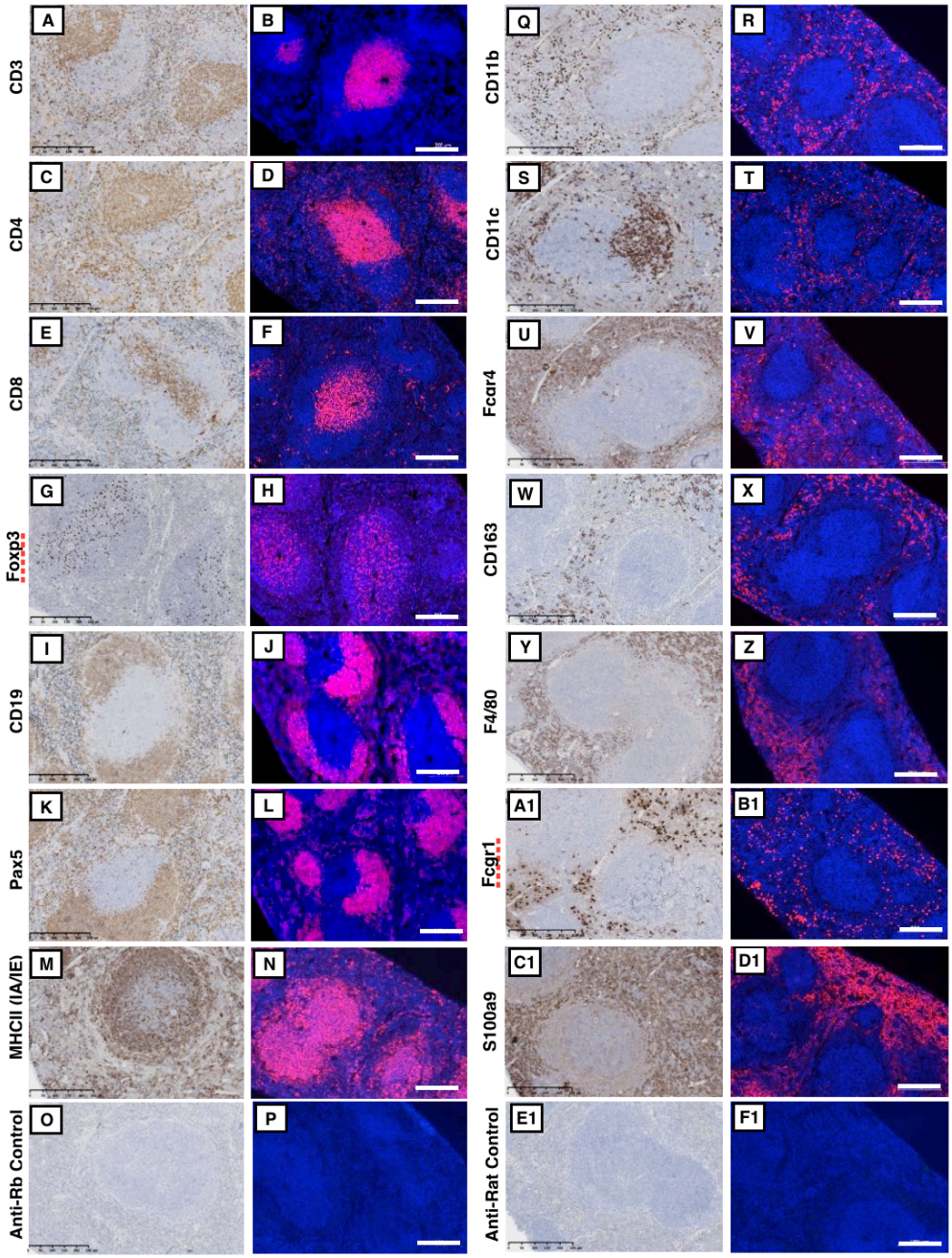

Figure 3.4: Chromogen and fluorescent staining of lymphoid lineage and myeloid lineage markers. BALB/c spleens were stained with antibodies specific for CD3 (PA1-29547; A, B), CD4 (EPR19514; C, D), CD8 (E, F), Foxp3 (G, H), CD19 (I, J), and Pax5 (K, L), MHCII (M, N), CD11b (Q, R), CD11c (S, T), FcgR4 (U, V), CD163 (W, X), F4/80 (Y, Z), FcgR1 (A1, B1) S100a9 (C1, D1), or secondary-only (O, P, anti-rabbit; E1, F1, anti-rat). Betazoid DAB and Opal 570 were used as the chromogenic and fluorescent substrates, respectively. Chromogen-stained sections were counterstained with hematoxylin, and fluorescence images were counterstained with DAPI. Chromogen-stained slides were scanned at 20X using the Hamamatsu NanoZoomer 2.0-HT. Slides Slides with fluorescent detection were scanned at 20X using the Zeiss Axioscan.Z1. Images represent a 10X field-of-view. Scale bar = 250 µm for chromogen images. Scale bar = 200 µm for 10X fluorescent images.

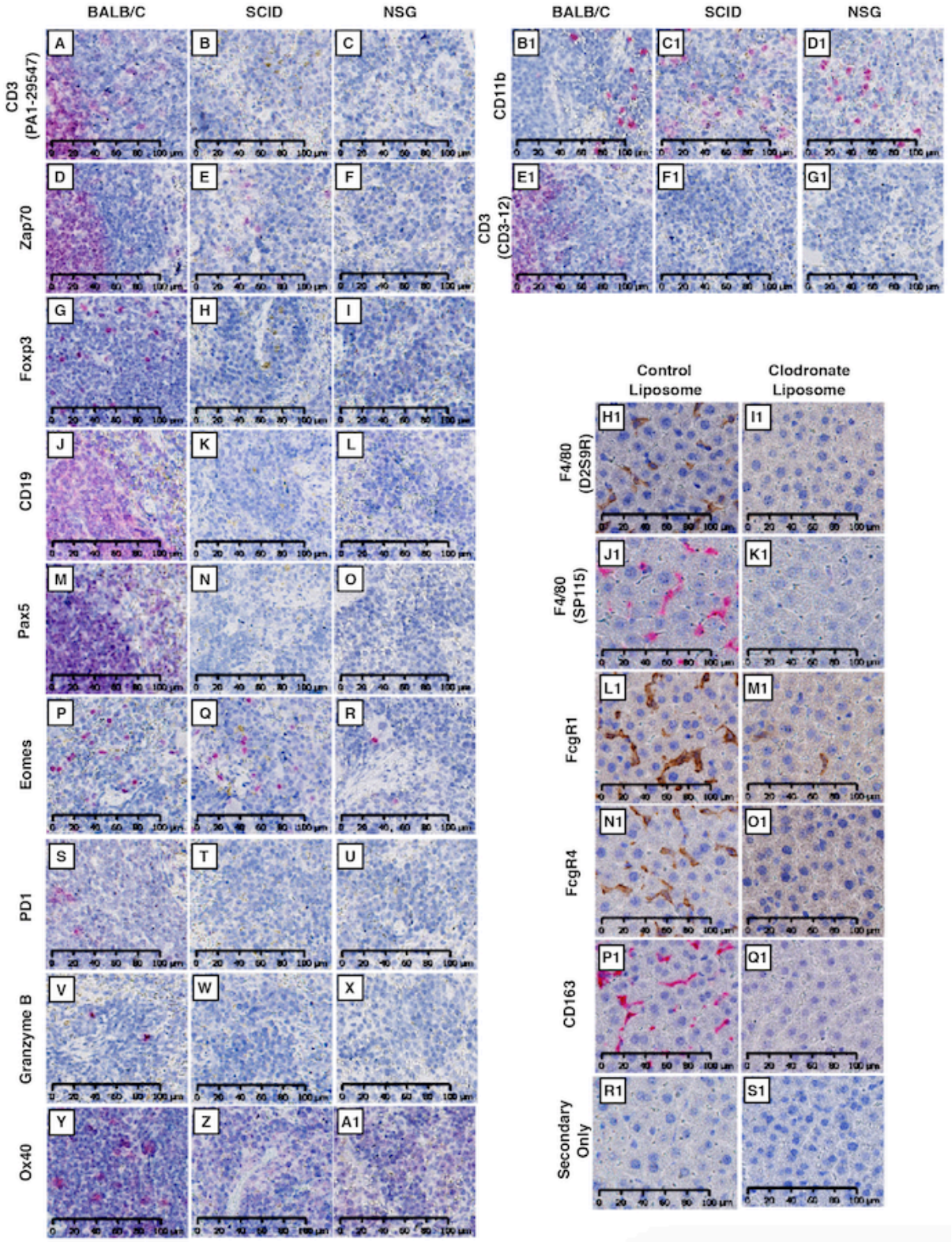
BALB/C
SCID
NSG
CD3 (PA1-29547)
Zap70
Foxp3
CD19
Pax5
Eomes
PD1
Granzyme B
Ox40
CD11b
CD3 (CD3-12)
Control Liposome
Clodronate Liposome
F4/80 (D2S9R)
F4/80 (SP115)
FcgR1
FcgR4
CD163
Secondary Only

Figure 3.5: Validation of antibody specificity. (**A-G1**) Wild type BALB/c, SCID, or NSG spleens were probed with antibodies specific for CD3 (PA1-29547; A, B, C), Zap70 (D, E, F), Foxp3 (G, H, I), CD19 (J, K, L), Pax5 (M, N, O), Eomes (P, Q, R), PD1(S, T, U), Granzyme B (V, W, X), Ox40 (Y, Z, A1), CD11b (B1, C1, D1), and CD3 (CD3-12; E1, F1, G1). For detection, Warp Red chromogenic substrate was used. Slides were counterstained with hematoxylin and scanned at 20X using Hamamatsu NanoZoomer 2.0-HT. (**H1-S1**) Livers from control- or clodronate-liposome treated BALB/c mice were stained for F4/80 (D2S9R and SP115; H1, I1 and J1, K1, respectively), FcgR1 (L1, M1), FcgR4 (N1, O1), CD163 (P1, Q1), or secondary-only (R1, S1). Slides were scanned at 20X using the Hamamatsu NanoZoomer 2.0-HT. All images represent a 40X field-of-view. Scale bar = 100 μm for all images.

For example, we developed a strategy to stain NK cells using CD3 and Zap70. *CD3* is expressed by T cells, but not NK cells (**Figure 3.3,**[1]. *Zap70* is expressed by T cells and NK cells (**Figure 3.3,**[1]. Because SCID and NSG mice lack T cells, CD3 staining is absent in SCID and NSG spleens compared to wild-type (**Figure 3.5:A-C**). In contrast, some $Zap70^+$ cells remain; presumably NK cells (**Figure 3.5:D-F**). Combining these markers, we stained spleens for CD3 and Zap70 using both chromagen and fluorescence detection methods, demonstrating the presence of $CD3^+$; $Zap70^+$ and $CD3^-$;$Zap70^+$ cells, corresponding to T cells and NK cells, respectively (**Figure 3.6:A, B**). In the case of chromagen staining, we first stained for CD3 using a dark brown chromagen (DAB), intentionally obscuring further staining wherever the chromagen is deposited. We subsequently performed Zap70 staining using a red chromagen ('Warp Red'). Through this strategy, it is easy to identify Zap70 single positive cells utilizing chromagen detection (**Figure 3.6:A,** inset).

We also developed a strategy to detect DCs. While *CD11c* has long been used as a DC marker, it is not cell-type exclusive as it is may be expressed by

macrophage subsets and other immune cells (**Figure 3.3,** [1]). *MHCII* (*H2-Ab1*) is also not exclusive, but it is expressed more consistently across DC subsets and is found on fewer cell types (**Figure 3.3,** [1]**).** Because *MHCII* is expressed by splenic B cells and macrophages, we first stained for B cell and macrophage markers, Pax5 and CD163, respectively. By combining CD163 and Pax5 signal with the same chromogen or fluorophore, we demonstrate the effective use of a "dump channel" applied in an IHC setting (**Figure 3.6:C, D)**. Staining for MHCII second with a different chromagen or fluorophore revealed a distinct population of $MHCII^{+}$; $Pax5^{-}$; $CD163^{-}$ cells, which we believe to be DCs (**Figure 3.6:C, D**).

Next, we developed a strategy to distinguish neutrophils from macrophages. Using knowledge from the literature and considering the available antibodies for mouse targets, we stained for CD163 and FcgR4. According to ImmGen (**Figure 3.3**,[1] and previous reports [154,155], *FcgR4* is expressed by macrophages and neutrophils. This is corroborated by flow cytometric analysis (**Figure 3.6:G**). Based on this information, we expect that splenic macrophages are $CD163^{+}$; $FcgR4^{+}$ and neutrophils are $CD163^{-}$; $FcgR4^{+}$. Performing this multiplex staining reveals cells that follow these staining patterns (**Figure 3.6:H, I**).

Examples of Effective Immune Cell Identification in Preclinical Models of Cancer

Finally, we tested our immune panels and multiplex staining on 4T1 tumors, which is an immune cell-heavy model of breast cancer. We did multiplex IHC

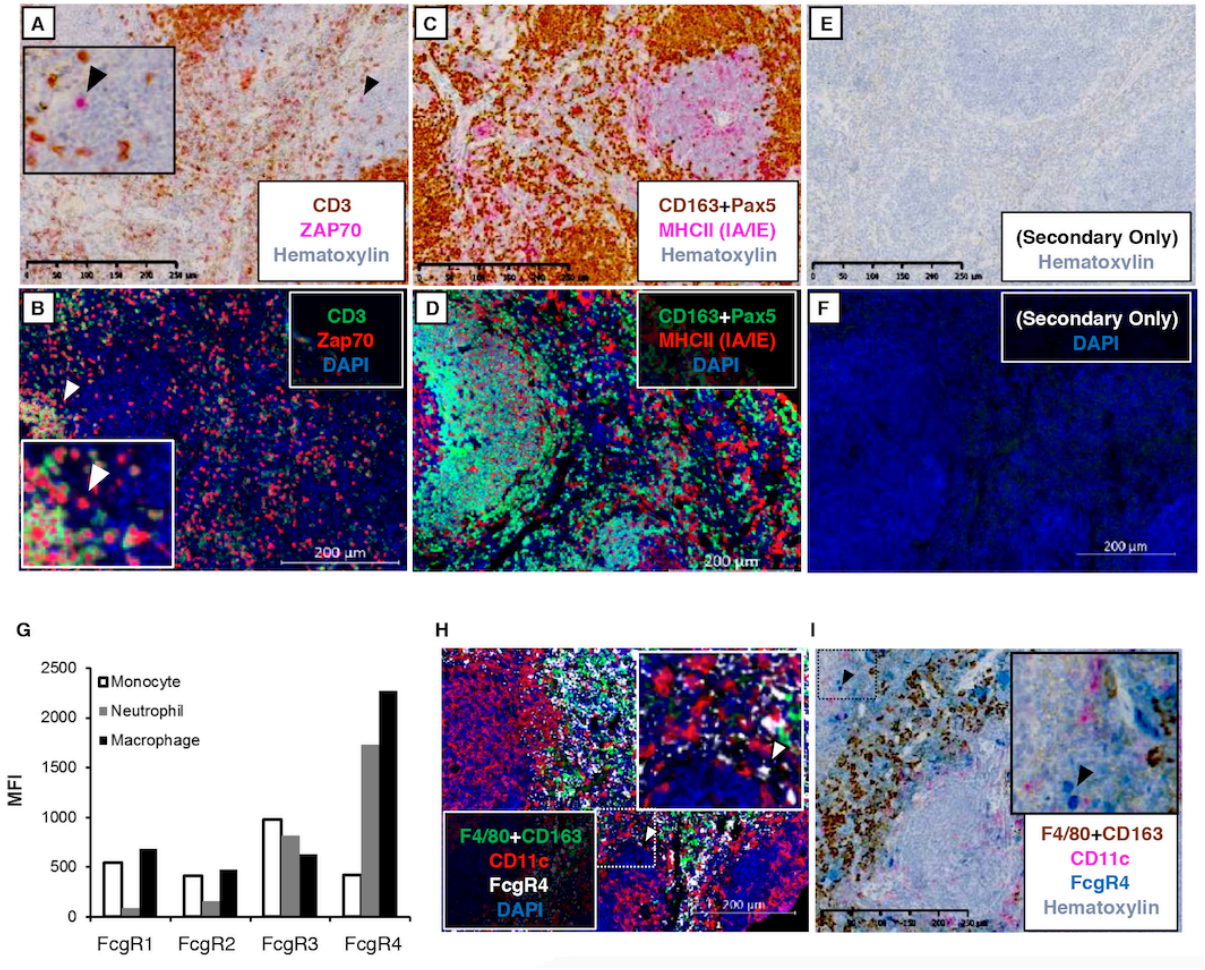

Figure 3.6: Multiplex IHC to stain Natural Killer Cells, Dendritic cells and Neutrophils. BALB/c spleens were stained for (**A, B**) CD3 (PA1-29547, T cells) and Zap70 (T cells, NK cells); (**C, D**) Pax5 (B cells), CD163 (majorly macrophages), and MHCII (IA/IE); (**H, I**) F4/80 (SP115), CD163, CD11c, and FcgR4. (**E, F**) Secondary-antibody-only (without addition of primary antibody) was used for negative controls. Chromogenic substrates used were Betazoid DAB (brown) and Warp Red (pink). Opal 520 (green), Opal 570 (red) and Opal 690 (white) were used for fluorescence detection. Chromogen-stained sections were counterstained with hematoxylin. For fluorescence detection, sections were counterstained with DAPI (blue). Slides were scanned at 20X using the Hamamatsu NanoZoomer 2.0-HT (chromagen detection) or the Zeiss Axioscan.Z1 (fluorescence detection). Images represent a 10x field-of-view.
(G) Total splenocytes were isolated from C57BL/6 mice. FcgR expression was evaluated on neutrophils ($CD11b^+$; $Ly6G^+$; $Ly6C^-$), macrophages ($F4/80^+$), and monocytes ($CD11b^+$; $Ly6c^+Ly6G^-$). FcgR signal is represented by mean fluorescence intensity. Scale bar = 250 µm for chromagen-stained images. Scale bar = 200 µm for fluorescent images.

staining using chromogen and fluorescent detection methods (**Figure 3.7**)**. Figure 3.7:AB** shows $CD3^+$; $CD4^+$ and $CD3^+$; $CD8^+$ T cells. We also detected $CD3^-$; $CD4^+$ and $CD3^-$; $CD8^+$ cells which may be NK or DCs. Notably, all CD3+ T cells were labeled with either CD4 or CD8, demonstrating the specificity and sensitivity of the staining, as the presence of double-negative or double-positive T-lineage cells are unreported in this model.

Figure 3.7:D (inset, right arrow) shows the presence of $CD11c^+$ macrophages. This corresponds to tumor-associated macrophages, as resident tissue macrophages in the mammary fat pad are $CD11c^-$ [162]. We also can detect $F4/80^-$; $CD163^-$; $CD11c^+$; $MHCII^+$ DCs (**Figure 3.7:D**, inset, left arrow).

Figure 3.7:JK shows quantitation of different immune cell types in 4T1 tumors normalized to the DAPI signal. 4T1 tumors have been reported to have high neutrophil infiltration [142]. Consistent with this, our analysis shows a high frequency of $F4/80^-$; $CD163^-$; $FcgR4^+$ cells which are presumably neutrophils (**Figure 3.7:E-F**).

Comparatively, we also found modest numbers of tissue macrophages ($F4/80^+$; $CD163^+$; $CD11c^-$), DCs ($F4/80^-$; $CD163^-$; $CD11c^+$; $MHCII^+$) and T cells ($CD3^+$; $CD4^+$ and $CD3^+$; $CD8^+$), data which is consistent the findings of other groups [163-165]. In sum, this data illustrates how an effective multiplex IHC strategy can be exploited to investigate the immune dynamics of the tumor microenvironment.

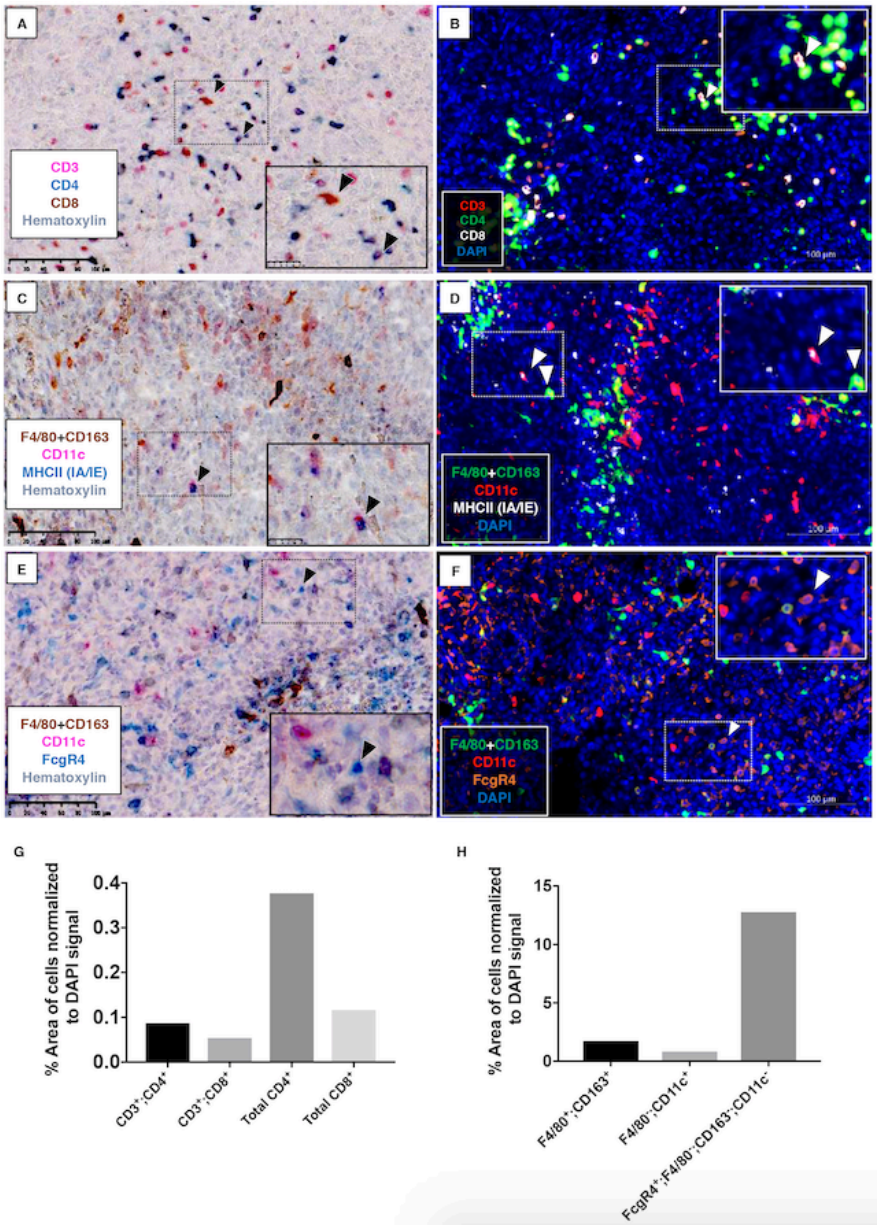

Figure 3.7. Multiplex IHC staining of 4T1 tumor tissues. 4T1 primary tumors were stained for (**A, B**) CD3 (PA1-29547; T cells), CD4 (EPR19514; T cells, NK cells, DCs), and CD8 (T cells, NK cells, DCs); (**C, D**), CD11c, FcgR4, and CD163+F4/80(SP115); (**E, F**) CD11c, MHCII (IA/IE), and CD163+F4/80(SP115). Chromogenic substrates used were Betazoid DAB (brown), Warp Red (pink), and Feranji Blue (blue) (A, C, E). Opal 520 (green), Opal 570 (red), and Opal 690 (white or orange) were used for fluorescent staining (B, D, F). Chromogen sections were counterstained with hematoxylin, whereas DAPI staining was used for fluorescence detetction. Slides were scanned at 20X using the Hamamatsu NanoZoomer 2.0-HT (chromagen detection) or the Zeiss Axioscan.Z1 (fluorescence detection). Images represent a 20x field-of-view. Inset: Higher magnification. (**B, C, D**) Arrows point to $CD3^{+}$;$CD8^{+}$ (B), $CD11c^{+}$;$MHCII^{+}$ (C; D, left arrow), or $CD163\&F4/80^{+}$;$CD11c^{+}$ cells (D, right arrow). (**E, F**) Arrows point to $FcgR4^{+}$; $CD11c^{-}$ $CD163\&F4/80^{-}$ cells. (**J, K**) Cell types in 4T1 tumor sections were quantitated as % area of positive cells normalized to DAPI signal. Scale bar = 100 µm for all images.

Discussion

In this study, we produced a modified FFPE IHC protocol for mouse tissue that provides a more effective antigen retrieval method. Antigen retrieval has been a longstanding challenge in the field, often requiring different retrieval protocols for different epitopes [150,166,167]. Our protocol works consistently well for all of the antibodies tested. The use of glycerol in the Tris-EDTA antigen retrieval buffer greatly increases the detection of multiple antigens and may be a better standard for mouse FFPE tissues. Also, the use of EDTA in the wash buffers prevents degradation of DNA by nucleases preserving nuclear morphology; a consideration that is absent in other multiplex protocols. Lastly, we found that treatment with 10% formalin immediately prior to antigen retrieval helps to maintain tissue integrity and reduces loss of tissue during multiple rounds of stripping and re-probing.

We also propose a novel strategy of using multiple markers to stain for cell types for which unique markers/antibodies have not been identified or are not available commercially. This strategy can be particularly helpful to identify DCs, neutrophils, and NK cells in the tumor microenvironment. With new emerging immune regulators [168] and therapies, this strategy provides an excellent tool to investigate the effect of drug treatment and prognosis of disease.

Overall, our protocol of multiplex IHC staining on mouse tissue provides an improved strategy for reproducible staining. Using our strategy and by properly planning the sequence of target antibodies, visualization of multiple epitopes is only

limited by the number of filter channels in the microscope. This protocol has the potential to improve the utility of multiplex IHC to investigate the immune system in vivo, including the analysis of the tumor immune microenvironment and mechanisms of action of immune-related drugs in preclinical models.

CHAPTER FOUR
Methodology

Cell Lines, Culture Conditions

The murine breast carcinoma cell line Met-1 was a kind gift of Dr. Philipp Scherer (UT Southwestern). Raw 264.7 and 4T1 cells were obtained from ATCC (Manassas, VA). E0771-LG and F246-6 were kind gifts from Dr. Jeffrey W. Pollard (Department of Developmental and Molecular Biology, Albert Einstein College of Medicine, Bronx, NY, USA). 3B10 hybridoma cells were a kind gift of Dr. Anton Wellstein (Department of Oncology, Georgetown University, Washington, DC, USA).

Cells were maintained at 37°C in a mixture of 5% CO_2 and 95% air in DMEM (for 4T1, Met-1, and F246-6) or RPMI (for E0771-LG) supplemented with 5% fetal calf serum (Rocky Mountain Biologicals, USA). DMEM and RPMI were obtained from Invitrogen (Carlsbad, CA).

Production of 3B10 monoclonal antibody

3B10 hybridoma cells were seeded in RPMI + 10% FBS at a concentration of $2x10^6$ cells/mL in T175 flasks. For passaging, cells were split once density reached approximately $8x10^6$ cells/mL.

For production, 3B10 cells were allowed to grow until viability dropped below 70%. Supernatant was collected and 100 mM sodium phosphate buffer (pH 8.4) and 3.2 M

NaCl were added. Protein A beads were equilibrated with 100 mM sodium phosphate buffer (pH 8.4) + 3.2 M NaCl before running 3B10 supernatant over the column. Once supernatant was run over the column, the column was washed with a decreasing concentration gradient of sodium phosphate buffer (100 mM to 10 mM; pH 8.4) + 3.2 M NaCl. Antibody was eluted using Pierce Gentle Ag/Ab Elution Buffer, pH 6.6 (ThermoFisher, 21013), dialyzed with PBS, and sterile-filtered (syringe filter; Whatman Puradisc, 0.2 um PVDF, 6791-1302) before use.

Mice

Female BALB/c (BALB/cfC3H strain) and C57BL/6 mice were purchased from the on-campus UT Southwestern Mouse Breeding Core (Dallas, TX). MMTV-PyMT mice were originally obtained from The Jackson Laboratory (Bar Harbor, ME) and were maintained on the FVB background. *Ptn*^{null} mice, originally produced by Muramatsu et al (2006)[7], were a kind gift from Dr. John P. Chute (Division of Hematology/Oncology, Department of Medicine, University of California, Los Angeles, Los Angeles, CA 90095, USA). *Ptn*^{null} mice were maintained on both the C57BL/6 and FVB backgrounds (backcrossed onto FVB for 8 generations).

Animal studies

For the orthotopic experiments, E0771-LG cells ($0.5x10^6$) were injected into the mammary fat pad of 8-10 week-old female *Ptn*$^{+/+}$ or *Ptn*$^{-/-}$ C57BL/6 mice. 4T1 cells ($1x10^6$) were injected in the mammary fat pad of 8 week-old female BALB/C mice.

Met-1 cells ($1x10^5$) were injected in the mammy fat pad of 8 week-old female FVB mice. Therapy was started when primary tumors reached 50 mm^3.

Mice were randomly assigned to treatment groups, treated with C44 (isotype control; 200 ug, 2x/week) or 3B10 (anti-Ptn; 200 µg, 2x/week). Mice were euthanized when primary tumor burden reached 1500 mm^3. For the transgenic experiments, female MMTV-PyMT mice received therapy with C44 or 3B10, starting at 8 weeks of age. Mice were euthanized at 14 weeks of age. Mice were monitored daily for signs of morbidity.

Following euthanization, tissues were fixed in 10% formalin or snap frozen in liquid nitrogen for further studies or prepared for flow cytometry analysis.

MTS Assay

The MTS colorimetric assay was performed as previously described[169]. Briefly, 2000 cells/well were plated in 96-well plates. Cells were treated with C44 (20 µg/mL) or 3B10 (dilution series from 0.31 to 20 µg/mL). On day 5, 20 µl MTS was added, followed by a 2-hour incubation at 37°C, and then the absorbance was read at 490 nm on a plate reader.

Transwell Migration Assay

The bottom of 5 μm (for macrophages and neutrophils) or 8 μm (for cancer cells) polycarbonate transwells (Costar, Corning, NY) were coated with 1-8 μg/mL recombinant Ptn <**source**> at 37°C for 3 hrs. For the cancer cell lines (4T1, Met-1, E0771-LG), $5x10^5$ cells were plated into the upper well of the chamber and allowed to migrate for 16 hrs. For the immune cells (macrophages and neutrophils), $1x10^6$ cells were plated into the upper well of the chamber and allowed to migrate for 3 hrs. After incubation, the wells were washed, fixed with cold methanol for 10 minutes, and cells on the top side of the membrane (unmigrated cells) were removed with a cotton swab. Remaining cells were counterstained with propidium iodide for 10 minutes. The transwells were then cut out and placed onto glass slides for analysis.

Cytokine/chemokine array

The Mouse Cytokine Antibody Array was performed as per the manufacturer's instructions (Abcam, ab133995). Briefly, tissue lysates were isolated from wild-type mammary fat pad (n=1) or tumor tissue from C44- or 3B10-treated Met-1 mice (n=2 and n=3, respectively). Each membrane was exposed to 100 μg of tissue lysate from a single mouse. Chemiluminescent signal was detected using the Licor Odyssey Imaging System. Relative signal intensities for each cytokine/chemokine were normalized to the loading controls.

Histology and immunohistochemistry

Histology and immunohistochemistry were performed as previously described (**IHC paper reference**):

Tissue fixation and sectioning. All tissues were fixed in 10% neutral buffered formalin for 48 h on a shaker at room temperature. Tissues were washed and stored in PBS at 4°C until embedded. Paraffin embedding was performed by the UT Southwestern Molecular Pathology Core. Before sectioning, FFPE tissue blocks were incubated in 70% ethanol with 10% glycerol for 5 minutes to soften followed by a quick rinse in distilled water. Then, 5 µm sections were cut using a Leitz 1512 rotary microtome and placed onto a water bath at 40°C for 2 minutes to reduce wrinkles. Sections were transferred to positively charged slides (#SFH1103; Biocare Medical) and allowed to dry overnight before staining.

Deparaffinization, staining, imaging. Slides were warmed for 10 minutes in a 60°C oven before following the de-paraffinization protocol. The de-paraffinization and rehydration protocol entails incubation in xylene (3x for 5 minutes), 100% ethanol (2x for 2 minutes), 95% ethanol (2x for 2 minutes), 70% ethanol (2x for 2 minutes), 50% ethanol (2x for 2 minutes) and PBS (1x 3 minutes). To prevent sections from folding or falling off the slides during antigen retrieval and antibody stripping, the de-paraffinized slides were fixed in 10% neutral buffered formalin for 30 minutes followed by incubation in PBS (2x for 3 minutes).

For antigen retrieval, 250 ml of antigen retrieval buffer (10 mM Tris-HCl 1 mM EDTA, 10% glycerol, pH 9.0) was preheated to 80°C in a bucket inside a pressure cooker (Biocare Medical) filled with 500 ml of water. Slides were then placed inside the buffer and heated at 110°C for 18 minutes (~4-5 psi). Slides were allowed to cool at room temperature for 30 minutes followed by a PBS rinse. Tissue sections were surrounded by a hydrophobic barrier using a PAP pen and blocked for 10 minutes with 2.5% goat serum, 2.5% horse serum (Vector Laboratories) or 30 minutes Rodent Block M (Biocare Medical) if the secondary host was goat, horse, or rat, respectively.

Incubation with primary antibody was performed on a shaker for 1 h at room temperature, or at 4°C overnight. Slides were washed in PBSt (0.05% tween + 2 mM EDTA; 3x for 5 minutes) before adding the 'polymer' HRP- or AP-conjugated secondary antibodies (ImmPress; Vector Laboratories). Sections were incubated with secondary antibody for 30 minutes on a shaker followed by one PBSt (0.2% tween + 2 mM EDTA) and two PBSt (0.05% tween + 2 mM EDTA) washes, 5 minutes each. Sections were then incubated with chromogenic or tyramide signal amplification substrates. For multiplex staining, antibody stripping was performed in 10 mM citrate buffer (pH 6.2, 10% glycerol) in a pressure cooker at 110°C for 2 minutes before probing with the next primary antibody.

For chromogenic detection, Betazoid DAB, Warp Red, and Ferangi Blue (BDB2004L, WR806S, and FB813H respectively; Biocare Medical) were used. Substrate incubation time was determined by monitoring signal development using a microscope. After developing with chromogenic substrates, slides were counterstained with hematoxylin. Bluing was performed by running tap water over the slides for 30 seconds. Slides were cover-slipped using VectaMount (H-5501, Vector Laboratories) and scanned at 20X using the Hamamatsu NanoZoomer 2.0-HT.

For fluorescence detection, we used tyramide signal amplification (OPAL; #NEL797001KT; PerkinElmer). The following fluorophores were used: OPAL 520, OPAL 570, and OPAL 690. DAPI was used for nuclear counterstaining. To reduce the auto-fluorescence, slides were incubated at the end in TrueBlack Lipofuscin Autofluorescence Quencher (#23007; Biotium) diluted 20-fold in 70% ethanol for 30 seconds. Slides were cover-slipped using ProLong Gold (#P36931, Life Technologies). Slides were scanned at 20X using the Zeiss Axioscan.Z1 (Whole Brain Microscopy Facility, UT Southwestern). DAPI, AF488 (for OPAL520), AF555 (for OPAL570) and AF660 (for OPAL 690) channels were used to acquire images. The exposure time for image acquisition was between 5 to 100 milliseconds. Image analysis was performed using ImageJ.

Real-time quantitative PCR

Total RNA was extracted using the Qiagen RNeasy Mini Kit (Qiagen, 74106). cDNA was produced from RNA using the Bio-Rad iScript cDNA Synthesis Kit. Expression of <**genes**> were assessed and detected using SYBR green (Bio-Rad). For primers, see **Supplemental Table X**.

Flow cytometry

Flow cytometric analysis was performed as previously described[169]:
Tumors were digested with a cocktail containing collagenase I (45 μ/ml; Worthington), collagenase II (15 μ/ml; Worthington), collagenase III (45 μ/ml; Worthington), collagenase IV (45 μ/ml; Worthington), elastase (0.075 μ/ml; Worthington), hyaluronidase (30 μ/ml; MilliporeSigma), and DNase type I (25 μ/ml; MilliporeSigma) for 40 minutes at 37°C and passed through a 70-μm cell strainer (Fal- con). Splenocytes were isolated from spleens and passed through a 70-μm cell strainer (Falcon). Suspensions were washed twice with PBS and stained with Fixable Viability Dye (Thermo Fisher) for 1 hour. The cell suspensions were then washed and stained with antibodies detecting CD11b (BD Bioscience, 557657), Ly-6C (BD Bioscience, 562728), Ly-6G (BD Bioscience, 740953), F4/80 (Biolegend, 123132), CD274 (PD-L1, BD Bioscience, 563369), CD11c (BD Bioscience, 564079), I-A/I-E (BD Bioscience, 562009), CD3 (BD Biosci- ence, 553061), CD4 (BD

Bioscience, 562891), CD8 (BD Bioscience, 563332), CD279 (PD-1, BD Bioscience, 563059), CD152 (CTLA-4, BD Bioscience, 565778), and CD25 (IL-2 receptor α, BD Bioscience, 562694) for 1 hour at 4°C. Surface-stained cells were fixed, permeabilized, and stained for intracellular markers arginase 1 (R&D Systems, IC5868P), iNOS (Thermo Fisher, 17-5920-82), FoxP3 (BD Bioscience, 560401), and Ki67 (Biolegend, 652404). Cells were analyzed using FACS LSRFortessa SORP, and analysis was performed using FlowJo, with the help of the Moody Foundation flow cytometry facility at University of Texas Southwestern Medical Center.

Statistics

Data are reported as the mean ± SD. Statistical analysis was performed using GraphPad Prism For comparisons of two groups, a 2-tailed student's T test. If the data did not fit a normal distribution, Kruskall-Wallace non-parametric test was performed instead.

Study Approval

Animal experiments in this study were approved by and performed in accordance with the Institutional Animal Care and Use Committee at the University of Texas Southwestern Medical Center at Dallas.

APPENDIX A
PTN and in vitro assays

It is now well-known that many experiments in the biology literature are unrepeatable. There are a plethora of factors that contribute to this issues, including experimental stringency (or lack thereof), contaminating factors, and variability in reagent quality. Also, key components of protocols may undocumented.

In the Ptn and Mdk field, there are many published reports of in vitro activities that are simply unrepeatable[5,31]. Perhaps unsurprisingly, there is a lack of published reports discussing such negative data. Despite this, numerous labs dedicated to the study of the Ptn/Mdk family are aware of this issue. For example, at the 2018 Midkine Symposium in Munich, Germany, there was a dedicated session towards discussion of the lack of robust in vitro functional assays concerning the Ptn/Mdk cytokine family. Out of this session came no definitive answers.

The irreproducibility of Ptn in vitro assays plagued the original direction of my thesis work. In this section, I will share some of my results in my attempts to repeat results from the literature.

I sought out a way to validate that our recombinant Ptn was functional. I performed a thorough review of the Ptn literature focusing on in vitro assays used to detect Ptn activity. During the 1990s, multiple labs reported that Ptn promotes

proliferation of NIH3T3 fibroblasts in vitro. Thus, I sought to use this assay as a positive control. I first titrated recombinant PTN to test it's efficacy over a wide range of concentration. I did not observe potentiation of NIH3T3 cell proliferation (**Appendix A: Figure 1a**). To test if PTN's activity may be cell density-dependent, I repeated the experiment, keeping PTN constant and titrating the number of plated cells. No change was observed (**Appendix A: Figure 1b**). I repeated these experiments with different timepoints and different media formulations +/- FBS, but still no proliferative activity was observed (data not shown). Some have suggested that Ptn may require proteolytic processing, with enzymes like plasmin, to produce "active" forms of the protein[10,97]. To test this, I first digested recombinant Ptn for different time points (**Appendix A: Figure 1c**). This produced cleaved products of various sizes dependent on incubation time (increasing from left to right). No proliferative activity was observed in any of the plasmin-processed fractions (**Appendix A: Figure 1d**).

It was suggested to us by a collaborator that mammalian cell-produced PTN was active, and during heparin-sepharose purification, there are lower MW PTN products that are most active. Thus, I produced PTN in HEK293 cells, fractionated the conditioned media over a heparin-sepharose column using a salt gradient, and tested the fractions for activity (**Appendix A: Figure 2**). PTN was detected most prominently in fraction 28 (black arrow). None of the PTN-containing fractions (F24-F27) exhibited proliferative activity (**Appendix A:**

Figure 2c). As expected, the positive control, bFGF, worked effectively. Fractions 20-23 had cytotoxic activity. Mass spec analysis reveals that this could be due to the presence of HMGB1, which can be cytotoxic in an extracellular context. A prominent band is detected in fraction 21, corresponding to the known molecular weight of HMGB1 (~25 kDa). This is also supported by the fact that the fractions with cytotoxic activity correspond to those which come off the column with when the gradient reaches ~600 mM NaCl, supported by previous reports[170]. I have yet to confirm whether or not PTN overexpression is causing HMGB1 secretion by the transfected HEK293 cells, but given that extracellular HMGB1 can function as a chemotactic signal[171], it may be worth investigating.

I also repeated these assays with other cell types, including cancer cells and immune cells. No proliferative activity was seen (data not shown).

Interestingly, Himburg et al. (2010) reported that Ptn can promote HSC growth in vitro, but this activity is very conditional, requiring the presence of three additional soluble factors: thrombopoietin, stem cell factor, and Fl3-ligand[16]. Recently, there was published example of conditional chemotactic activity for Ptn. When Qin et al. (2017) performed a proteomic screen for chemoattractants produced by neural precursor cells, they identified 8 differentially expressed proteins relative to control[172]. Ptn was one of the top hits. They observed, however, that no single factor, including Ptn, could reproduce the chemotactic activity of the NPC conditioned-media. Qin et al. then tested all possible

combinations of the 8 factors and observed that the activity required the presence of Ptn, SPARC, SPARCL1, and Hsp90B. Qin et al. observed that these proteins form a heterotetramer required for activity[172]. The conditional requirements of these reported assays suggests that the irreproducibility issues in the field are far from accidental.

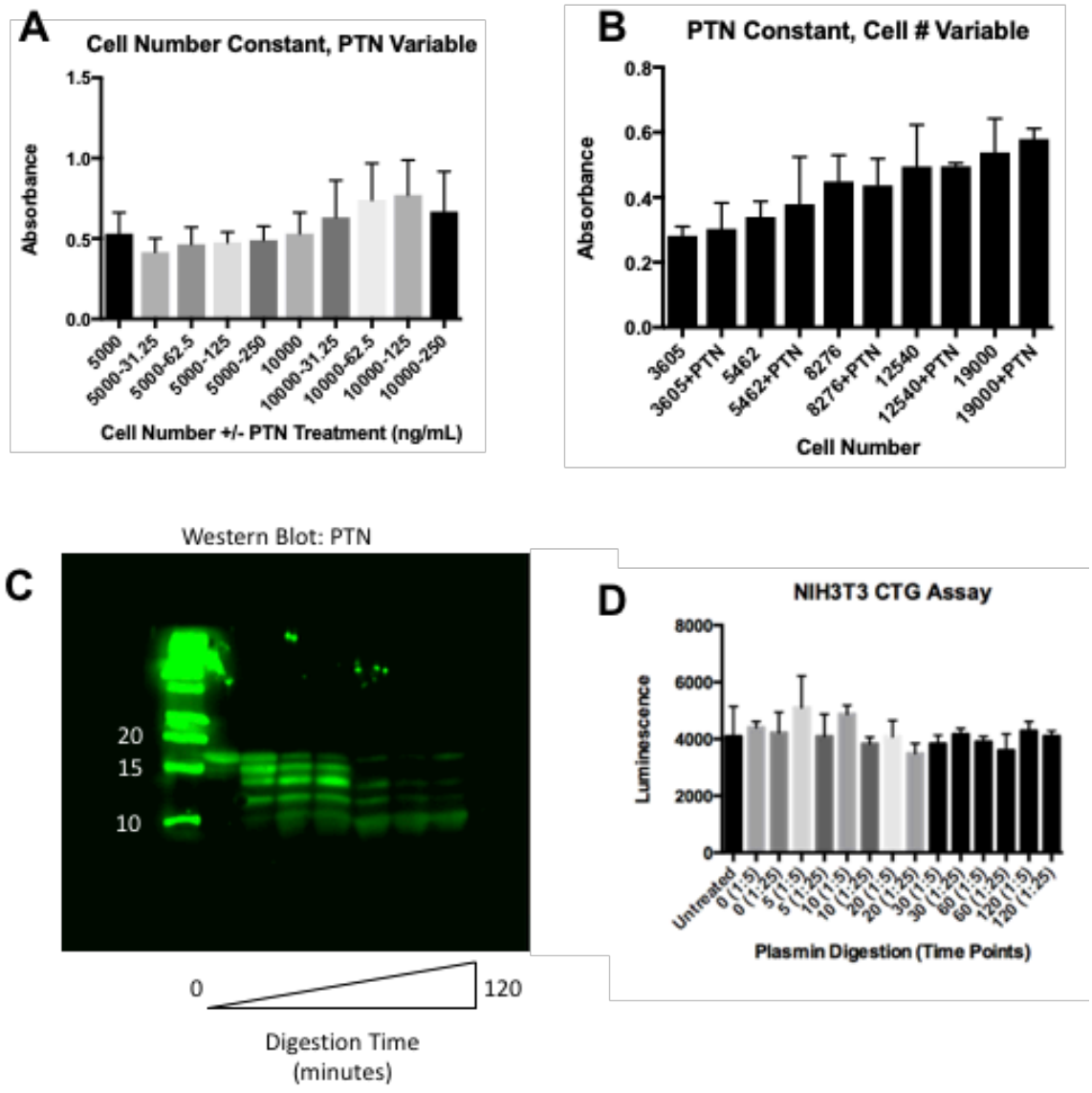

Appendix Figure A1: **Testing the mitogenicity of recombinant Ptn**. A) MTS assay of 3T3 cells treated with titrated recombinatn Ptn. B) Ptn concentration was constant and 3T3 cell number was titrated to determine if Ptn effects are cell density dependent. C,D) Recombinant Ptn was treated with plasmin for various time points. Digested fragments were used to determine if any proteolytically processed fragments had activity.

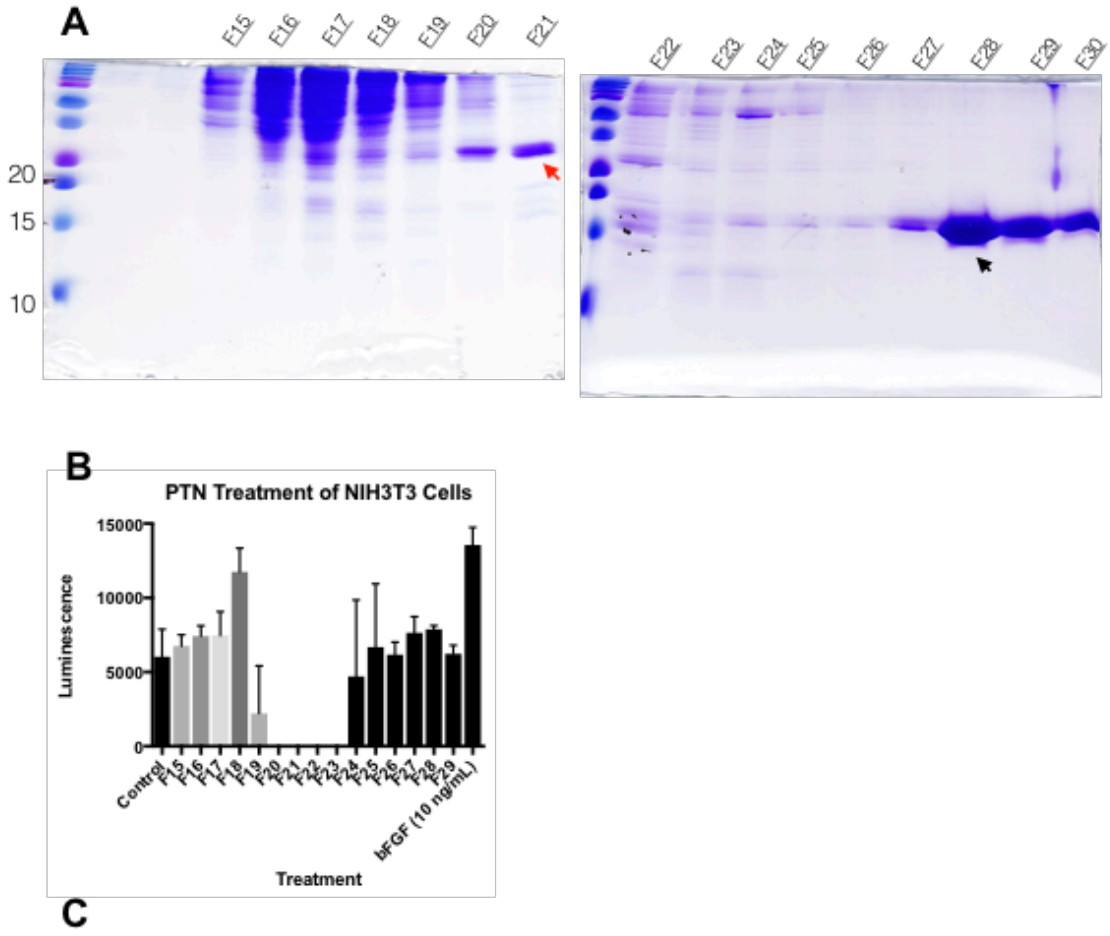

C

Protein	Description	Length (AA)	mw (Da)	PSMs	Peptide Seqs	% Coverage
P09429	HMGB1_HUMAN High mobility group protein B1 (	215	24932.20	829	40	81.90
Q8TEA8	DTD1_HUMAN D-tyrosyl-tRNA(Tyr) deacylase 1 O	209	23463.00	437	22	87.60
Q00688	FKBP3_HUMAN Peptidyl-prolyl cis-trans isomeras	224	25215.30	403	31	82.60
P26583	HMGB2_HUMAN High mobility group protein B2 (	209	24072.80	386	43	84.70
O15347	HMGB3_HUMAN High mobility group protein B3 (	200	23019.50	362	30	78.50
P09661	RU2A_HUMAN U2 small nuclear ribonucleoprotei	255	28470.20	178	27	71.00
Q17R31	TATD3_HUMAN Putative deoxyribonuclease TATD	274	31174.70	130	19	86.40
P13984	T2FB_HUMAN General transcription factor IIF sub	249	28434.90	124	24	81.50

Appendix Figure A2: **Production, purification, and testing of mammalian cell produced recombinant Ptn**. A Ptn-expression vector was transfected into Hek293 cells. 3 days post transfection, conditioned media was collected and run over a heparin-sepharose column. Protein was eluted using a salt concentration gradient. A) Coomassie blue staining of SDS-PAGE gels. Each lane represents a fraction. The red arrow points to what is assumed to be Hmgb1. The black arrow is Ptn. B) Fractions were tested for mitogenicity on NIH3T3 cells. C) Mass spec of F21 to identify the cytotoxic factor.

BIBLIOGRAPHY

1 Heng, T. S., Painter, M. W. & Immunological Genome Project, C. The Immunological Genome Project: networks of gene expression in immune cells. *Nat Immunol* **9**, 1091-1094, doi:10.1038/ni1008-1091 (2008).

2 Muramatsu, T. Structure and function of midkine as a basis of its pharmacological effects. *Br J Pharmacol* **171**, 814-826 (2014).

3 Fu C., L. M., Maminta-Smith D., Chan G., Deuel T. Cloning and sequence of the Xenopus laevis homologue of the midkine cDNA. *Gene* **146**, 311-312 (1994).

4 Kadomatsu K, T. M., Muramatsu T. cDNA cloning and sequencing of a new gene intensely expressed in early differentiation stages of embryonal carcinoma cells and in mid-gestation period of mouse embryogenesis. *Biochem Biophys Res Commun* **151**, 1312-1318 (1988).

5 Courty J, D. M., Caruelle D, Perderiset M, Barritault D. Mitogenic properties of a new endothelial cell growth factor related to pleiotrophin. *Biochem Biophys Res Commun* **180**, 145-151 (1991).

6 Rauvala, H. An 18-kd heparin-binding protein of developing brain that is distinct from fibroblast growth factors. *EMBO J* **8**, 2933-2941 (1989).

7 Muramatsu H, Z. P., Kurosawa N, Ichihara-Tanaka K, Maruyama K, Inoh K, Sakai T, Chen L, Sato M, Muramatsu T. Female infertility in mice deficient in midkine and pleiotrophin, which form a distinct family of growth factors. *Genes Cells* **11**, 1405-1417 (2006).

8 Kadomatsu K, K. S., Tsubota S. The heparin-binding growth factor midkine: the biological activities and candidate receptors. *J Biochem* **153**, 511-521 (2013).

9 Rosenfield SM, B. E., Cohen-Missner S, Gibby KA, Ory V, Henke RT, Riegel AT, Wellstein A. Pleiotrophin (PTN) Expression and Function and in the Mouse Mammary Gland and Mammary Epithelial Cells. *PLoS One* **7**, e47876 (2012).

10 Papadimitriou E, P. E., Castana P, Tsalios T, Polyzos A, Beis D. Pleiotrophin and its receptor protein tyrosine phosphatase beta/zeta as regulators of angiogenesis and cancer. *Biochim Biophys Acta* **1866**, 252-265 (2016).

11 Kadomatsu K, H. R., Suganuma T, Murata F, Muramatsu T. A retinoic acid responsive gene MK found in the teratocarcinoma system is expressed in spatially and temporally controlled manner during mouse embryogenesis. *J Cell Biol* **110**, 607–616 (1990).

12 Aridome K, T. J., Takao S, Kadomatsu K, Ozawa M, Aikou T et al. Increased midkine gene expression in human gastrointestinal cancers. *Jpn J Cancer Res* **86**, 655–661 (1995).

13 Inazumi T, T. S., Nishikawa T, Kadomatsu K, Muramatsu H, Muramatsu T. Expression of the retinoid-inducible polypeptide, midkine, in human epidermal keratinocytes. *Arch Dermatol Res* **289**, 471-475 (1997).

14 Nordin SL, A. C., Bjermer L, Bjartell A, Morgelin M, Egesten A. Midkine is part of the antibacterial activity released at the surface of differentiated bronchial epithelial cells. *J Innate Immun* **5**, 519-330 (2013).

15 Herradon G, E. L., Nguyen T, Silos-Santiago I, Deuel TF. Midkine regulates pleiotrophin organ-specific gene expression: evidence for transcriptional regulation and functional redundancy within the pleiotrophin/midkine developmental gene family. *Biochem Biophys Res Commun* **333**, 714-721 (2005).

16 Himburg HA, M. G., Daher P, Meadows SK, Russell JL, Doan P, Chi JT, Salter AB, Lento WE, Reya T, Chao NJ, Chute JP. Pleiotrophin regulates the expansion and regeneration of hematopoietic stem cells. *Nature Medicine* **16**, 475-483 (2010).

17 Himburg HA, H. J., Ito T, Daher P, Russell JL, Quarmyne M, Doan PL, Helms K, Nakamura M, Fixsen E, Herradon G, Reya T, Chao NJ, Harroch S, Chute JP. Pleiotrophin regulates the retention and self-renewal of hematopoietic stem cells in the bone marrow vascular niche. *Cell Reports* **2**, 964-975, doi:doi:10.1016/j.celrep.2012.09.002 (2012).

18 Himburg HA, Y. X., Doan PL, Quarmyne M, Micewicz E, McBride W, Chao NJ, Slamon DJ, Chute JP. Pleiotrophin mediates hematopoietic regeneration via activation of RAS. *J Clin Invest.* **124**, 4753-4758, doi:doi:10.1172/JCI76838 (2014).

19 Braun BS, T. D., Kong N, Le DT, Kogan SC, Rozmus J, Le Beau MM, Jacks TE, Shannon KM. Somatic activation of oncogenic KRas in hematopoietic cells initiates a rapidly fatal myeloproliferative disorder. *Proc Natl Acad Sci U S A.* **101**, 597-602 (2004).

20 Dorrell C, T. K., Minden MD, Hawley RG, Dick JE. Hematopoietic cell fate and the initia- tion of leukemic properties in primitive primary human cells are influenced by Ras activity and fernesyltransferase inhibition. *Mol Cell Biol* **24**, 6993-7702 (2004).

21 Uehara K, M. S., Kadomatsu K, Tsutsui J, Muramatsu T. Genomic structure of human midkine (MK), a retinoic acid-responsive growth/differentiation factor. *J Biochem* **111**, 563-567 (1992).

22 Satoh J, K. Y. Differing effects of IFN beta vs IFN gamma in MS: gene expression in cultured astrocytes. *Neurology* **57**, 681-685 (2001).

23 Li F, T. F., Wang L, Williamson IK, Sharifi BG, Shah PK. Pleiotrophin (PTN) is expressed in vascularized human atherosclerotic plaques: IFN-{gamma}/JAK/STAT1 signaling is critical for the expression of PTN in macrophages. *FASEB J* **24**, 810-822 (2010).

24 Asari A, K. T., Kurihara H. Oral Administration of High Molecular Weight Hyaluronan (900 kDa) Controls Immune System via Toll-like Receptor 4 in the Intestinal Epithelium. *J Biol Chem* **285**, 24751-24758 (2010).

25 Pufe T, B. M., Petersen W, Tillmann B, Mentlein R. Expression of pleiotrophin, an embryonic growth and differentia- tion factor, in rheumatoid arthritis. *Arthritis Rheum* **48**, 660-667 (2003).

26 Sharifi BG, Z. Z., Wang L, Song L, Chen H, Qin M, Sierra-Honigmann MR, Wachsmann-Hogiu S, Shah PK. Pleiotrophin Induces Transdifferentiation of Monocytes Into Functional Endothelial Cells. *Arterioscler Thromb Vasc Biol* **26**, 1273-1280, doi:doi:10.1161/01.ATV. 0000222017.05085.8e. (2006).

27 Rawnaq T, D. L., Wolters-Eisfeld G, Uzunoglu FG, Vashist YK, Bachmann K, Simon R, Izbicki JR, Bockhorn M, Güngör C. The multifunctional growth factor midkine promotes proliferation and migration in pancreatic cancer. *Mol Cancer Res* **12**, 670-680 (2014).

28 Callebaut C, N. S., Briand JP, Krust B, Hovanessian AG. Inhibition of HIV infection by the cytokine midkine. *Virology* **281**, 248-264 (2001).

29 Mitsiadis TA, C. J., De Bari C, Bluteau G. The large functional spectrum of the heparin-binding cytokines MK and HB-GAM in continuously growing organs: The rodent incisor as a model. *Dev Biol* **320**, 256-266 (2008).

30 Hatziapostolou M, P. C., Katsoris P, Courty J, Papadimitriou E. Heparin affin regulatory peptide/ pleiotrophin mediates fibroblast growth factor 2 stimulatory effects on human prostate cancer cells. *J Biol Chem* **281**, 32217-32226 (2006).

31 Li YS, G. M., Deuel TF. Pleiotrophin gene expression is highly restricted and is regulated by platelet-derived growth factor. *Biochem Biophys Res Commun* **184**, 427-432 (1992).

32 Antoine M, T. C., Wirz W, Borkham-Kamphorst E, Sawitza I, Gressner AM, Kiefer P. Upregulation of pleiotrophin expression in rat hepatic stellate cells by PDGF and hypoxia: Implications for its role in experimental biliary liver fibrogenesis. *Biochem Biophys Res Commun* **337**, 1153-1164 (2005).

33 Poimenidi E, T. C., Koutsioumpa M, Skondra L, Droggiti E, van den Broek M, Koolwijk P, Papadimitriou E. Vascular endothelial growth factor A (VEGF-A) decreases expression and secretion of pleiotrophin in a VEGF receptor-independent manner. *Vascul Pharmacol* **80**, 11-19, doi:doi: 10.1016/j.vph.2016.02.008 (2016).

34 Zhao G, N. Y., Lv M, He L, Wang T, Hou Y. ERβ-mediated estradiol enhances epithelial mesenchymal transition of lung adenocarcinoma through increasing transcription of midkine. *Mol Endocrinol* **26**, 1304-1315 (2012).

35 Zhang H, O. M., Panzhinskiy E, Zawada WM, Das M. PKCδ/midkine pathway drives hypoxia-induced proliferation and differentiation of human lung epithelial cells. *Am J Physiol Cell Physiol* **306**, C648-658 (2014).

36 Kondoh S, I. K., Igarashi K, Sugizaki H, Shirode-Fukuda Y, Inoue E, Yu T, Takeuchi JK, Kanno J, Bonewald LF, Imai Y. Estrogen receptor α in osteocytes regulates trabecular bone formation in female mice. *Bone* **60**, 68-77 (2014).

37 Kaplan F, C. J., Sladek R, Hudson TJ, Muglia LJ, Macrae T, Gagnon S, Asada M, Brewer JA, Sweezey NB. The growth factor midkine is modulated by both glucocorticoid and retinoid in fetal lung development. *Am J Respir Cell Mol Biol* **28**, 33-41 (2003).

38 Milhiet PE, V. F., Caruelle JP, Barritault D, Caruelle D, Courty J. Upregulation of the angiogenic factor heparin affin regulatory peptide by progesterone in rat uterus. *J Endocrinol* **158**, 389-399 (1998).

39 Gu D, Y. B., Zhao C, Ye W, Lv Q, Hua Z, Ma J, Zhang Y. The effect of pleiotrophin signaling on adipogenesis. *FEBS Lett* **581**, 382-388 (2007).

40 Achour A, M. b. J., Baudouin F, Caruelle D, Courty J. Pleiotrophin induces expression of inflammatory cytokines in peripheral blood mononuclear cells. *Biochimie* **90**, 1791-1795 (2008).

41 M'Bika JP, B. F., Courty J, Achour A. Host factor pleiotrophin induces human immunodeficiency virus type 1 replication associated with inflammatory cytokine expression. *J Gen Virol* **91**, 1346-1353 (2010).

42 Kong Y, B. P., Nan KJ, Sun H, Chen NZ, Qi XG. Pleiotrophin is a potential colorectal cancer prognostic factor that promotes VEGF expression and induces angiogenesisin colorectal cancer. *Int J Colorectal Dis* **27**, 287-298 (2012).

43 Fan JB, L. W., Yuan K, Zhu XH, Xu DW, Chen JJ, Cui ZM. EGFR trans-activation mediates pleiotrophin-induced activation of Akt and Erk in cultured osteoblasts. *Biochem Biophys Res Commun* **447**, 425-430 (2014).

44 Sato W, K. K., Yuzawa Y, Muramatsu H, Hotta N, Matsuo S, Muramatsu T. Midkine is involved in neutrophil infiltration into the tubulointerstitium in ischemic renal injury. *J Immunol* **167**, 3463-3469 (2001).

45 Said EA, K. B., Nisole S, Svab J, Briand JP, Hovanessian AG. The Anti-HIV Cytokine Midkine Binds the Cell Surface-expressed Nucleolin as a Low Affinity Receptor. *J Biol Chem* **277**, 37492-37502 (2002).

46 Said EA, C. J., Svab J, Delbé J, Krust B, Hovanessian AG. Pleiotrophin inhibits HIV infection by binding the cell surface-expressed nucleolin. *FEBS J* **272**, 4646-4659 (2005).

47 Cohen S, S. O., Zelman-Toister E, Maharshak N, Binsky-Ehrenreich I, Gordin M, Hazan-Halevy I, Herishanu Y, Shvidel L, Haran M, Leng L, Bucala R, Harroch S, Shachar I. The cytokine midkine and its receptor RPTPζ regulate B cell survival in a pathway induced by CD74. *J Immunol* **188**, 259-269 (2012).

48 Yoshida Y, G. M., Tsutsui J, Ozawa M, Sato E, Osame M, Muramatsu T. Midkine is present in the early stage of cerebral infarct. *Brain Res Dev Brain Res* **85**, 25-30 (1995).

49 Yeh HJ, H. Y., Xu J, Hsu CY, Deuel TF. Upregulation of pleiotrophin gene expression in developing microvasculature, macrophages, and astrocytes after acute ischemic brain injury. *J Neurosci* **18**, 3699-3707 (1998).

50 Horiba M, K. K., Nakamura E, Muramatsu H, Ikematsu S, Sakuma S, Hayashi K, Yuzawa Y, Matsuo S, Kuzuya M, Kaname T, Hirai M, Saito H, Muramatsu T. Neointima formation in a restenosis model is suppressed in midkine-deficient mice. *J Clin Invest.* **105**, 489-495 (2000).

51 Obama H, B. S., Tashiro T, Tsutsui J, Ozawa M, Yoshida H, Tanaka H, Muramatsu T. Myocardial infarction induces expression of midkine, a heparin-binding growth factor with reparative activity. *Anticancer Res* **18**, 145-152 (1998).

52 Horiba M, K. K., Yasui K, Lee JK, Takenaka H, Sumida A, Kamiya K, Chen S, Sakuma S, Muramatsu T, Kodama I. Midkine plays a protective role against cardiac ischemia/reperfusion injury through a reduction of apoptotic reaction. *Circulation* **114**, 1713-1720 (2006).

53 Himburg HA, S. J., Yan X, Kan J, Dressman H, Chute JP. A Molecular Profile of the Endothelial Cell Response to Ionizing Radiation. *Radiat Res* **186**, 141-152 (2016).

54 Wan B, F. J., Schultz TW, Sayler GS. In Vitro Immune Toxicity of Depleted Uranium: Effects on Murine Macrophages, CD4+ T Cells, and Gene Expression Profiles. *Environ Health Perspect* **114**, 85-91 (2006).

55 Polytarchou C, H. M., Papadimitriou E. Hydrogen peroxide stimulates proliferation and migration of human prostate cancer cells through activation of activator protein-1 and up-regulation of the heparin affin regulatory peptide gene. *J Biol Chem* **280**, 40428-40435 (2005).

56 Vicente-Rodríguez M, P.-G. C., Ferrer-Alcón M, Uribarri M, Sánchez-Alonso MG, Ramos MP, Herradón G. Pleiotrophin differentially regulates the rewarding and sedative effects of ethanol. *J Neurochem* **131**, 688-695 (2014).

57 He D, C. H., Muramatsu H, Lasek AW. Ethanol activates midkine and anaplastic lymphoma kinase signaling in neuroblastoma cells and in the brain. *J Neurochem* **135**, 508-521 (2015).

58 Weckbach LT, G. L., Borgolte J, Pagel JI, Pogoda F, Schymeinsky J, Müller-Höcker J, Shakibaei M, Muramatsu T, Deindl E, Walzog B. Midkine acts as a proangiogenic cytokine in hypoxia-induced angiogenesis. *Am J Physiol Heart Circ Physiol* **303**, H429-438, doi:doi: 10.1152/ajpheart.00934.2011 (2012).

59 Reynolds PR, M. M., Le Cras TD, Nichols WC, Whitsett JA. Midkine is regulated by hypoxia and causes pulmonary vascular remodeling. *J Biol Chem* **27**, 37124-37132 (2004).

60 Souttou B, R. D., Vigny M. Pleiotrophin induces angiogenesis: involvement of the phosphoinositide-3 kinase but not the nitric oxide synthase pathways. *J Cell Physiol* **187**, 59-64 (2001).

61 Christman KL, F. Q., Kim AJ, Sievers RE, Fok HH, Candia AF, Colley KJ, Herradon G, Ezquerra L, Deuel TF, Lee RJ. Pleiotrophin induces formation of functional neovasculature in vivo. *Biochem Biophys Res Commun* **332**, 1146-1152 (2005).

62 Liu X, M. G., Webster HF, Kurtz A. Basic FGF and FGF receptor 1 are expressed in microglia during experimental autoimmune encephalomyelitis: temporally distinct expression of midkine and pleiotrophin. *Glia* **24**, 390-397 (1998).

63 Wang J, T. H., Sonobe Y, Jin S, Mizuno T, Miyakawa S, Fujiwara M, Nakamura Y, Kato T, Muramatsu H, Muramatsu T, Suzumura A. Inhibition of midkine alleviates experimental autoimmune encephalomyelitis through the expansion of regulatory T cell population. *Proc Natl Acad Sci U S A.* **105**, 3915-3920 (2008).

64 Takada T, T. K., Muramatsu H, Song XJ, Torii S, Muramatsu T. Midkine, a retinoic acid-inducible heparin-binding cytokine in inflammatory responses: chemotactic activity to neutrophils and association with inflammatory synovitis. *J Biochem* **122**, 453-458 (1997).

65 Maruyama K, M. H., Ishiguro N, Muramatsu T. Midkine, a heparin-binding growth factor, is fundamentally involved in the pathogenesis of rheumatoid arthritis. *Arthritis Rheum* **50**, 1420-1429 (2004).

66 Sonobe Y, L. H., Jin S, Kishida S, Kadomatsu K, Takeuchi H, Mizuno T, Suzumura A. Midkine inhibits inducible regulatory T cell differentiation by suppressing the development of tolerogenic dendritic cells. *J Immunol* **188**, 2602-2611 (2012).

67 Chung JS, T. K., Akiyoshi H, Cruz PD Jr, Ariizumi K. The DC-HIL/syndecan-4 pathway regulates autoimmune responses through myeloid-derived suppressor cells. *J Immunol* **192**, 2576-2584 (2014).

68 Chung JS, B. M., Tomihari M, Cruz PD Jr, Ariizumi K. The DC-HIL/syndecan-4 pathway inhibits human allogeneic T-cell responses. *Eur J Immunol* **39**, 965-974 (2009).

69 Muto J, Y. K., Taylor KR, Gallo RL. Engagement of CD44 by hyaluronan suppresses TLR4 signaling and the septic response to LPS. *Mol Immunol* **47**, 449-456 (2009).

70 Birmpas C, B. J., Courty J, Katsoris P. The pseudopeptide HB-19 binds to cell surface nucleolin and inhibits angiogenesis. *Vasc Cell* **4**, 21 (2012).

71 Koutsioumpa M, D. G., Mikelis C, Theochari K, Vourtsis D, Katsoris P, Giannopoulou E, Courty J, Petrou C, Magafa V, Cordopatis P, Papadimitriou E. Pleiotrophin expression and role in physiological angiogenesis in vivo: Potential involvement of nucleolin. *Vasc Cell* **4** (2012).

72 Destouches D, E. K. D., Hamma-Kourbali Y, Krust B, Albanese P, Katsoris P, Guichard G, Briand JP, Courty J, Hovanessian AG. Suppression of tumor growth and angiogenesis by a specific antagonist of the cell-surface expressed nucleolin. *PLoS One* **3**, e2518 (2008).

73 Mitsiadis TA, S. M., Muramatsu T, Muramatsu H, Rauvala H, Lehtonen E, Jalkanen M, Thesleff I. Expression of the heparin-binding cytokines, midkine (MK) and HB-GAM (pleiotrophin) is associated with epithelial-mesenchymal interactions during fetal development and organogenesis. *Development* **121**, 37-51 (1995).

74 Götte, M. Syndecans in inflammation. *FASEB J* **17**, 575-591 (2003).

75 Elenius K, V. S., Laato M, Salmivirta M, Thesleff I, Jalkanen M. Induced expression of syndecan in healing wounds. *J Cell Biol* **114**, 585-595 (1991).

76 Clasper S, V. S., Fiore M, Plebanski M, Wordsworth P, David G, Jackson DG. Inducible expression of the cell surface heparan sulfate proteoglycan syndecan-2 (fibroglycan) on human activated macrophages can regulate fibroblast growth factor action. *J Biol Chem* **274**, 24113-24123 (1999).

77 Sebestyén A, G. M., Knittel T, Ambrust T, Ramadori G, Kovalszky I. Cytokine regulation of syndecan expression in cells of liver origin. *Cytokine* **12**, 1557-1560 (2000).

78 Ishiguro K, K. K., Kojima T, Muramatsu H, Iwase M, Yoshikai Y, Yanada M, Yamamoto K, Matsushita T, Nishimura M, Kusugami K, Saito H, Muramatsu T. Syndecan-4 deficiency leads to high mortality of lipopolysaccharide-injected mice. *J Biol Chem* **276**, 47483-47488 (2001).

79 Sanderson RD, L. P., Bernfield M. B lymphocytes express and lose syndecan at specific stages of differentiation. *Cell Regul* **1**, 27-35 (1989).

80 Yeaman C, R. A. Post-transcriptional regulation of syndecan-1 expression by cAMP in peritoneal macrophages. *J Cell Biol* **122**, 941-950 (1993).
81 Li J, B. L., Laham RJ, Volk R, Simons M. Macrophage-dependent regulation of syndecan gene expression. *Circ Res* **81**, 785-796 (1997).
82 Yamashita Y, O. K., Miyoshi EK, Wall R, Bernfield M, Kincade PW. Syndecan-4 is expressed by B lineage lymphocytes and can transmit a signal for formation of dendritic processes. *J Immunol* **162**, 5940-5948 (1999).
83 Kaneider NC, E. P., Dunzendorfer S, Wiedermann CJ. Syndecan-4 as antithrombin receptor of human neutrophils. *Biochem Biophys Res Commun* **287**, 42-46 (2001).
84 Saphire AC, B. M., Zhang Z, David G, Gallay PA. Syndecans serve as attachment receptors for human immunodeficiency virus type 1 on macrophages. *J Virol* **75**, 9187-9200 (2001).
85 Wegrowski Y, M. A., Kotlarz G, Toulmonde E, Maquart FX, Bernard J. Cell surface proteoglycan expression during maturation of human monocytes-derived dendritic cells and macrophages. *Clin Exp Immunol* **144**, 485-493 (2006).
86 Chung JS, D. I., Cruz PD Jr, Ariizumi K. Syndecan-4 mediates the coinhibitory function of DC-HIL on T cell activation. *J Immunol* **179**, 5778-5784 (2007).
87 Teixé T, N.-B. P., Vilella R, Engel P, Reina M, Espel E. Syndecan-2 and -4 expressed on activated primary human CD4+ lymphocytes can regulate T cell activation. *Mol Immunol* **45**, 2905-2919 (2008).
88 Hayashida K, P. W., Park PW. Syndecan-1 shedding facilitates the resolution of neutrophilic inflammation by removing sequestered CXC chemokines. *Blood* **114**, 3033-3043 (2009).
89 Gautier EL, S. T., Miller J, Greter M, Jakubzick C, Ivanov S, Helft J, Chow A, Elpek KG, Gordonov S, Mazloom AR, Ma'ayan A, Chua WJ, Hansen TH, Turley SJ, Merad M, Randolph GJ; Immunological Genome Consortium. Gene-expression profiles and transcriptional regulatory pathways that underlie the identity and diversity of mouse tissue macrophages. *Nat Immunol* **13**, 1118-1128 (2012).
90 Rovira-Clavé X, A.-I. M., Noguer O, Espel E, Reina M. Syndecan-2 can promote clearance of T-cell receptor/CD3 from the cell surface. *Immunology* **137**, 214-225 (2012).
91 Kehoe O, K. N., King S, Eustace A, Boyes C, Reizes O, Williams A, Patterson A, Middleton J. Syndecan-3 is selectively pro-inflammatory in the joint and contributes to antigen-induced arthritis in mice. *Arthritis Res Ther* **16**, R148 (2014).
92 Segaliny AI, B. R., Mortier E, Maillasson M, Cherel M, Jacques Y, Le Goff B, Heymann D. Syndecan-1 regulates the biological activities of interleukin-34. *Biochim Biophys Acta* **1853**, 1010-1021 (2015).
93 Raulo E, C. M., Carey DJ, Nolo R, Rauvala H. Isolation of a neuronal cell surface receptor of heparin binding growth-associated molecule (HB-GAM). Identification as N-syndecan (syndecan-3). *J Biol Chem* **269**, 12999-13004 (1994).

94 Imai S, K. M., Raulo E, Kinnunen T, Fages C, Meng X, Lakso M, Rauvala H. Osteoblast recruitment and bone formation enhanced by cell matrix-associated heparin-binding growth-associated molecule (HB-GAM). *J Cell Biol* **143**, 1113-1128 (1998).

95 Asai T, W. K., Ichihara-Tanaka K, Kaneda N, Kojima S, Iguchi A, Inagaki F, Muramatsu T. Identification of Heparin-Binding Sites in Midkine and Their Role in Neurite-Promotion. *Biochem Biophys Res Commun* **236**, 66-70 (1997).

96 Muramatsu H, Z. P., Suzuki H, Oda Y, Chen GY, Sakaguchi N, Sakuma S, Maeda N, Noda M, Takada Y, Muramatsu T. α4β1- and α6β1-integrins are functional receptors for midkine, a heparin-binding growth factor. *Journal of Cell Science* **117**, 5405-5415 (2004).

97 Mikelis C, S. E., Koutsioumpa M, Kieffer N, Papadimitriou E. Integrin alpha(v)beta(3) is a pleiotrophin receptor required for pleiotrophin-induced endothelial cell migration through receptor protein tyrosine phosphatase beta/zeta. *FASEB J* **23**, 1459-1469 (2009).

98 Koutsioumpa M, P. C., Courty J, Zhang Y, Kieffer N, Mikelis C, Skandalis SS, Hellman U, Iliopoulos D, Papadimitriou E. Interplay between αvβ3 integrin and nucleolin regulates human endothelial and glioma cell migration. *J Biol Chem* **288**, 343-354 (2013).

99 Weckbach LT, G. A., Winkelmann M, Jakob SM, Groesser L, Borgolte J, Pogoda F, Pick R, Pruenster M, Müller-Höcker J, Deindl E, Sperandio M, Walzog B. The cytokine midkine supports neutrophil trafficking during acute inflammation by promoting adhesion via β2 integrins (CD11/CD18). *Blood* **123**, 1887-1896 (2014).

100 Shibata Y, M. T., Hirai M, Inui T, Kimura T, Saito H, McCormick LM, Bu G, Kadomatsu K. Nuclear Targeting by the Growth Factor Midkine. *Mol Cell Biol* **22**, 6788-6796 (2002).

101 Perez-Pinera P, Z. W., et al. Anaplastic lymphoma kinase (ALK) is activated through the pleiotrophin (PTN)/receptor protein tyrosine phosphatase (RPTP)β/ζ signaling pathway: an "Alternative Mechanism" of receptor tyrosine kinase (RTK) activation. *J. Biol. Chem.* **282**, 28683-28690 (2007).

102 Stoica GE, K. A., Aigner A, Sunitha I, Souttou B, Malerczyk C, Caughey DJ, Wen D, Karavanov A, Riegel AT, Wellstein A. Identification of Anaplastic Lymphoma Kinase as a Receptor for the Growth Factor Pleiotrophin. *J. Biol. Chem.* **276**, 16772-16779 (2001).

103 Stoica GE, K. A., Powers C, Bowden ET, Sale EB, Riegel AT, Wellstein A. Midkine binds to anaplastic lymphoma kinase (ALK) and acts as a growth factor for different cell types. *J. Biol. Chem.* **277**, 35990-35998 (2002).

104 Mathivet T, M. P., Vigny M. In contrast to agonist monoclonal antibodies, both C-terminal truncated form and full length form of Pleiotrophin failed to activate vertebrate ALK (anaplastic lymphoma kinase)? *Cell Signal* **19**, 2434-2443 (2007).

105 TF, D. Anaplastic lymphoma kinase: "Ligand Independent Activation" mediated by the PTN/RPTPβ/ζ signaling pathway. *Biochim Biophys Acta* **1834**, 2219-2223 (2013).

106 Guan J, U. G., Yamazaki Y, Wolfstetter G, Mendoza P, Pfeifer K, Mohammed A, Hugosson F, Zhang H, Hsu AW, Halenbeck R, Hallberg B, Palmer RH. FAM150A and FAM150B are activating ligands for anaplastic lymphoma kinase. *Elife* **4:eLife.09811** (2015).

107 Reshetnyak AV, M. P., Shi X, Mo ES, Mohanty J, Tome F, Bai H, Gunel M, Lax I, Schlessinger J. Augmentor α and β (FAM150) are ligands of the receptor tyrosine kinases ALK and LTK: Hierarchy and specificity of ligand-receptor interactions. *Proc Natl Acad Sci U S A* **112**, 15862-15867 (2015).

108 Arroyo AG, Y. J., Rayburn H, Hynes RO. Differential requirements for alpha4 integrins during fetal and adult hematopoiesis. *Cell* **85**, 997-1008 (1996).

109 Albert ML, K. J., Birge RB. alphavbeta5 integrin recruits the CrkII-Dock180-rac1 complex for phagocytosis of apoptotic cells. *Nat Cell Biol* **2**, 899-905 (2000).

110 Bishop GG, M. J., Sanders JM, Hesselbacher SE, Feldman MJ, McNamara CA, Gimple LW, Powers ER, Mousa SA, Sarembock IJ. Selective alpha(v)beta(3)-receptor blockade reduces macrophage infiltration and restenosis after balloon angioplasty in the atherosclerotic rabbit. *Circulation* **103**, 1906-1911 (2001).

111 Jin H, S. J., Garmy-Susini B, Kleeman J, Varner J. Integrin alpha4beta1 promotes monocyte trafficking and angiogenesis in tumors. *Cancer Res* **66**, 2146-2152 (2006).

112 Voisin MB, N. S. *Adhesion Molecules: Function and Inhibition*. (Birkhäuser Basel, 2007).

113 Randolph GJ, O. J., Partida-Sánchez S. Migration of dendritic cell subsets and their precursors. *Annu Rev Immunol* **26**, 293316 (2008).

114 Muramatsu H, Z. K., Sakaguchi N, Ikematsu S, Sakuma S, Muramatsu T. LDL receptor-related protein as a component of the midkine receptor. *Biochem Biophys Res Commun* **270**, 936-941 (2000).

115 Mantuano E, B. C., Lam MS, Azmoon P, Gilder AS, Gonias SL. LDL receptor-related protein-1 regulates NFκB and microRNA-155 in macrophages to control the inflammatory response. *Proc Natl Acad Sci U S A*. **113**, 1369-1374 (2016).

116 Chen S, B. G., Takei Y, Sakamoto K, Ikematsu S, Muramatsu T, Kadomatsu K. Midkine and LDL-receptor-related protein 1 contribute to the anchorage-independent cell growth of cancer cells. *J Cell Science* **120**, 4009-4015 (2007).

117 Mongelard F, B. P. Nucleolin: a multiFACeTed protein. *Trends Cell Biol* **17**, 80-86 (2007).

118 Hirano K, M. Y., Hirai Y, Sato R, Itoh T, Hayashi A, Yamanaka M, Eda S, Beppu M. A multifunctional shuttling protein nucleolin is a macrophage receptor for apoptotic cells. *J Biol Chem* **280**, 39284-39293 (2005).

119 van Spriel AB, L. J., van Egmond M, Dijkman HB, Assmann KJ, Mayadas TN, van de Winkel JG. Mac-1 (CD11b/CD18) is essential for Fc receptor–mediated neutrophil cytotoxicity and immunologic synapse formation. *Blood* **97**, 2478-2486 (2001).

120 Ho MK, S. T. Mac-1 antigen: quantitative expression in macrophage populations and tissues, and immunofluorescent localization in spleen. *J Immunol* **128**, 2281–2286 (1982).

121 Shen D, P. N., Yakubenko VP, Ardell CL, Balabiyev A, Ugarova TP, Wang X. Pleiotrophin, a multifunctional cytokine and growth factor, induces leukocyte responses through the integrin Mac-1. *J Biol Chem* **292**, 18848-18861 (2017).

122 Solovjov DA, P. E., Plow EF. Distinct roles for the alpha and beta subunits in the functions of integrin alphaMbeta2. *J Biol Chem* **280**, 1336–1345 (2005).

123 Maruyama K, M. H., Ishiguro N, Muramatsu T. Midkine, a heparin-binding growth factor, is fundamentally involved in the pathogenesis of rheumatoid arthritis. *Arthritis Rhem* **50**, 1420-1429 (2004).

124 Horiba M, K. K., Nakamura E, Muramatsu H, Ikematsu S, Sakuma S, Hayashi K, Yuzawa Y, Matsuo S, Kuzuya M, Kaname T, Hirai M, Saito H, Muramatsu T. Neointima formation in a restenosis model is suppressed in midkine-deficient mice. *J Clin Invest* **105**, 489-495 (2000).

125 Banno H, T. Y., Muramatsu T, Komori K, Kadomatsu K. Controlled release of small interfering RNA targeting midkine attenuates intimal hyperplasia in vein grafts. *J Vasc Surg* **44**, 633-641 (2006).

126 Wang J, T. H., Sonobe Y, Jin S, Mizuno T, Miyakawa S, Fujiwara M, Nakamura Y, Kato T, Muramatsu H, Muramatsu T, Suzumura A. Inhibition of midkine alleviates experimental autoimmune encephalomyelitis through the expansion of regulatory T cell population. *PNAS* **105**, 3915-3920 (2008).

127 Sato W, K. K., Yuzawa Y, Muramatsu H, Hotta N, Matsuo S, Muramatsu T. Midkine is involved in neutrophil infiltration into the tubulointerstitium in ischemic renal injury. *J Immunol* **167**, 3463-3469 (2001).

128 Kawai H, S. W., Yuzawa Y, Kosugi T, Matsuo S, Takei Y, Kadomatsu K, Muramatsu T. Lack of the growth factor midkine enhances survival against cisplatin-induced renal damage. *Am J Pathol* **165**, 1603-1612 (2004).

129 Kosugi T, Y. Y., Sato W, Arata-Kawai H, Suzuki N, Kato N, Matsuo S, Kadomatsu K. Midkine is involved in tubulointerstitial inflammation associated with diabetic nephropathy. *Lab Invest* **87**, 903-913 (2007).

130 Takada T, T. K., Muramatsu H, Song XJ, Torii S, Muramatsu T. Midkine, a retinoic acid-inducible heparin-binding cytokine in inflammatory responses: chemotactic activity to neutrophils and association with inflammatory synovitis. *122* **2** (1997).

131 Wellstein A, F. W., Khatri A, Lu Y, Swain SS, Dickson RB, Sasse J, Riegel AT, Lippman ME. A Heparin-binding Growth Factor Secreted from Breast Cancer Cells Homologous to a Developmentally Regulated Cytokine. *J Biol Chem* **267**, 2582-2587 (1992).

132 Chang Y, Z. M., Perez-Pinera P, Astudillo A, Mortimer J, Berenson JR, Deuel TF. Secretion of pleiotrophin stimulates breast cancer progression through remodeling of the tumor microenvironment. *Proc Natl Acad Sci U S A.* **104**, 10888-10893 (2007).

133 Nozoe T, O. T., Mori E, Uramoto H, Takenoyama M, Hanagiri T, Sugio K, Yasumoto K. Clinicopathologic significance of an immunohistochemical expression of p27 in scirrhous carcinoma of the breast. *Breast Cancer* **14**, 277-280 (2007).

134 Zhang N, Z. R., Perez-Pinera P, Herradon G, Ezquerra L, Wang ZY, Deuel TF. Identification of the angiogenesis signaling domain in pleiotrophin defines a mechanism of the angiogenic switch. *Biochem Biophys Res Commun* **343**, 653-658 (2006).

135 Hao H, M. Y., Fukazawa T, Yamatsuji T, Takaoka M, Bao XH, Matsuoka J, Okui T, Shimo T, Takigawa N, Tomono Y, Nakajima M, Fink-Baldauf IM, Nelson S, Seibel W, Papoian R, Whitsett JA, Naomoto Y. Inhibition of the Growth Factor MDK/Midkine by a Novel Small Molecule Compound to Treat Non-Small Cell Lung Cancer. *PLoS One* **8**, e71093 (2013).

136 Salama R, M. H., Zou P, Okayama M, Muramatsu T. Midkine, a heparin-binding growth factor, produced by the host enhances metastasis of Lewis lung carcinoma cells. *Cancer Letters* **233**, 16-20 (2006).

137 van der Horst EH, F. B., Chinn L, Coxon A, Li S, Polesso F, Slavin A, Ruefli-Brasse A, Wesche H. The growth factor Midkine antagonizes VEGF signaling in vitro and in vivo. *Neoplasia* **10**, 340-347 (2008).

138 Giamanco NM, J. Y., Wellstein A, Shriver CD, Summers TA, Baron J. Midkine and pleiotrophin concentrations in needle biopsies of breast and lung masses. *Cancer Biomark* **20**, 299-307 (2017).

139 Ma J, K. Y., Nan H, Qu S, Fu X, Jiang L, Wang W, Guo H, Zhao S, He J, Nan K. Pleiotrophin as a potential biomarker in breast cancer patients. *Clin Chim Acta* **466**, 6-12 (2017).

140 Sanz R, A. R., Stresing V, Martín B, Landemaine T, Oliva B, Driouch K, Lidereau R, Sierra A. Functional pathways shared by liver and lung metastases: a mitochondrial chaperone machine is up-regulated in soft-tissue breast cancer metastasis. *Clin Exp Metastasis.* **24**, 673-683 (2007).

141 Chung B, E. A., Gopalakrishna-Pillai S, Murad JP, Andersen ES, Kumar Reddy N, Srinivasan G, Armstrong B, Chu C, Kim Y, Tong T, Waisman J, Yim JH, Badie B, Lee PP. Human brain metastatic stroma attracts breast cancer cells via chemokines CXCL16 and CXCL12. *NPJ Breast Cancer* **3:6** (2017).

142 Park, J. *et al.* Cancer cells induce metastasis-supporting neutrophil extracellular DNA traps. *Sci Transl Med* **8**, 361ra138, doi:10.1126/scitranslmed.aag1711 (2016).

143 Heerboth S, H. G., Leary M, Longacre M3, Byler S, Lapinska K, Willbanks A, Sarkar S. EMT and tumor metastasis. *Clin Transl Med* **4:6** (2015).

144 Diamantopoulou Z, K. P., Menashi S, Courty J, Katsoris P. Loss of Receptor Protein Tyrosine Phosphatase β/ζ (RPTPβ/ζ) Promotes Prostate Cancer Metastasis. *J Biol Chem* **287**, 40339-40349 (2012).

145 Szantho, E. *et al.* Comparative Analysis of Multicolor Flow Cytometry and Immunohistochemistry for the Detection of Disseminated Tumor Cells. *Appl Immunohistochem Mol Morphol* **26**, 305-315, doi:10.1097/PAI.0000000000000519 (2018).

146 Saravanan, L. & Juneja, S. Immunohistochemistry is a more sensitive marker for the detection of myeloperoxidase in acute myeloid leukemia compared with flow

cytometry and cytochemistry. *Int J Lab Hematol* **32**, e132-136, doi:10.1111/j.1751-553X.2008.01124.x (2010).

147 Koyama, S. *et al.* STK11/LKB1 Deficiency Promotes Neutrophil Recruitment and Proinflammatory Cytokine Production to Suppress T-cell Activity in the Lung Tumor Microenvironment. *Cancer Res* **76**, 999-1008, doi:10.1158/0008-5472.CAN-15-1439 (2016).

148 Sridharan, V. *et al.* Immune Profiling of Adenoid Cystic Carcinoma: PD-L2 Expression and Associations with Tumor-Infiltrating Lymphocytes. *Cancer Immunol Res* **4**, 679-687, doi:10.1158/2326-6066.CIR-16-0031 (2016).

149 Beckstead, J. H. A simple technique for preservation of fixation-sensitive antigens in paraffin-embedded tissues. *J Histochem Cytochem* **42**, 1127-1134, doi:10.1177/42.8.8027531 (1994).

150 Feng, Z. *et al.* Multispectral Imaging of T and B Cells in Murine Spleen and Tumor. *J Immunol* **196**, 3943-3950, doi:10.4049/jimmunol.1502635 (2016).

151 Lykidis, D. *et al.* Novel zinc-based fixative for high quality DNA, RNA and protein analysis. *Nucleic Acids Res* **35**, e85, doi:10.1093/nar/gkm433 (2007).

152 Pileri, S. A. *et al.* Antigen retrieval techniques in immunohistochemistry: comparison of different methods. *J Pathol* **183**, 116-123, doi:10.1002/(SICI)1096-9896(199709)183:1<116::AID-PATH1087>3.0.CO;2-2 (1997).

153 Au-Yeung, B. B. *et al.* The structure, regulation, and function of ZAP-70. *Immunol Rev* **228**, 41-57, doi:10.1111/j.1600-065X.2008.00753.x (2009).

154 Dahal, L. N., Gadd, A., Edwards, A. D., Cragg, M. S. & Beers, S. A. UC-1V150, a potent TLR7 agonist capable of activating macrophages and potentiating mAb-mediated target cell deletion. *Scand J Immunol* **87**, e12666, doi:10.1111/sji.12666 (2018).

155 Tutt, A. L. *et al.* Development and Characterization of Monoclonal Antibodies Specific for Mouse and Human Fcgamma Receptors. *J Immunol* **195**, 5503-5516, doi:10.4049/jimmunol.1402988 (2015).

156 Shiraishi, D. *et al.* CD163 Is Required for Protumoral Activation of Macrophages in Human and Murine Sarcoma. *Cancer Res* **78**, 3255-3266, doi:10.1158/0008-5472.CAN-17-2011 (2018).

157 Gabrilovich, D. I., Ostrand-Rosenberg, S. & Bronte, V. Coordinated regulation of myeloid cells by tumours. *Nat Rev Immunol* **12**, 253-268, doi:10.1038/nri3175 (2012).

158 Cobaleda, C., Schebesta, A., Delogu, A. & Busslinger, M. Pax5: the guardian of B cell identity and function. *Nat Immunol* **8**, 463-470, doi:10.1038/ni1454 (2007).

159 Bronte, V. & Pittet, M. J. The spleen in local and systemic regulation of immunity. *Immunity* **39**, 806-818, doi:10.1016/j.immuni.2013.10.010 (2013).

160 Claassen, E. & Van Rooijen, N. The effect of elimination of macrophages on the tissue distribution of liposomes containing [3H]methotrexate. *Biochim Biophys Acta* **802**, 428-434 (1984).

161 Seiler, P. *et al.* Crucial role of marginal zone macrophages and marginal zone metallophils in the clearance of lymphocytic choriomeningitis virus infection. *Eur J Immunol* **27**, 2626-2633, doi:10.1002/eji.1830271023 (1997).

162 Franklin, R. A. *et al.* The cellular and molecular origin of tumor-associated macrophages. *Science* **344**, 921-925, doi:10.1126/science.1252510 (2014).
163 Huang, Y. *et al.* CD4+ and CD8+ T cells have opposing roles in breast cancer progression and outcome. *Oncotarget* **6**, 17462-17478, doi:10.18632/oncotarget.3958 (2015).
164 Song, H. *et al.* Inhibition of tumor progression by oral piceatannol in mouse 4T1 mammary cancer is associated with decreased angiogenesis and macrophage infiltration. *J Nutr Biochem* **26**, 1368-1378, doi:10.1016/j.jnutbio.2015.07.005 (2015).
165 Roland, C. L. *et al.* Cytokine levels correlate with immune cell infiltration after anti-VEGF therapy in preclinical mouse models of breast cancer. *PLoS One* **4**, e7669, doi:10.1371/journal.pone.0007669 (2009).
166 Shi, S. R., Key, M. E. & Kalra, K. L. Antigen retrieval in formalin-fixed, paraffin-embedded tissues: an enhancement method for immunohistochemical staining based on microwave oven heating of tissue sections. *J Histochem Cytochem* **39**, 741-748, doi:10.1177/39.6.1709656 (1991).
167 Shi, S. R., Liu, C. & Taylor, C. R. Standardization of immunohistochemistry for formalin-fixed, paraffin-embedded tissue sections based on the antigen-retrieval technique: from experiments to hypothesis. *J Histochem Cytochem* **55**, 105-109, doi:10.1369/jhc.6P7080.2006 (2007).
168 Sorrelle, N., Dominguez, A. T. A. & Brekken, R. A. From top to bottom: midkine and pleiotrophin as emerging players in immune regulation. *J Leukoc Biol* **102**, 277-286, doi:10.1189/jlb.3MR1116-475R (2017).
169 Du W, H. H., Sorrelle N, Brekken RA. Sitravatinib potentiates immune checkpoint blockade in refractory cancer models. *JCI Insight* **3** (2018).
170 Xu D, Y. J., Song D, Esko JD. Heparan sulfate is essential for high mobility group protein 1 (HMGB1) signaling by the receptor for advanced glycation end products (RAGE). *J Biol Chem* **286**, 41736-41744 (2011).
171 Wu L, Y. L. The function and mechanism of HMGB1 in lung cancer and its potential therapeutic implications. *Oncol Lett.* **15**, 6799-6805 (2018).
172 Qin EY, C. D., Abbott KL, Lennon J, Nagaraja S, Mackay A, Jones C, Vogel H, Jackson PK, Monje M. Neural Precursor-Derived Pleiotrophin Mediates Subventricular Zone Invasion by Glioma. *CEll* **170**, 845-859 (2017).